AD-A112 162 ROCKWELL INTERNATIONAL THOUSAND OAKS CA SCIENCE CENTER F/G 19/1
RAPID ULTRASONIC INSPECTION OF ARTILLERY PROJECTILES.(U)
MAY 78 C M FORTUNKO, R B THOMPSON DAAK10-77-C-2020
UNCLASSIFIED SC5113.4FR NL

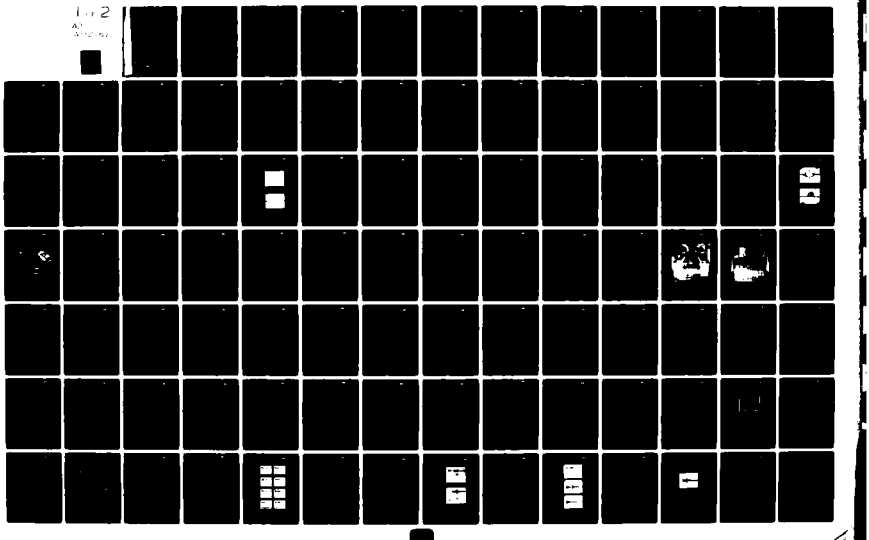

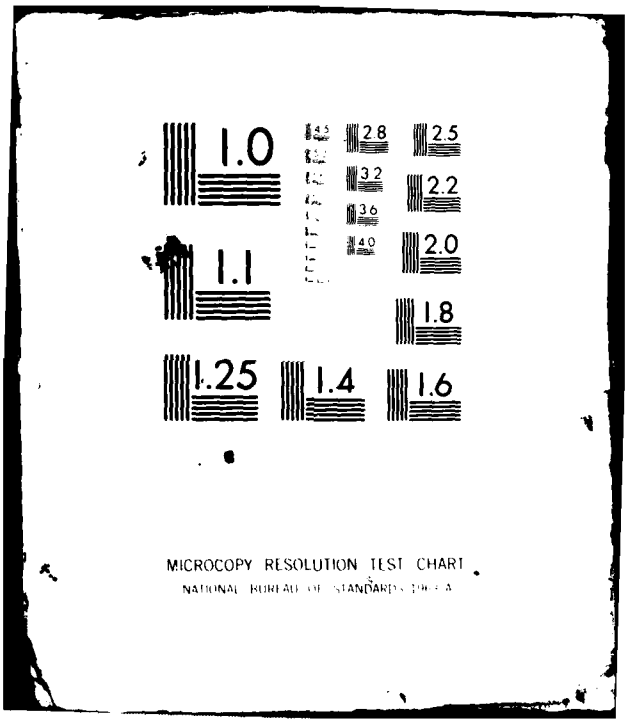
1.0
1.1
1.25
1.4
1.6
1.8
2.0
2.2
2.5
2.8
3.2
3.6
4.0
MICROCOPY RESOLUTION TEST CHART
NATIONAL BUREAU OF STANDARDS 1963-A

May 1978 SC5113.4FR

RAPID ULTRASONIC INSPECTION OF ARTILLERY PROJECTILES

FINAL REPORT FOR THE PERIOD
MAY 25, 1977 TO NOVEMBER 25, 1977

GENERAL ORDER NO. 5113

CONTRACT NO. DAAK10-77-2020

Prepared for:

ARRADCOM
Dover, New Jersey

by

C. M. Fortunko and R. B. Thompson
Principal Investigators

and

M. W. Mahoney
Program Manager

Approved for public release; distribution unlimited.

Rockwell International
Science Center

UNCLASSIFIED

SECURITY CLASSIFICATION OF THIS PAGE (When Data Entered)

REPORT DOCUMENTATION PAGE	READ INSTRUCTIONS BEFORE COMPLETING FORM
1. REPORT NUMBER	2. GOVT ACCESSION NO. AD-A112162 / 3. RECIPIENT'S CATALOG NUMBER
4. TITLE (and Subtitle) RAPID ULTRASONIC INSPECTION OF ARTILLERY PROJECTILES	5. TYPE OF REPORT & PERIOD COVERED Final Report 05/25/77 through 11/25/77
	6. PERFORMING ORG. REPORT NUMBER SC5113.4FR
7. AUTHOR(s) C. M. Fortunko, R. B. Thompson, M. W. Mahoney	8. CONTRACT OR GRANT NUMBER(s) DAAK10-77-C-2020
9. PERFORMING ORGANIZATION NAME AND ADDRESS Rockwell International Science Center 1049 Camino Dos Rios Thousand Oaks, California 91360	10. PROGRAM ELEMENT, PROJECT, TASK AREA & WORK UNIT NUMBERS
11. CONTROLLING OFFICE NAME AND ADDRESS ARRADCOM, Building 3409 Dover, New Jersey 07801	12. REPORT DATE May 1978 / 13. NUMBER OF PAGES 107
14. MONITORING AGENCY NAME & ADDRESS(if different from Controlling Office)	15. SECURITY CLASS. (of this report) Unclassified / 15a. DECLASSIFICATION/ DOWNGRADING SCHEDULE

16. DISTRIBUTION STATEMENT (of this Report)

Approved for public release; distribution unlimited.

17. DISTRIBUTION STATEMENT (of the abstract entered in Block 20, if different from Report)

18. SUPPLEMENTARY NOTES

19. KEY WORDS (Continue on reverse side if necessary and identify by block number)

Ultrasonics, Defects, Nondestructive Evaluation, Artillery Projectiles, Automated Inspection, EMAT's

20. ABSTRACT (Continue on reverse side if necessary and identify by block number)

This report describes the results of the second phase of a three phase program to develop an on-line, rapid ultrasonic inspection system for artillery projectiles using noncontact, electromagnetic acoustic transducers (EMATs). In Phase I, feasibility was demonstrated using the M-107 projectile as a medium. Based on these successful results, the present Phase II was initiated with the purpose of adapting these results to the geometry of the M-549 (RAP) projectile. It had as specifications the development of a system design, construction of key hardware

(over)

DD FORM 1 JAN 73 1473 EDITION OF 1 NOV 65 IS OBSOLETE

UNCLASSIFIED

SECURITY CLASSIFICATION OF THIS PAGE (When Data Entered)

#20 Abstract (continued).

components, and experimental evaluation of hardware performance.

Herein are described in detail the technical results of Phase II. Included are discussions of the conceptual layout of a rapid, fully automatic, microprocessor controlled inspection system based on the EMAT technology; the detailed design of the projectile handling system necessary to assure the reliable flow of projectiles through the system, including provisions for handling of rejected parts and consideration of compatibility with the production line of Norris Industries, in Vernon, California; the design and construction of an electromagnet to produce the magnetic bias necessary for optimum inspection; the design and construction of two ultrasonic channels; the demonstration of their ability to detect and locate EDM notches and naturally occurring defects in the M-549 projectile; and the possible effects of material variations such as surface decarburization.

Based on the successful execution of these tasks, it is recommended that a complete prototype system be constructed and installed on a projectile production line in Phase III of this program.

TABLE OF CONTENTS

TABLE OF CONTENTS (Cont'd)

ABSTRACT

This report describes the results of the second phase of a three phase program to develop an on-line, rapid ultrasonic inspection system for artillery projectiles using noncontact, electromagnetic acoustic transducers (EMATs). In Phase I, feasibility was demonstrated using the M-107 projectile as a medium. Based on these successful results, the present Phase II was initiated with the purpose of adapting these results to the geometry of the M-549 (RAP) projectile. It had as specifications the development of a system design, construction of key hardware components, and experimental evaluation of hardware performance.

Herein are described in detail the technical results of Phase II. Included are discussions of the conceptual layout of a rapid, fully automatic, microprocessor controlled inspection system based on the EMAT technology; the detailed design of the projectile handling system necessary to assure the reliable flow of projectiles through the system, including provisions for handling of rejected parts and consideration of compatibility with the production line of Norris Industries, in Vernon, California; the design and construction of an electromagnet to produce the magnetic bias necessary for optimum inspection; the design and construction of two ultrasonic channels; the demonstration of their ability to detect and locate EDM notches and naturally occurring defects in the M-549 projectile; and the possible effects of material variations such as surface decarburization.

Based on the successful execution of these tasks, it is recommended that a complete prototype system be constructed and installed on a projectile production line in Phase III of this program.

I. INTRODUCTION

The electromagnetic-acoustic transducer (EMAT) is a device of particular interest for nondestructive evaluation (NDE) because of its practical advantage of noncontact operation which for many applications can result in a high rate of ultrasonic inspection with an attendant large reduction in quality control costs. The program discussed in this writing specifically addresses the use of EMATs for near complete ultrasonic inspection of the 155 mm M-549 (RAP) artillery projectile in one inspection station.

Although the M-549 is of current interest, the emphasis of this program has been generic in nature in that the overall objective is to demonstrate a type of inspection system which can be used, with suitable modifications, to inspect the metal parts of any existing or anticipated artillery projectile in a more cost effective and reliable manner than is presently possible with standard ultrasonic equipment. For the purpose of performing this demonstration, a three-phase program has been planned of which this report describes progress during the second phase with results from the previous feasibility study reported elsewhere[1]. A review of the feasibility is provided in the background section of this report, however, for greater detail see Ref. 1. Efforts from the feasibility study and the second-phase study have all been directed toward the third and final phase which includes the construction and installation of an inspection system capable of fully automated inspection of the 155 mm M-549 (RPA) artillery projectile in a production environment.

Specific objectives of the second-phase study have included: (1) construction of transducers and circuits for one ultrasonic channel, (2) design and construction of an electromagnet capable of magnetizing the 155 mm M-549 projectile (a different projectile from that previously evaluated) to a degree necessary for inspection with noncontact, electromagnetic transducers, (3) completion of fabrication drawings for a projectile handling system designed to operate in concert with an inspection station which uses noncontact, electromagnetic transducers to excite and detect ultrasonic waves, and (4) demonstration of ability to inspect the M-549 projectile with noncontact electromagnetic transducers. These objectives have been successfully completed with results described herein.

II. BACKGROUND

The electromagnetic transducer for generating and detecting ultrasonic waves is a rapidly emerging technology that has been under development at the Science Center for the last six years.[2-5] Figure 1 illustrates the basic principles. When a wire carrying a dynamic current is placed adjacent to a metal part, eddy currents are induced within the material. If, in addition, a static magnetic field is present, these induced currents will experience a force (as in an electric motor) which can be used to launch ultrasonic waves. Conversely, if the surface of the material is moving as a result of an ultrasonic wave impinging upon it from some remote location, there will be eddy currents induced in the metal as it passes through the static magnetic field (as in an electric generator). These

PRINCIPLES OF NONCONTACT TRANSDUCTION

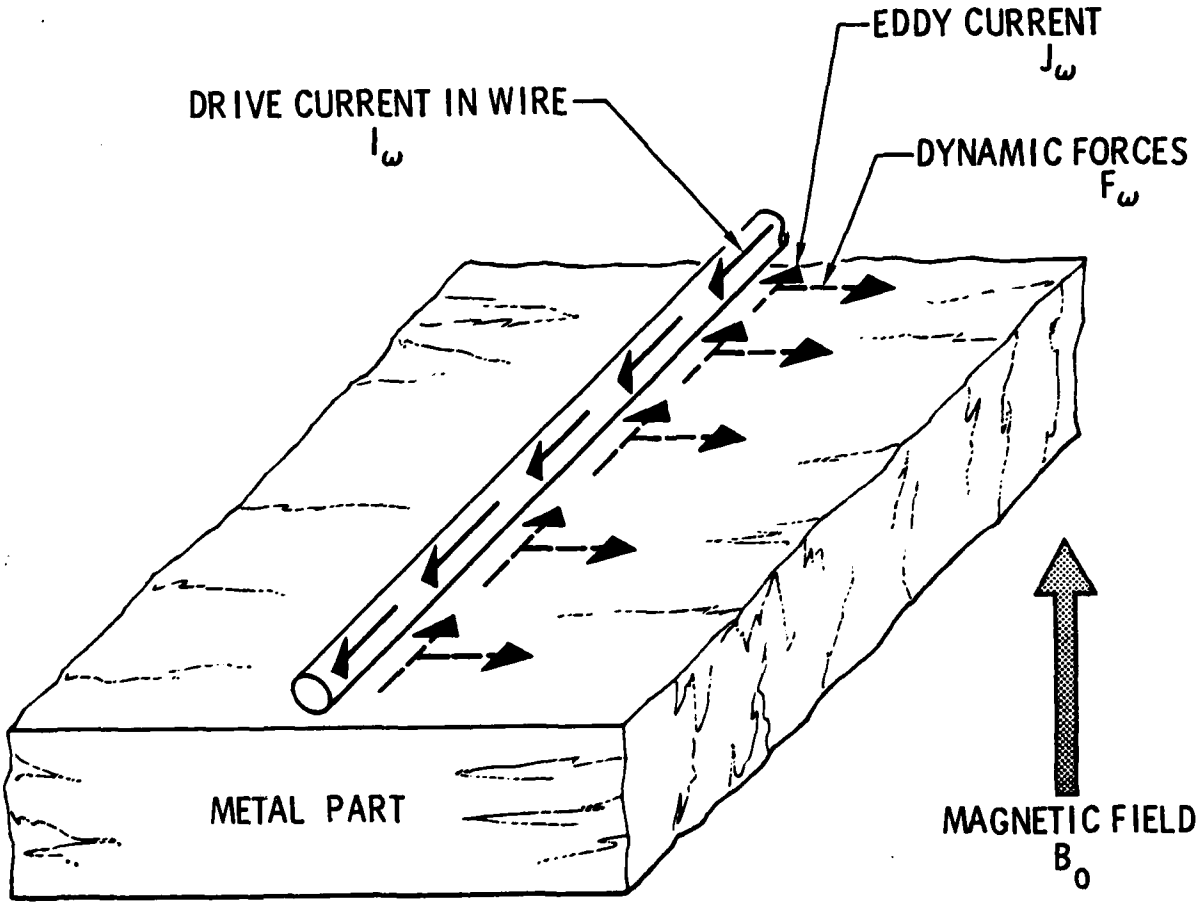

LORENTZ FORCE
(AS IN ELECTRIC MOTOR)

$$\vec{F}_\omega = \vec{J}_\omega \times \vec{B}_0$$

Fig. 1 Distribution of currents and forces on the lattice of a metal part contributing to generation of ultrasonic signals under normal field bias.

currents will be inductively detected by the wire and appropriate electronic receivers. Hence, the same transducer structure, a coil of wire and a magnet, can be used to both excite and detect ultrasonic waves in metals with no physical contact.

In ferromagnetic metals, the above discussions again apply. However, there is an additional transduction mechanism, due to magnetostriction, which can significantly increase transducer efficiency.(6) Figure 2 illustrates this by showing the variations of the amplitude of the ultrasonic wave generated as a function of the static magnetic field in low carbon steel. At high fields, the material is saturated and the amplitude varies linearly with field as in nonmagnetic metals. At low fields, there is a large peak in transducer efficiency caused by magnetostriction. A bias of only 300 Oe produces signals as large as are observed at 10 kOe. This effect is used to great advantage in projectile inspection.

Transducers can be constructed to excite surface waves, bulk shear waves, angle shear waves, and angle longitudinal waves. In the former two cases, which are of interest in this report, the transducer coil is wound in the meander, or serpentine fashion as shown at the top of Fig. 3. If such a coil, along with the magnet necessary to produce the static field (not shown) is placed on the material surface, either of these two wave types can be selected by varying the frequency. When the frequency f is chosen according to the relation:

$$fD = V_R \qquad (1)$$

where D is the coil period and V_R is the Rayleigh (surface) wave velocity,

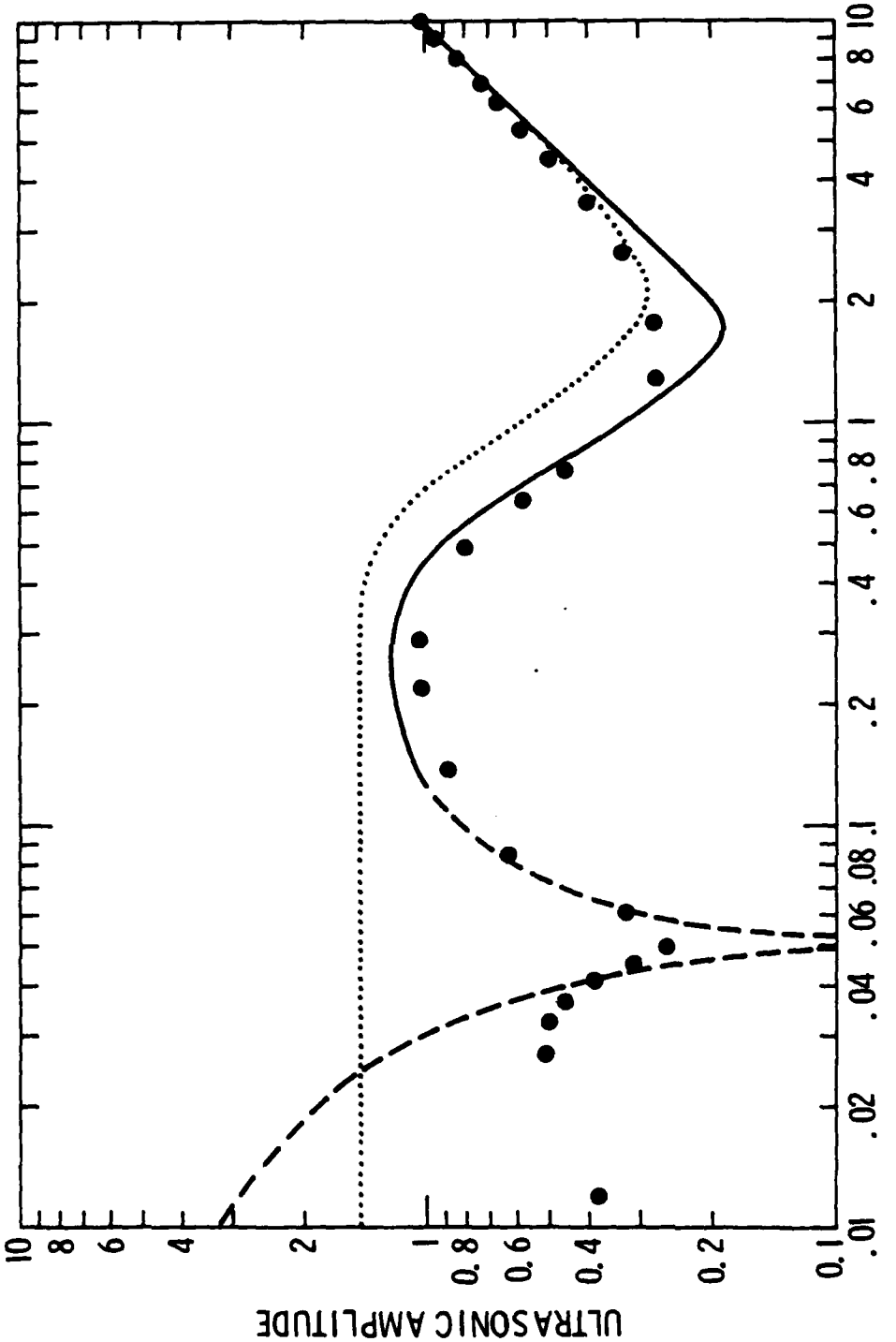

Fig. 2 Variation of ultrasonic amplitude in a 1018 steel plate at 130 kHz. The amplitude is maximized at approximately 300 Oe. Curves are theoretical results.

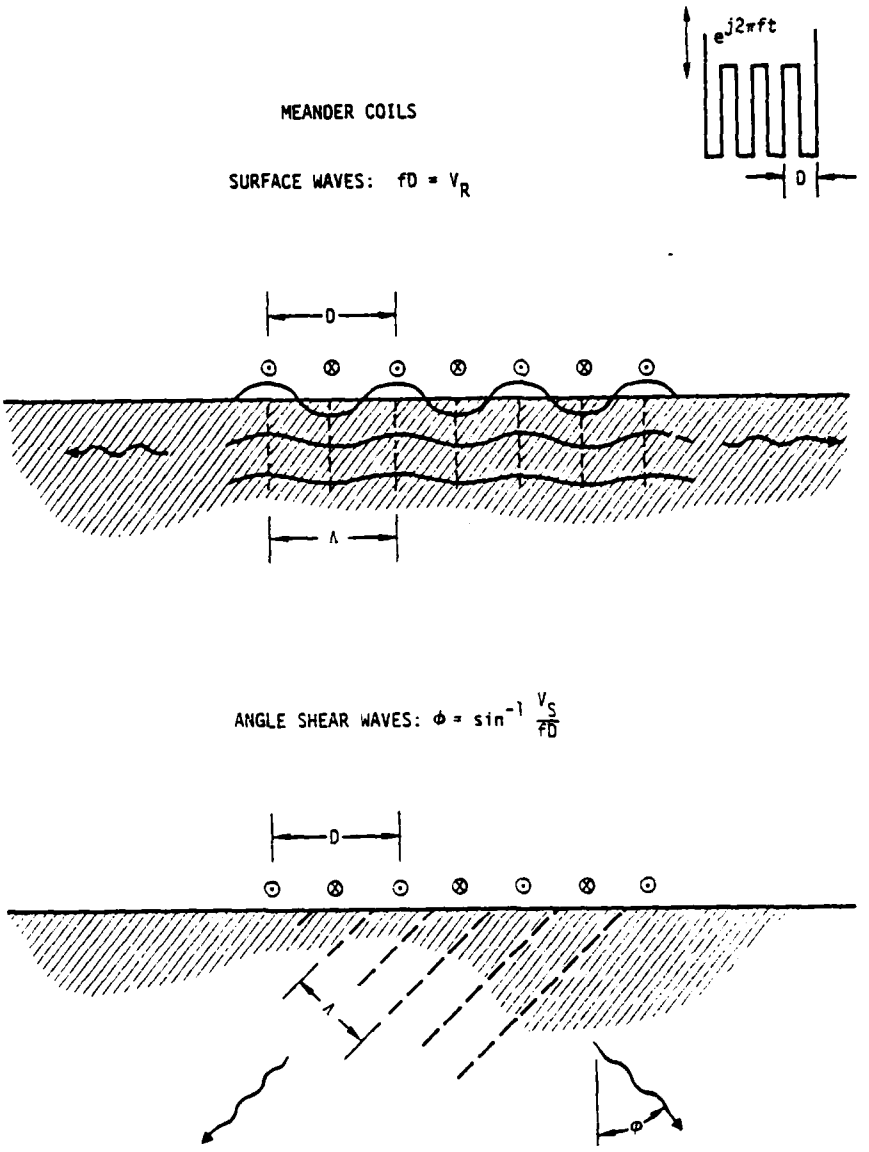

Fig. 3 Principle of generation of surface waves and angle bulk waves by meander coil electromagnetic transducers.

then surface waves will be efficiently generated since their wavelength is just equal to the coil period.(2) At higher frequencies, angle shear waves can be generated(3) since the shorter wavelength can still match the coil period when the wave is traveling at an angle into the material as shown in the bottom of Fig. 3. This angle measured with respect to surface normal is given by:

$$\theta = \sin^{-1}(V_S/fD) \qquad (2)$$

where V_S is the shear wave velocity.

Using the basic principles described above, the feasibility of ultrasonically inspecting artillery projectiles with electromagnetic transducers was previously demonstrated.(1) EDM notches of 0.051 cm (0.020 in.) depths and 0.508 cm (0.200 in.) lengths were placed in several locations on both the interior and exterior of three different 155 mm projectiles (M-107, M-107E1, M-121). The outer surface defects were detected using both surface (Rayleigh) waves and angle shear waves excited by exterior probes. The interior surface defects were detected by angle shear waves excited by exterior probes and surface waves excited by interior probes. In each case, the signal-to-noise ratio of the defect indication was on the order of 30 dB or greater. These demonstrated sensitivities, coupled with the fact that the transducers require no couplant, clearly indicated that an automatic inspection system for on-line use at production rates was practical.

III. PRINCIPAL RESULTS

The objective of the present phase has been to lay the groundwork necessary to transfer the technological innovations demonstrated during the

Phase I feasibility study into an operational prototype system to be completed during Phase III, to follow. Since Phase I used the M-107 projectile as a medium for demonstration of capability, a part of this program has addressed the changes entailed in adapting the results to the M-549 (RAP) geometry, which has a higher long term NDE priority. The remainder of the program has been directed at the definition of a total inspection system configuration and the design and development of key technical components so that, when initiated, Phase III can be primarily concerned with system development using components of known performance.

Specifically, the scope of work of Phase II calls for technical activity in three areas: on-site consultation with government personnel to evaluate system compatibility with an existing production line, design of the total system layout and specific components, and construction and evaluation of key hardware components. These results are summarized below and then discussed in greater depth in Sections IV, V, and VI. Since this document is intended to be the basis for the construction of the prototype system, considerable technical detail has been included. The reader not concerned with great detail may read this section and then proceed to Sections VII and VIII for a summary and conclusions and recommendations without serious loss of continuity. Again, since this is viewed as a design document, Sections IV, V, and VI contain relevant material developed under other support as it pertains to the present program. This is identified as such in the text.

Under the direction of the Army, the inspection system is being designed to be installed in the M-549 production line operated by Norris Industries in Vernon, California. Through consultation with representatives

of both the Army and Norris Industries, it has been established that such a system is compatible with the layout and operational procedures of their line at Vernon. Based on these discussions, an overview of the system operation is as follows.

Once a projectile is delivered to the EMAT inspection station, via the designed handling machine, it is lifted hydraulically and positioned between the poles of an electromagnet where a raster of approximately 30 transducers is brought into contact with the projectile. In order to eliminate lift-off sensitivity, the transducer element maintains a constant separation distance from the surface by means of a spring/tension type tracking mechanism. The contact is not intimate, however, and wear shoes are provided to prevent transducer degradation by abrasion. Each transducer is positioned so as to inspect a specific location of the M-549 projectile, while in total, almost the entire part is inspected. The electromagnet is then activated to produce a field of sufficient strength to achieve maximum magnetostrictive enhancement of ultrasonic signals in the projectile. After sufficient magnetic field strength is attained, the projectile is rotated in the field while the EMAT transducers are sequentially fired to achieve near-complete ID and OD surface area and volume inspection. Ultrasonic signals reflected from specific locations within the projectile are received by the EMAT transducers and delivered to a central processor where they are compared to accept/reject criteria established for different regions of the projectile. The projectile is removed from the EMAT test station and it then either continues in the fabrication line, if acceptable, or is subsequently removed if found to be defective. It should be understood that all projectile

movement, power requirements, launching of ultrasonic signals, switching of electromagnet coil current, and necessary accept/reject decisions are centrally controlled through the same processor. As such the inspection process, as designed, is completely automated.

During this second phase effort, system control designs, specific pieces of hardware, and fabrication drawings for a metal parts handling machine have reached various stages of development in accordance with the program plan. These efforts are described in Section IV.

In Section IV.A, the electronic system architecture for control of the handling machine and ultrasonic signal processing is schematically described. This system makes use of a digital, central processing unit that manages asynchronous functions such as the projectile handling machinery and control of the electromagnet power supplies, and synchronous functions such as the multiplexing of the individual ultrasonic channels. Included in this section is a detailed discussion of the ultrasonic signal processing scheme, which is somewhat novel to the field of nondestructive testing. In traditional systems, ultrasonic signals are converted to numeric flaw indications by the use of a properly positioned gate and a threshold detector of adjustable level. We have gone one step further in sophistication, and performance, through the use of a correlation receiver, as is commonly done in many sonar and radar systems. This device performs the same function alluded to above, but does so with a better rejection of random electronic noise, impulsive noise produced by electronic machinery in the production environment, and possibly grain noise in the material. Since this is a new concept in NDE, a timing diagram is included tracing the progress of an

ultrasonic signal through the receiver as it is converted to a digital number for comparison to an accept/reject criteria stored in the memory of the central processor. Among the other advantages of this approach is the fact that variable acceptance levels can be implemented on a channel by channel basis.

In Section IV.B, a detailed discussion of the electronic hardware making up the one ultrasonic channel constructed in this program is given. This includes a high power transmitter amplifier, a linear receiver amplifier, a transmit-receive switch and the correlation receiver cited above. The present electronics package has a signal-to-noise ratio of approximately 70 dB in the angle shear mode - i.e. a signal transmitted directly from a transmitting transducer to the receiving transducer in the pitch-catch mode is 70 dB above the noise. As will be shown, in a later section, this provides sufficient sensitivity to detect EDM notches as small as 0.023cm (0.009 in) deep by 0.29cm (0.116 in) long with good signal-to-noise ratios.

In Section IV.C, a discussion is presented of the design and construction of the large electromagnet required to simultaneously place the entire projectile at the magnetic bias required for optimum transduction efficiency. This task is particularly important since the simple magnet design used in Phase I did not produce this result, and separate pole pieces had to be used to provide the proper bias to different regions of the projectile. The magnet design in Phase II incorporates several new innovations, including pole pieces of tapered thickness so that more flux can be provided in the base region, where the projectile is also thicker and shunted by its base, contoured pole pieces to match the curvature of the projectile, and a laminated yoke to improve the switching speed. Measurements

on the completed magnet show that it does provide the required bias level throughout the entire projectile. The only problem encountered was an excessive field strength in the nose region which exceeds the level required for maximum transduction efficiency. This will be overcome during construction of the prototype by increasing the gap in this region to reduce the field to the required level.

Section IV.D describes the design of the projectile handling machine. This aspect of the work was subcontracted to K.J. Law Associates, Inc., a firm experienced in the automation of NDE tests using closely related eddy current technology. The system makes use of a walking beam movement which simultaneously moves projectiles through a series of stations. In addition to the inspection station, provisions are included for cleaning, rejection of faulty parts, and demagnetization as needed. Included is a discussion of the compatibility of this handling machine with both the production line at Vernon and the requirements for high reliability inspection with EMATs.

In Section V, the performance of the ultrasonic channels is discussed in detail. Previous results in Phase I had shown that an EMAT system could detect EDM notches as small as 0 051cm (0.020 in) deep and 0.51cm (0.200 in) long on both the interior and exterior surfaces of the M-107. The purpose of this study was to establish that these results could also be obtained on the M-549, and to demonstrate the performance of the improved ultrasonic signal processing channels. Measurements on the M-549 reported in Section V.A shows that there were in fact differences between it and the M-107. These are caused by the fact that the wall thickness does not taper as rapidly and is

essentially constant along much of the length of the projectile, and the fact that this thickness is somewhat less. This result implies that the ultrasonic pulses begin to break up into plate modes, and when the flaw is far from the transducer, it can produce multiple signals corresponding to the individual ultrasonic modes which travel at different velocities. However, when the flaw is close to the transducer, these modes coalesce into a single signal as is usually found in familiar angle beam techniques. The range gates in the prototype system will be placed in this regime.

Section V.B presents a detailed discussion of the operation of the ultrasonic channel showing the output of the correlation receiver as an artificially flawed projectile is rotated under a fixed transducer, simulating the mode of operation of the prototype system. Finally, in Section V.C, the results of survey experiments are discussed in which the detectability of EDM notches and naturally occurring defects were demonstrated. Included are demonstrations for both axial and circumferential notches on the OD and circumferential notches on the ID in either the ogive on bourrelet regions. The smallest notch studied, an EDM notch 0.023cm(0.009 in) deep and 0.29cm(0.116 in) long was easily detected. Also, naturally occurring defects previously located by other techniques were readily located using EMAT transducers and in one case verified by destructive analysis. Some difficulties remain in the base region, but it is believed that these will be overcome by advances being made in other ongoing programs before the initiation of Phase III.

One potentially serious problem was uncovered during Phase II. As described in Section VI, it was found that certain production M-549

projectiles have decarburized surface layers in which the transduction efficiency is significantly reduced. As this was discovered late in the program, and was not a part of the scope of work, a definitive study has not yet been performed. However, based on an IR&D study of the mechanisms of transduction, certain simple solutions are suggested which should overcome the problem with little cost. The conclusions of the program and recommendations are discussed separately in Section VIII.

IV. INSPECTION SYSTEM DESIGN AND HARDWARE

During this second-phase effort, system control designs, specific pieces of hardware, and fabrication drawings for a metal parts handling machine have been completed. The details are given below.

The basic layout and design of circuits described in this section, including the correlation receiver, was carried out under industrial research and development support. These circuits were then adapted to the specific requirements of the artillery projectile inspection system and constructed under the support of this contract.

A. Electronic System Architecture for Handling Machine Control and Ultrasonic Signal Processing.

This section describes an overall plan for management and processing of the ultrasonic data from a large number of electromagnetic transducers and for controlling the projectile handling machinery and magnet power supply.

The signal processing scheme for the M-549 projectile ultrasonic inspection system involves a departure from conventional techniques in that a correlation receiver is used to achieve nearly matched filtering and demodulation of the received ultrasonic data.[7] The main advantage of this type of receiver is that filtering of received data from all ultrasonic channels can be accomplished by the same receiver with uniform fidelity. Other departures from conventional design practices include a novel non-linear power amplifier for exciting the ultrasonic signals, an electrical matching network for optimizing the noise figure of the receiver-preamplifier, and a

transmit receive circuit (TR switch) to protect the sensitive receiver electronics from overloading and possible damage by the transmitter output signal. These details are discussed in the following sections.

The layout of the data processing and process control is shown, in block diagram form, in Fig. 4. A step-by-step timing diagram of analog and digital waveforms involved in the generation and processing of the ultrasonic signals by a typical ultrasonic channel is summarized in Fig. 5. A detailed description of the system's operation is given below.

A typical ultrasonic inspection channel can function either in a "pulse-echo" mode using the same electromagnetic transducer for generating and receiving ultrasonic signals, or in a "pitch-catch" mode using separate transducers. Provisions for each mode are shown because both will be included in the system.

Because electromagnetic transducers are subject to different breakdown limitations than piezoelectric transducers and exhibit higher insertion losses, the ultrasonic channels are subject to severe crosstalk interference and must be operated sequentially rather than in-parallel. The sequencing is accomplished by analog multiplexing of RF signals on transmission and reception. The multiplexers can be thought of as tandem rotary switches controlled by digital signals from the central processor.

The reference waveforms used to drive the transmitter circuitry and to correlate the received signals after linear preamplification are generated by the programmable waveform generator which can be considered a part of the correlation receiver.

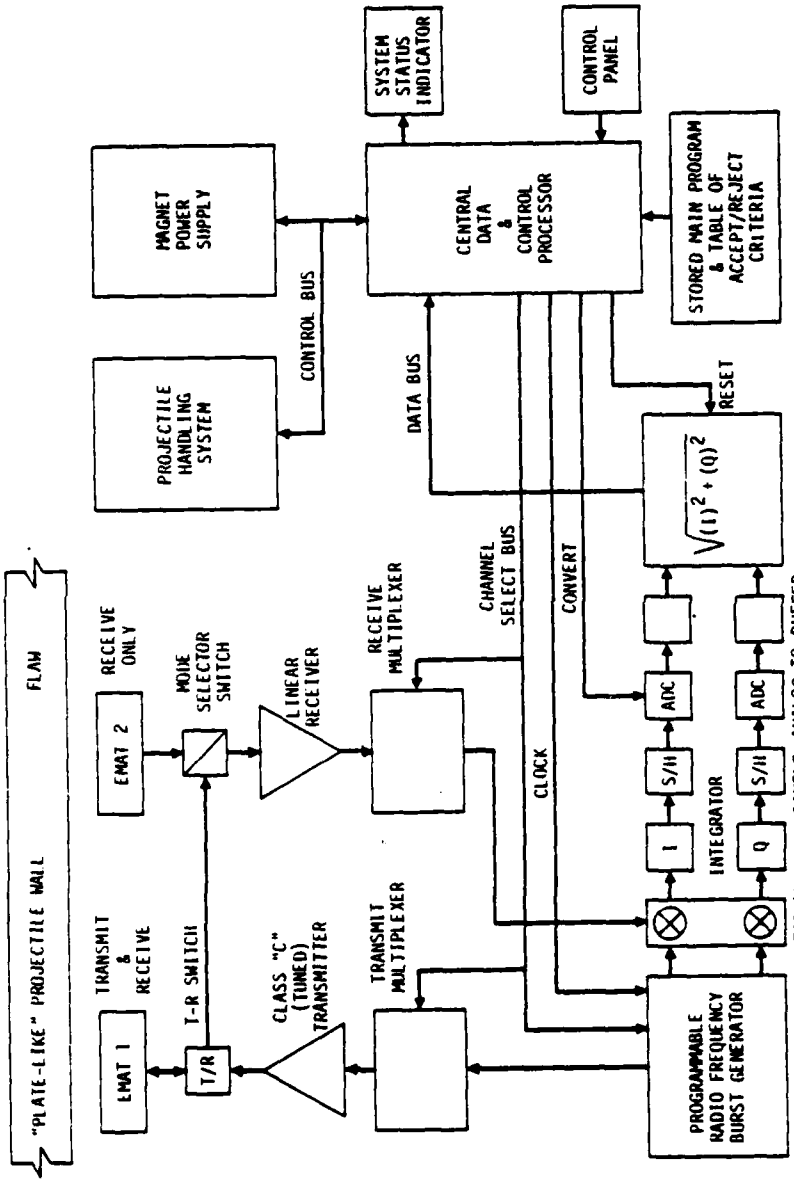

Fig. 4 Block diagram of the planned system for processing of ultrasonic signals, control of projectile handling machinery and making of accept-reject decisions.

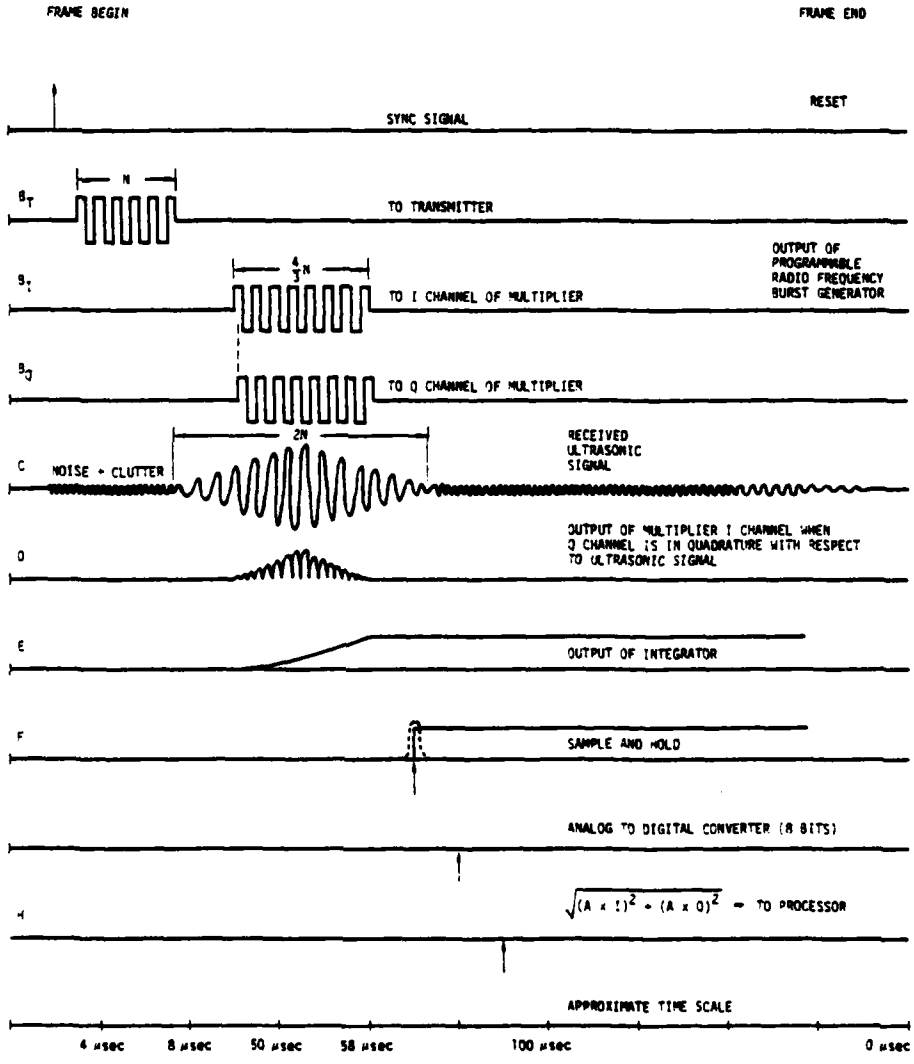

Fig. 5 Time diagram of analog signal processing steps and conversion of the analog data to digital format for further processing of central data and control processors.

The synchronous operation of the transmit receive electronics, the multiplexing system and the correlation receiver is digitally controlled by the central data and control processor which also manages asynchronous functions such as projectile handling and controls of the electromagnet power supplies. The processor also determines the final disposition of each projectile on the basis of received ultrasonic data and a permanently stored set of accept-reject standards.

The sequence of waveforms involved in the processing of ultrasonic data is best explained by referring to Fig. 5. This figure shows the generation of the driving signals as well as the steps involved in the processing of the received ultrasonic signals within a single frame of approximately 400 microseconds. This scan length is compatible with the time required to generate and receive the ultrasonic waveform, and to accomplish all processing functions including the making of the accept-reject decision. Assuming no interruptions of the data processing system, it is estimated that information from 2500 ultrasonic scans can be processed by the central data and control processor in a time of 1 second which is the time interval presently allowed for the inspection of the whole projectile (not including handling time). Thus, there is more than ample time to inspect the whole projectile and to perform all signal processing functions in real-time.

At the beginning of each scan cycle, the central data and control processor transmits an address code to the multiplexers and the programmable RF burst generator. The programmable RF burst generator is internally programmed to generate a reference waveform B_T of N cycles of RF which drives the class "C" transmitter amplifier. The output of the power amplifier

drives the transmit electromagnetic transducer and is partially converted to ultrasonic energy.

After a time delay corresponding to the ultrasonic range of a resolution element within the component being inspected for the presence of flaws, the programmable RF burst generator generates two additional tone bursts B_I and B_Q which are approximately 4/3 N cycles long and are phase shifted by 90 electrical degrees with respect to each other. The two signals serve as reference in-phase and in-quadrature waveforms for demodulating the received ultrasonic signal C after preamplification and demultiplexing. The demodulation of the received signals is accomplished by linear multiplication of the received ultrasonic signal C by the two reference signals B_I and B_Q. The products are then integrated separately to remove second harmonic frequency components, and to produce a voltage level corresponding to the signal energy in each channel.

The use of two channels for detection is required because the exact electrical phase of the ultrasonic signal scattered by a flaw cannot be known in advance. For example, a single channel receiver would produce no output when the reference is phase shifted by 180 electrical degrees with respect to the received ultrasonic signal. (The receiver produces no output when either the received ultrasonic signal C or the reference signals B_I and B_Q are not present simultaneously.)

The outputs of the two integrators E are then sampled individually and stored as analog voltage levels F which can be readily converted to a digital format G. An additional operation is needed involving the computation of the square root of the sum of the squares of the two integrator output

signals. This operation is necessary in order to preserve the linearity of the detection process The result can then be transmitted directly to the central data and control processor which compares the received data with internally stored accept-reject criteria for the purpose of determining whether a flaw has been detected.

The main advantage of the correlation receiver is that because of its programmable features, a number of different waveforms can be demodulated with nearly optimum signal-to-noise performance by the same device. In addition, the correlation receiver tends to discriminate against sharp noise pulses far better than ordinary fixed tuned receivers. For this reason, only a single illumination of the resolution cell within the part being inspected is necessary to discriminate against random electromagnetic interference and electrical noise generated within the signal processing system itself. The major disadvantage of the correlation technique is that it tends to be less effective when the received signals are substantially different from the input signals due to propagation effects such as dispersion or beats caused by strong interferences of several signals.

B. Electronic Hardware for Ultrasonic Channels

Two complete electronic packages have been assembled for generating and receiving ultrasonic signals using the same electromagnetic transducers for both functions. This single transducer development represents a significant improvement over the previous experimental configuration which used separate transducers for generation and reception of ultrasonic signals. Additionally, this new electronic package is a second generation design which

lends itself to miniaturization and modular fabrication. It is expected that the present design will be used in the final inspection station with only very minor engineering changes.

In order to define the best inspection configuration for the M-549 projectile, one of the two electronic packages was tuned to a surface wave frequency (1 MHz). This method of inspection is presently being considered for detection of small defects located on the outer surface of the base. The second electronic channel was tuned to an angle-shear wave frequency (1.8 MHz). Both channels were tested on the surface of M-549 projectiles with good results. A further presentation of the ultrasonic performance of these electronic packages is presented in Section V of this report whereas a detailed discussion of the design of individual components within the electronic package follows below.

1. Transmitter Power Amplifier

A circuit diagram of the power amplifier module is shown in Fig. 6. Because of the need for good crosstalk supression between adjacent receiver modules, the transmitter amplifier features highly non-linear gain characteristics which insures an excellent off-on ratio. The amplifier is presently rated at approximately 1 kilowatt peak RF power at a duty cycle of 1%, or less. It is directly connected to the input of the linear preamplifier receiver via a transmit-receive circuit for "pulse-echo" work. The recovery time is restricted by the electrical "Q" of the matching network and is better than 25 microseconds at 1.8 MHz. Shorter recovery times can be achieved only by operation at higher RF carrier frequencies.

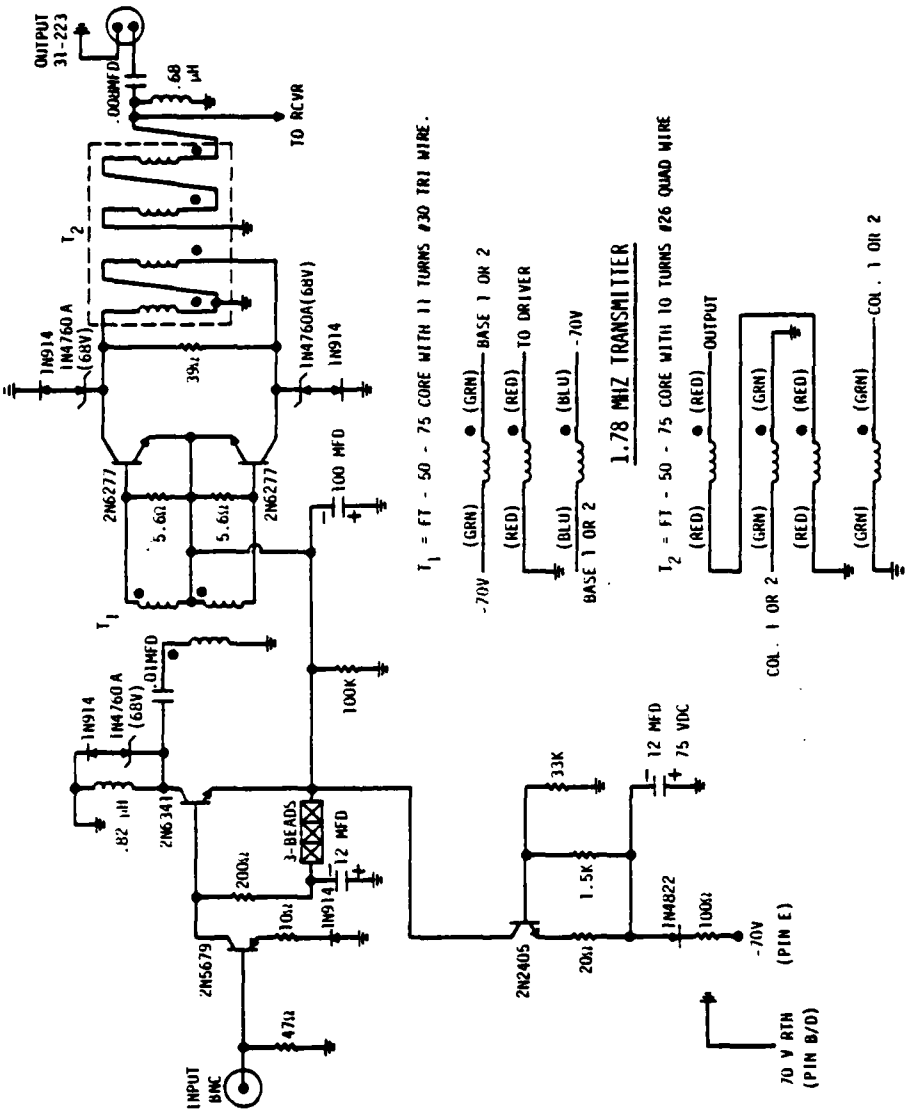

Fig. 6 Circuit diagram of a 1.8 MHz transmitter power amplifier module.

The amplifier is designed to operate at full rated output when driven by a digital level waveform such as shown in Fig. 5(b). The high power output is generated by switching energy stored in a capacitor through a pair of push-pull RF transistors with maximum peak current output of approximately 80 amperes. Heat sinking of the RF power stage is not required because the thermal time constant of the semiconductor substrates is shorter than the duration of the ultrasonic tone burst and because this type of amplifier configuration (class"C") features very high collector efficiencies. The output stage also includes Zener diodes to protect the power stage from secondary breakdown which can occur when the transmitting transducer is accidentally damaged. Typical current waveforms are shown in Fig. 7. The current waveform at the collector of one of the switching transistors is shown in Fig. 7(a) and the transducer current is shown in Fig. 7(b). The horizontal and vertical scales are 2μ-sec/div and 10 amperes/div in both photos.

The stand by power consumption of the amplifier is approximately 1 watt at a dc power supply voltage of 75 volts.

2. Linear Receiver Preamplifier

The low level ultrasonic signals detected by the receiving transducer must be preamplified before multiplexing in order to prevent degradation of their signal-to-noise ratio by the switching and transmission circuitry. A new linear preamplifier was designed for this purpose. In addition, a new impedance matching network using broadband transmission line transformers to minimize the noise figure of the linear receiver preamplifier and a new

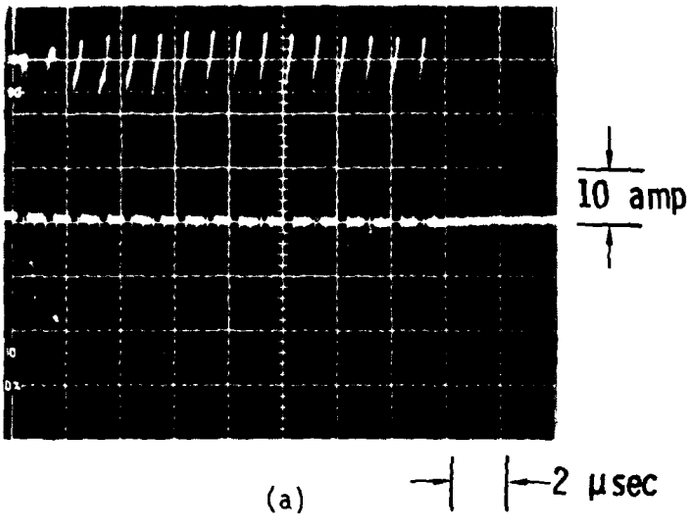

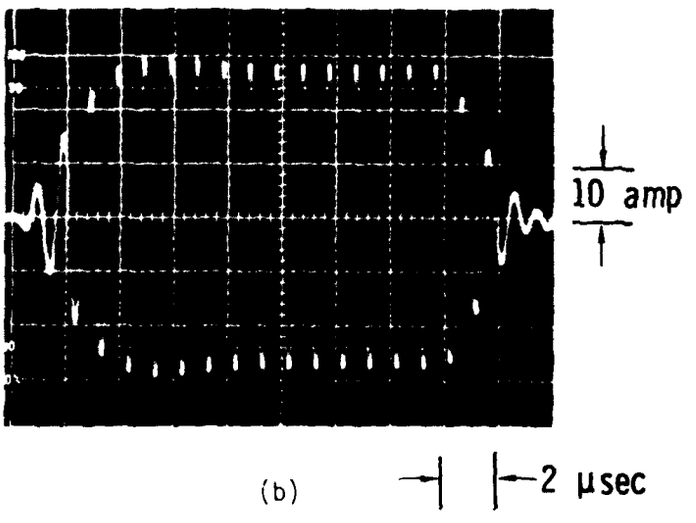

Fig. 7 Transmitter waveforms

transmit-receive switch to protect the receiver during transmission were developed.

A circuit diagram of the new receiver design and of the associated matching network and transmit-receive switch is shown in Fig. 8. The receiver uses N-channel FET transistors with diode limiters for overload protection. A standard +15V 1 watt power supply is required. Although the circuit diagram shown in Fig. 8 specifies component values for operation at approximately 1.8 MHz, operation at other frequencies is possible by readjusting the interstage tuning. The tuned circuits are intended primarily to improve the recovery characteristics of the preamplifier, and are sufficiently broadband to prevent phase distortion of the received ultrasonic signals. In this way, faithful reproduction of the received signals is achieved, thereby assuring proper operation of the correlation receiver which also serves as a filter. This feature of the system will be described in a following section.

The preamplifier does not contain an automatic gain control circuit except for the transmit-receive switch. Instead, the gain is fixed but can be manually adjusted over a range in excess of 80 dB. Measurements of typical signal levels on flat plates and actual M-549 projectiles indicate that the present design has sufficient linear dynamic range to assure undistorted reception of all ultrasonic signals. In fact, the amplifier is fairly linear over 80 dB which exceeds the expected maximum signal-to-noise ratio of the ultrasonic signals of approximately 70 dB. The latter figure can be arrived at by assuming an input RF power level of +60 dBM and conservatively allowing 10 dB for transducer coupling losses and a 4 dB noise figure for the preamplifier and correlation receiver combined with -124 dBM Johnson noise

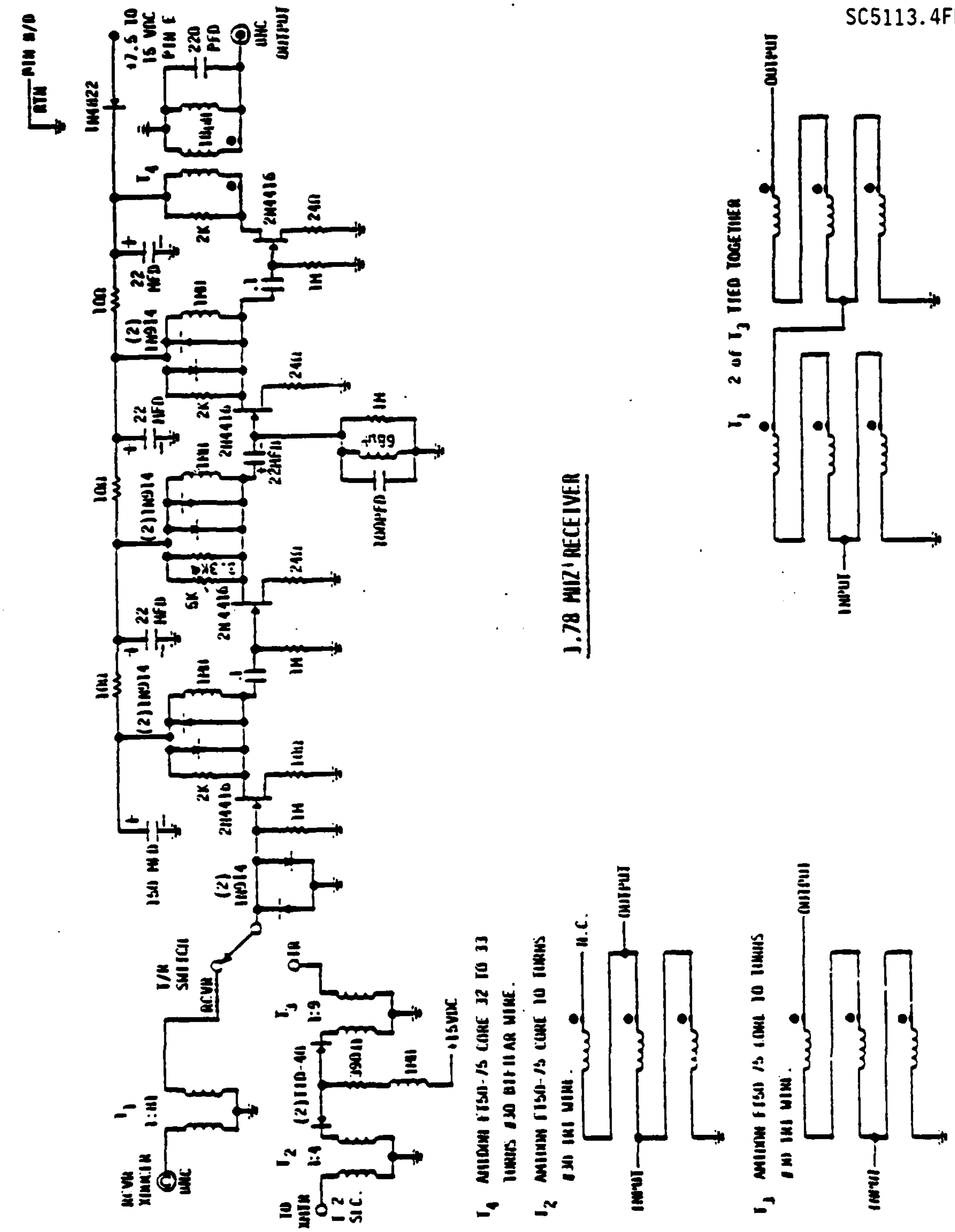

Fig. 8 Circuit diagram of a 1.8 MHz receiver preamplifier.

power in a 100 kHz bandwidth. This high linearity means that all signals from the weakest flaw echo to the strongest direct transmission, can be detected without clipping. This is an important property for use with a correlation receiver, as will be discussed below. Therefore, it is believed that the sensitivity of the present system is sufficient providing transducer efficiency is not impaired by unexpected materials effects.

3. Transmit-Receive Switch

When the same transducer is used for generation and reception of ultrasonic signals, the transmit-receive switch functions as a protective device which prevents damaging the sensitive receiver preamplifier by direct leakage from the transmitter.

A schematic diagram of the T/R circuit is included in Fig. 8. the device is located in close proximity to the receiver front end for maximum protection of the receiver. A pair of back-to-back "catch" diodes (TID-40) is employed to block transmitter currents. Another pair of diodes (1N-914), acting as a limiter, is used to provide additional damping and "cross-bar" protection on the input FET transistor. Further improvements are expected because the effectiveness of the transmit-receive switch is directly related to receiver recovery following a transmitter shutdown and, therefore, to the range resolution limits of the system.

The present design concept envisions the location of the transmit-receive electronics in close proximity to the transducer elements but outside the leakage fields of the electromagnet. The correlation receiver would be located near the central processor.

4. Correlation Receiver

The peak signal-to-noise ratio of RF signals of finite duration can be seriously degraded by the filtering characteristics of receiver amplifiers. In particular, it is difficult to design an amplifier for matched filtering of the triangularly shaped waveforms characteristic of ultrasonic inspection systems using electromagnetic transducers for generation and reception of ultrasonic signals. An alternative approach involves the use of time domain correlation which can result in matched filtering if the shape of the waveform and its time of arrival are known in advance. Both of the above requirements can be satisfied in this case because the distribution of the signal in time is known and complete coverage of the component is provided by scanning the projectile under the fixed transducer element, using a fixed range gate. In addition to its filtering characteristics, one of the major advantages of the correlation receiver is that time delay adjustments can be made electronically to compensate for variations in propagation delays of signals in different channels. Because of this, a single, digitally controlled correlation receiver is used to process the ultrasonic data from all ultrasonic channels.

In order to maximize the peak signal-to-noise ratio on reception, it is necessary that the receiver exhibit an impulse response which replicates the time reversed input waveform. Although such filters have the advantage of being time-invariant, they require unique hardware implementation for specific waveforms which is often impractical. If the range information is not required or is specified in advance, a simpler implementation is possible. One such approach, involving correlation with a time delayed replica of the

input signal, is illustrated in Fig. 9. In this implementation, the received ultrasonic signal, after preamplification is first multiplied by an appropriate reference waveform. The multiplier output is then intergrated and the output of the integrator is sampled by a sample-and-hold circuit. The output of the sample-and-hold circuit can be readily converted to digital format for further processing.

A two-channel correlation receiver is required when the exact phase relationship between the received ultrasonic signal and the reference waveform cannot be determined in advance. Although two-channel receivers exhibit a 3 dB noise figure degradation due to the presence of noise in both channels, their output is not sensitive to phase uncertainties in the received signal. A two-channel receiver functions as two separate receiver channels except that products of the input signal are formed by multiplication by in-phase (I) and quadrature (Q) reference waveforms. The total output of the receiver is then obtained by computing the square root of the sum of the squares of the I and the Q channel outputs. Because of its obvious advantages, this receiver configuration has been included in the proposed ultrasonic signal processing scheme of Fig. 5.

Recent advances in integrated circuit multipliers have made it possible to design such a correlator for real time use. A general design has been developed as a part of the Rockwell IR&D program, and a specific embodiment has been assembled as a part of this program. Because the design has not yet been finalized, the publication of a detailed circuit diagram is not deemed appropriate at this time. A photo of the receiver breadboard is shown in Fig. 12.

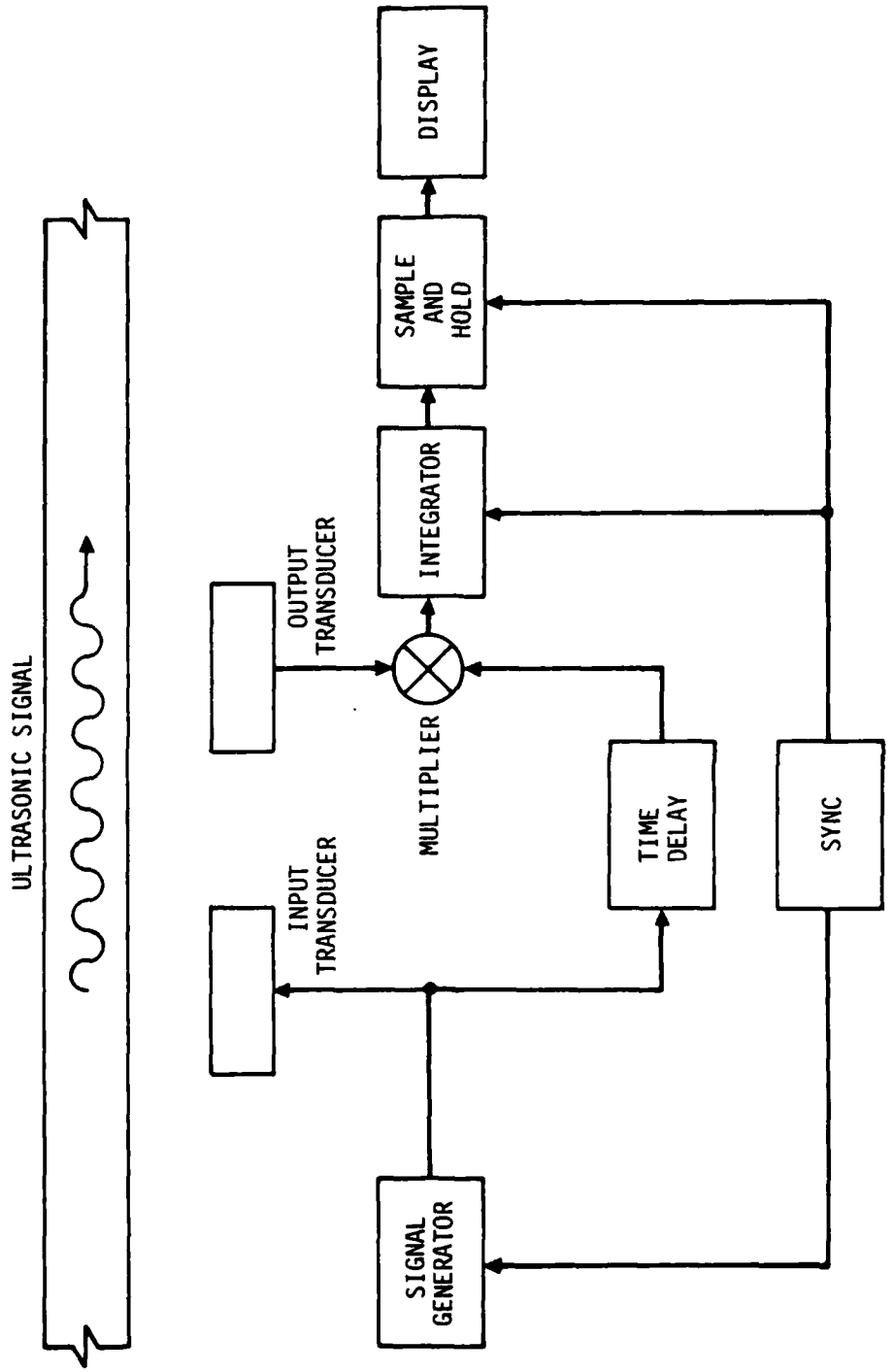

Fig. 9 Functional block diagram of a correlation receiver using a timed delayed replica of the input signal to demodulate the received ultrasonic signal.

The results of preliminary tests of the receiver response linearity are summarized in Fig. 10 for a combination of two reference voltages (5 and 10 V peak-to-peak) and integrator time constants. The carrier frequency and pulse duration in these experiments were 500 kHz and 12 microseconds, respectively. Typical waveforms observed at the input and output of the multiplier circuit are illustrated by the lower and the upper photos in Fig. 11. The horizontal time scale is 5 microseconds per division.

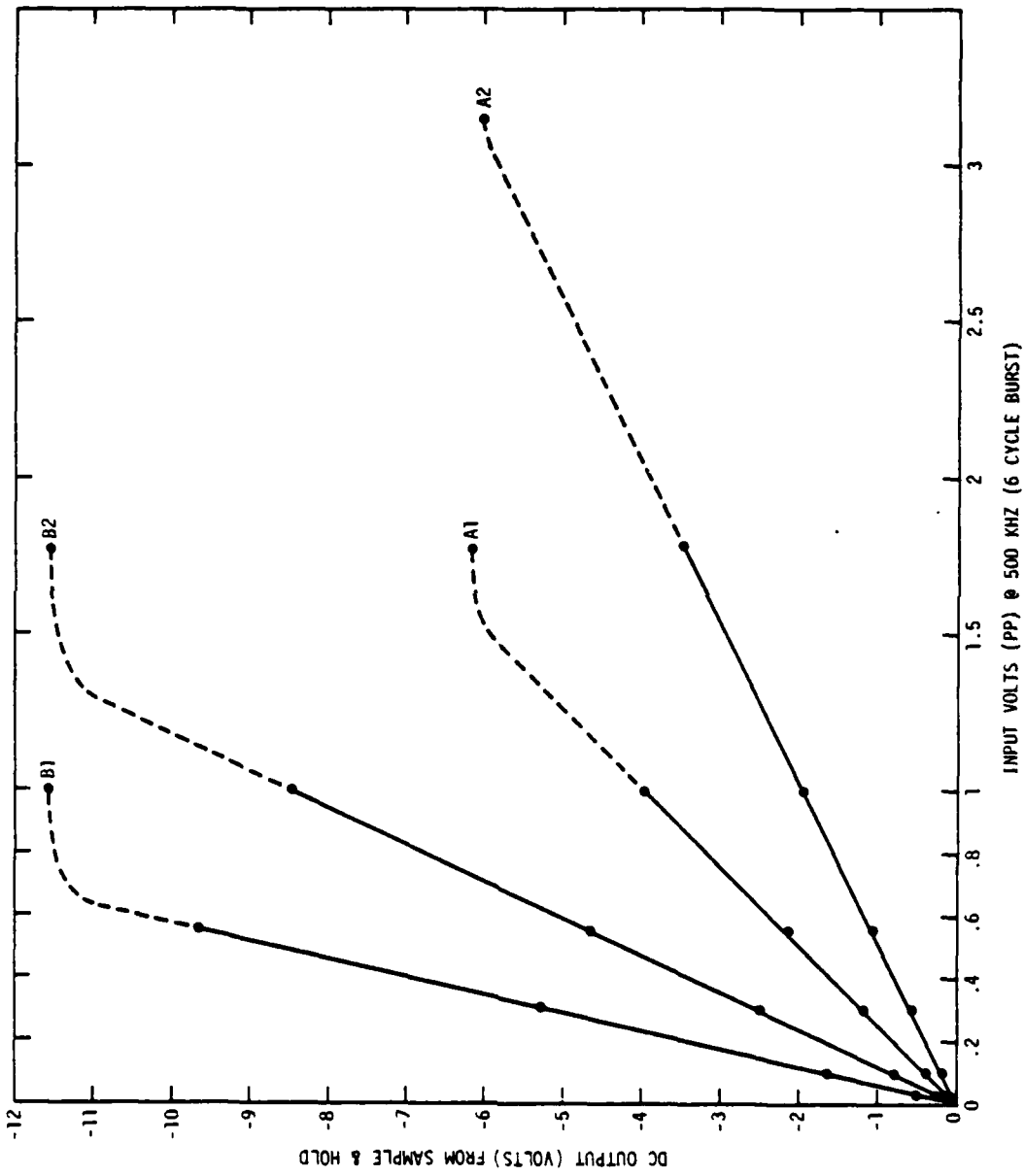

Fig. 10 Correlation receiver response for different integration time constants.

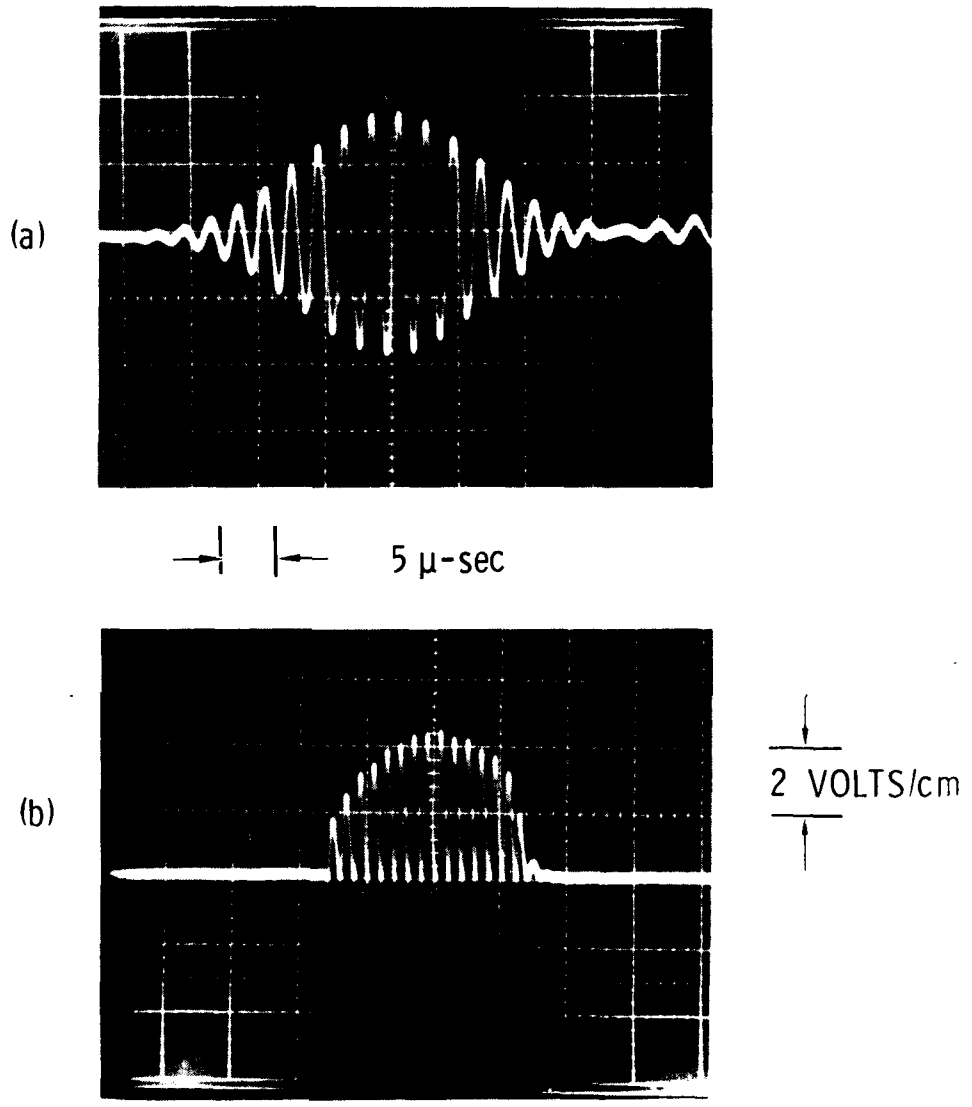

Fig. 11 Typical waveform observed at the (a) input and (b) output of the multiplier circuits at 500 KHz.

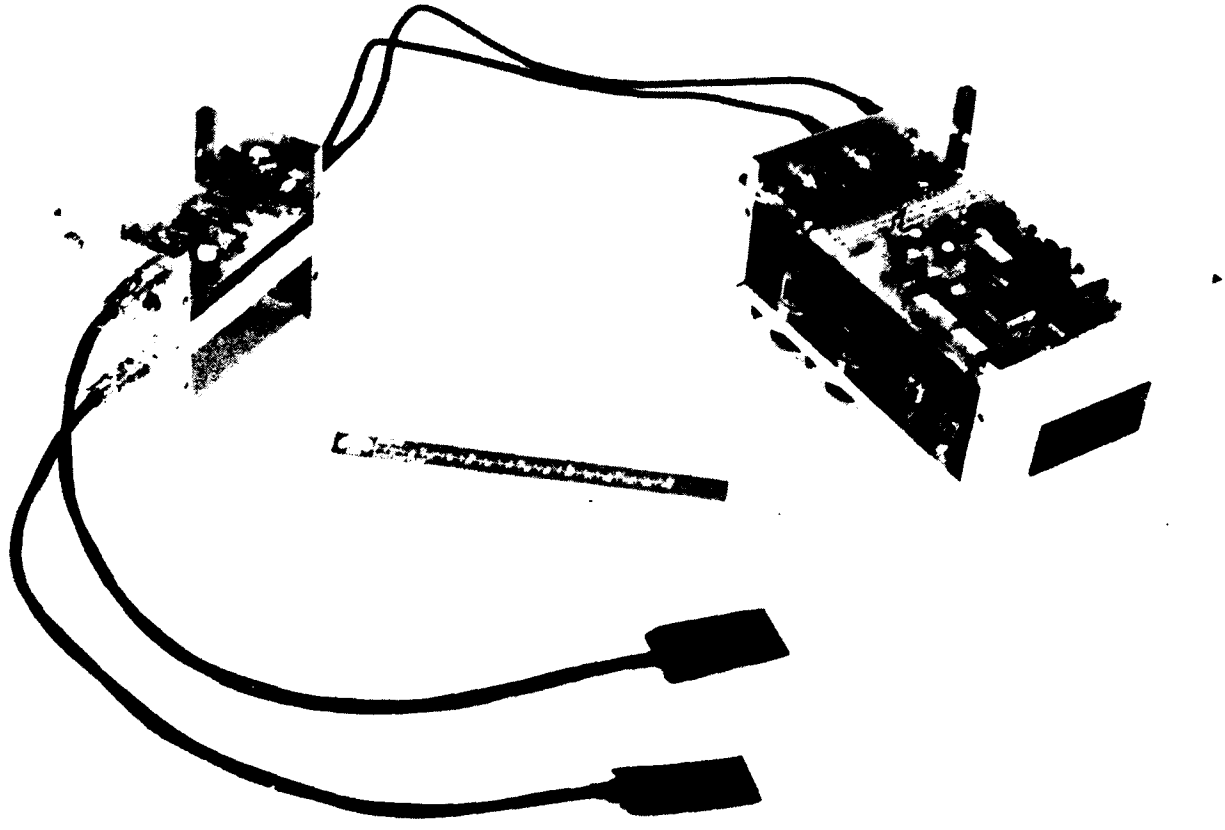

Fig. 12 Photograph of a single channel receiver breadboard.

C. Electromagnet Design and Fabrication

1. Principles

This section describes the design principles and construction details of the new electromagnet for providing a nearly uniform magnetic bias throughout the M-549 projectile. This arrangement eliminates the need for separate electromagnets for each transducer and results in a simple inspection configuration. The magnetic bias configuration for inspecting the periphery of the M-549 projectile is shown in Fig. 13. The main advantage of the inspection configuration illustrated in Fig. 13 is that electromagnetic transducer elements can be placed anywhere on the periphery of the projectile in the ogive and bourrelet. Additional transducer elements for inspecting the base region will be biased by the leakage fields shunted through the base.

Two distinctly different magnetic bias configurations are possible. The electromagnetic transducer elements can be placed either in the air gap separating the projectile from the pole pieces of the electromagnet or above the projectile as illustrated in Fig. 13. Transducers placed directly in the air gap operate in near normal magnetic fields, and, therefore, can be pointed in any direction. On the other hand, transducers placed as illustrated in Fig. 13 can only be pointed along the lines of magnetic flux which follow the circumference of the projectile.

The placement of the transducers outside the air gap is advantageous because ample space exists for multiple transducers in all sections of the projectile. This is an important consideration since additional transducers

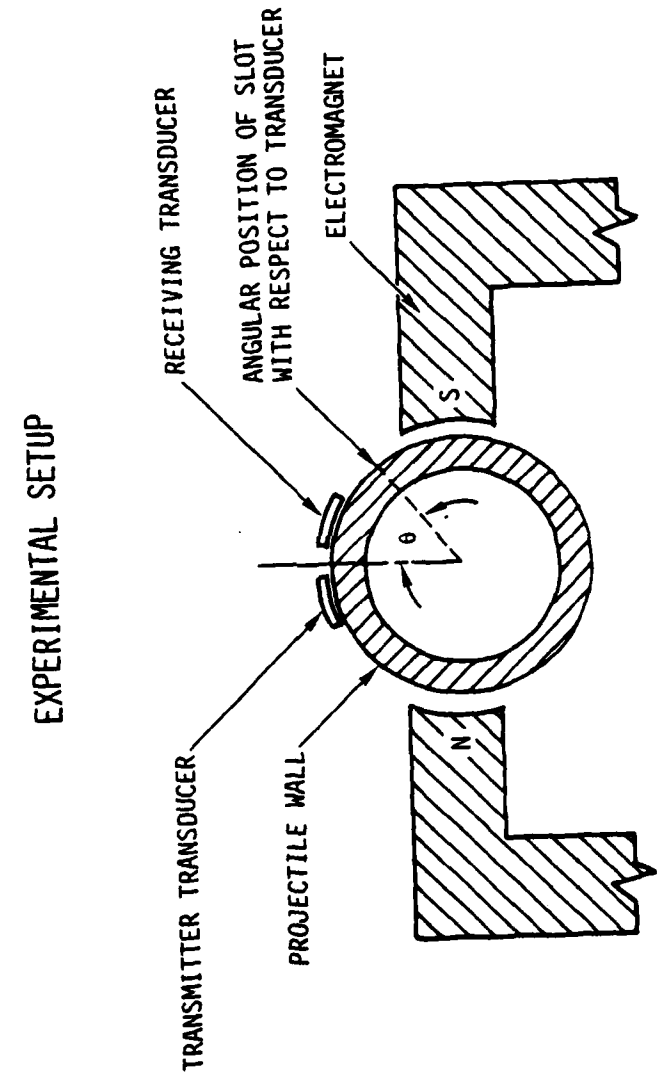

Fig. 13 Magnet configuration for inspecting the M-549 projectile.

may be needed to provide expanded scattering data bases for improved defect characterization.

In the present inspection scheme as outlined in Fig. 13, considerable economies in electric power requirements as well as improved magnet switching times can be realized by adjusting the magnitude of the static magnetic field bias for maximum magnetostrictive transduction efficiencies of electromagnetic transducers placed outside the air gap. It has been determined experimentally as shown in Fig. 2, that the optimum ultrasonic signal strength for a low carbon steel with a ferrite structure is obtained when the tangential magnetic field is in the range 150 Oe< H < 450 Oe at the surface of the projectile and directly beneath the electromagnetic transducer. The magnetostrictive enhancement process is not present when the electromagnet transducer is biased in a nearly normal magnetic field. However, a comparable level of efficiency can be attained by maintaining the magnetic flux density in the air gap in the range 6-10 kG.

Measurements of electromagnetic transducer conversion efficiencies show that strong magnetostrictive enhancement processes also exist in the martensitic HF-1 steel used in the M-549 projectile, but that their magnitude can be dependent on the metallurgical conditions near the surfaces. In particular, it has been determined that a thin decarburized layer can exist at the exterior surfaces of some projectiles and that its presence can lead to a significant reduction in transducer efficiencies. However, this reduction does not appear to extend to the normal field case.

Measurements of transducer generation efficiencies have been carried out in the presence and absence of decarburization on actual M-549 projectiles using 1.8 MHz shear waves launched at approximately 30^{o} with respect to surface normal. The relative dependence of the transducer conversion efficiency on applied parallel magnetic field is shown in Fig. 14. The upper trace shows the existence of a broad maximum in the conversion efficiency as measured on an M-549 projectile which was machined to remove the decarburized layer. A peak in the maximum is observed at approximately 400 Oe level in this measurement, although routine measurements on most projectiles indicate a somewhat lower optimum field level. The lower trace shows the measured transducer conversion efficiency prior to the removal of the decarburized layer.

Two features of the lower curve are significant in comparison to the upper curve. First, the presence of a decarburized layer can be associated with an approximately 25 dB degradation in transducer efficiency. Second, the position of the maximum in the transducer efficiency curve is shifted by approximately 400 Oe in favor of the decarburized sample. The exact nature of the above effects is not fully understood at this time and will become the subject for a further study.

Another feature of the data presented in Fig. 14 is that the transducer efficiency at high bias fields appears to be significantly lower than that of the bias levels for maximum magnetostriction in contrast to the results shown in Fig. 2. This effect is well understood and can be explained in terms of the direction of the dominant driving stresses at the surface of the projectile beneath the transducer. In fact, theoretical calculations

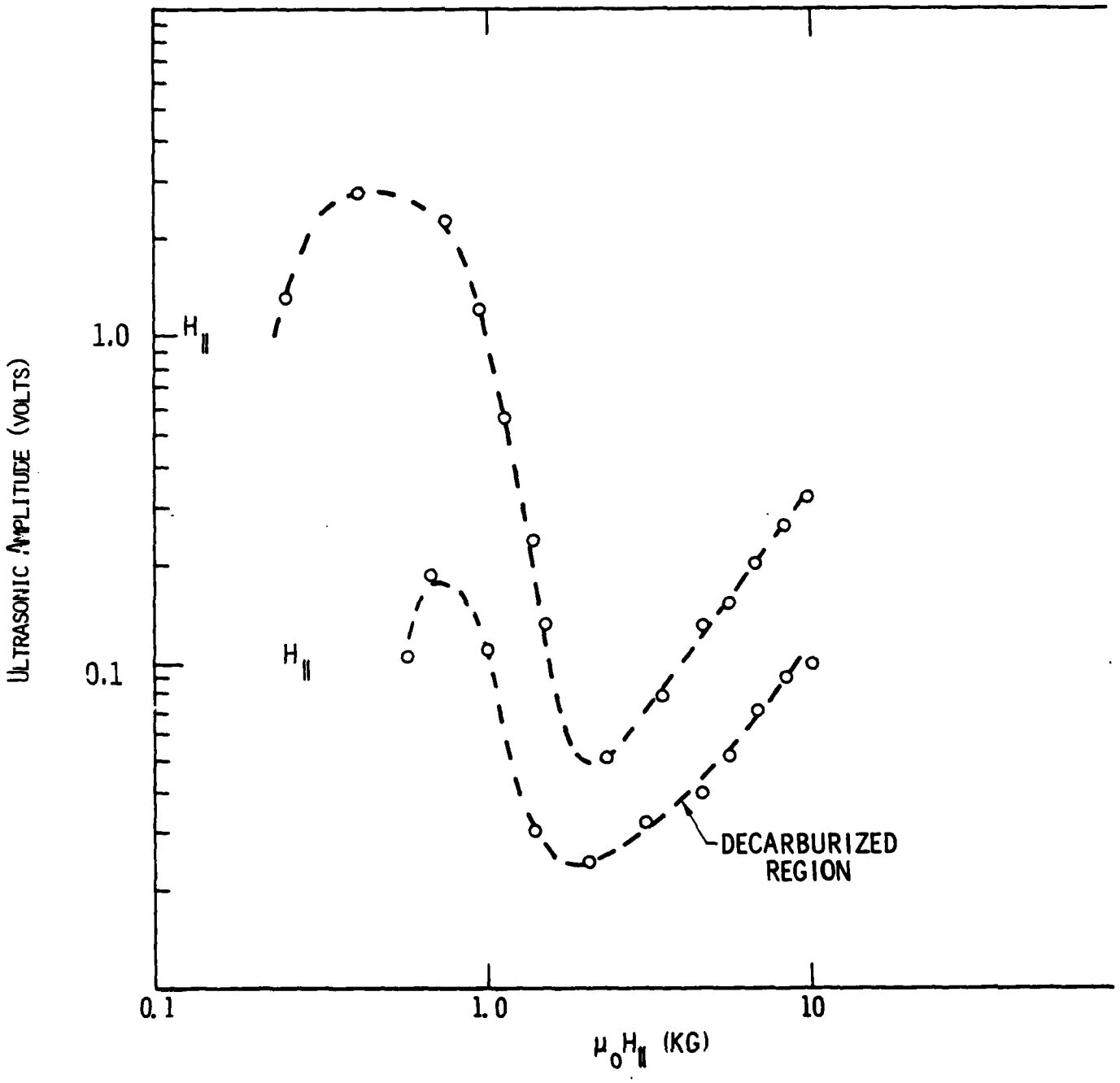

Fig. 14 Relative dependence of transducer generation efficiency on parallel magnetic field in the presence and absence of decarburization.

confirmed by experimental evidence show that under these particular conditions, no generation should occur when the bias field is parallel to the surface. The observed nonzero generation efficiency can be explained by the presence of leakage fields and the finite length of the transducer and projectile wall thickness.

Experimental studies have shown that magnetostrictive effects are not present under normal magnetic field bias and in that this configuration the transducer efficiencies are not sensitive to decarburization and the transduction efficiencies increase monotonically with the magnetic field as predicted by the Lorentz force excitation model. The received ultrasonic signal strength is primarily sensitive to changes in material bulk resistivity and does not exhibit large variations.

The use of normal magnetic field biases has not been fully evaluated and as such, has not been considered for inspection of the M-549 projectile because of obvious limitations associated with this bias, e.g. 1) positioning of transducer would be restricted to the gap between the pole pieces and the projectile, thus limiting system versatility and resulting in a significantly more complicated transducer-tracking device, 2) it would become more difficult to maintain a sufficiently large magnetic field over the entire portion of the projectile surface area, 3) large normal fields would greatly increase electric power consumption requirements, and 4) the generic applicability of EMAT inspection associated with magnetostrictive enhancement would not be demonstrated.

The full implications of the decarburization problem and proposed solutions will be described in detail in Section VI. For the purpose of the remainder of this section, it will be assumed that one of the remedies

proposed therein has been implemented so that advantage can be taken of the strong magnetostrictive peak illustrated in Fig. 2.

2. Improvements in Electromagnet Design and Construction

Under the current phase of this program, a new electromagnet was designed and constructed for magnetizing the entire M-549 projectile to a nearly uniform level. The new design incorporates several improvements over the previous design which proved to be deficient in a number of ways.

A new analytical model was developed utilizing a more complete understanding of magnetic non-linear behavior as well as experimental results from measurements on scale models and the previous magnet. Previously, it was recognized that the magnetic reluctance would vary along the axis due to the complex shape and non-uniform distribution of metal within the projectile, but is was erroneously assumed that the flux within the yoke of the electromagnet would readjust itself to produce a nearly uniform magnetization of the projectile. In fact, the first electromagnet provided a highly non-uniform field distribution because excess flux was concentrated in the nose and not enough flux was available at the base of the projectile.(1) It was realized that this problem could be overcome by varying the thickness of the pole pieces so as to balance the variation in the flux distribution along the axis of the projectile. In addition, it was decided that the new electromagnet should be laminated in order to improve magnet switching speeds and make them compatible with expected transit times of one projectile through the ultrasonic inspection station. In this regard, it was estimated that a

switching delay to eddy currents should be approximately one second, since it would constitute less than 10% of the total time required for the passage of one projectile through the system.

A major requirement of the analytical model of the magnetic biasing structure was that it should predict the approximate shape of the magnet pole pieces which would place the entire projectile at the magnetic bias level needed for maximizing the magnetostrictive enhancement of the transduction efficiency. In addition, the magnetic structure was required to provide a sufficiently high magnetic flux density (6-10 KG) in the air gap separating the walls of the projectiles from the pole pieces to insure that the efficiencies of transducers biased by the nearly normal magnetic fields be comparable to the transduction efficiencies of transducers placed outside the air gaps.

The electromagnet designed during the previous feasibility study did not meet the above requirements and current drive levels had to be readjusted depending on the position of the transducer in order to obtain maximum transduction efficiencies. During the current phase of the program, these deficiencies were overcome largely through the development of an improved analytical model and experiments performed on ¼ scale models.

Figure 15 shows the results of flux density measurements made on a scale model of the projectile which neglected the tapering in the ogive region. The existence of the taper carries fields to higher levels in the real magnet at the nose. However, this effect can be easily compensated for by thinning of the final pole pieces or by increasing the air gap width. The principal objective of this study was to evaluate the magnetic flux densities

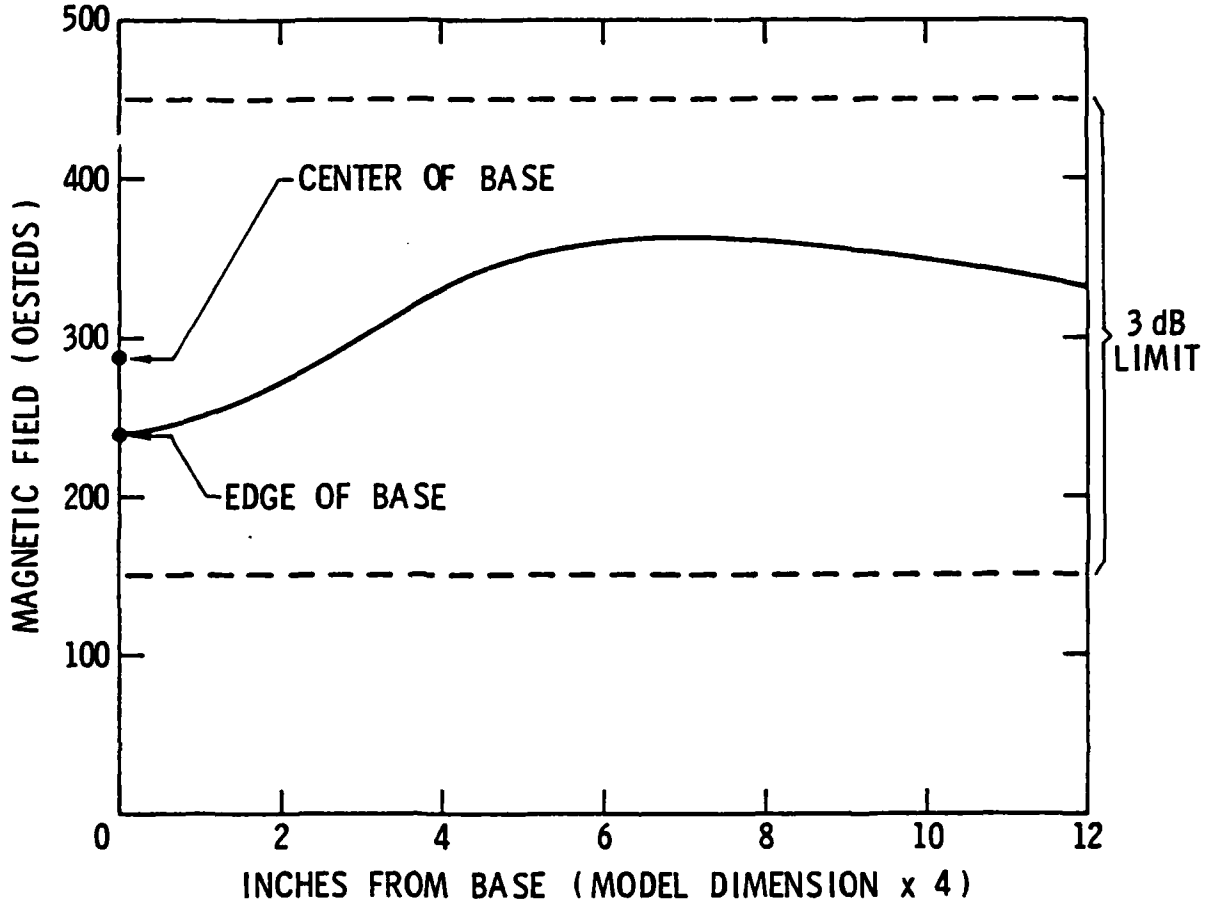

Fig. 15 Tangential magnetic field as measured in a ½ scale model of the M-549 projectile. The projectile model neglected the tapering in the ogive.

in the base region which is difficult to predict analytically. The results show that the magnetic flux densities vary from 240 to 265 Oe along the sides of the model and from 240 to 365 Oe at the base. The normal flux density in the air gap ranges from 6 kG at the nose to 8 kG at the base. This higher flux level at the base can be explained by lower reluctance due to a higher concentration of magnetic metal. Thus, it should be expected that magnetostrictive transduction efficiencies should vary no more than 3 dB along the scale model and that sufficient flux densities could be established in the air gaps to produce normal field excitation of comparable efficiency.

Based on these results, a new electromagnet was constructed as shown in Figs. 16 and 17. The key features of this design include: (1) a tapered construction of the electromagnet pole piece to provide more magnetic flux at the base of the M-549 projectile where the magnetic reluctance of the shell is the lowest, (2) a split coil construction with the segments located on either side of the projectile to minimize magnetic leakage, and (3) a laminated electromagnet yoke with one-quarter inch sections to reduce eddy current effects and increase the switching speed of the magnet. Each coil consists of approximately 250 turns of copper conductor with a square cross-sectional area of 0.25cm^2 (0.010 in^2). An air gap of approximately .64cm (¼ in) has been allowed on each side of the projectile to provide ample space for the transducer coils which require normal field biasing.

Another novel feature of the electromagnet construction involves air cooling of the coils. It is believed that sufficient cooling of the coils can be provided by free air flow through the air spaces provided between

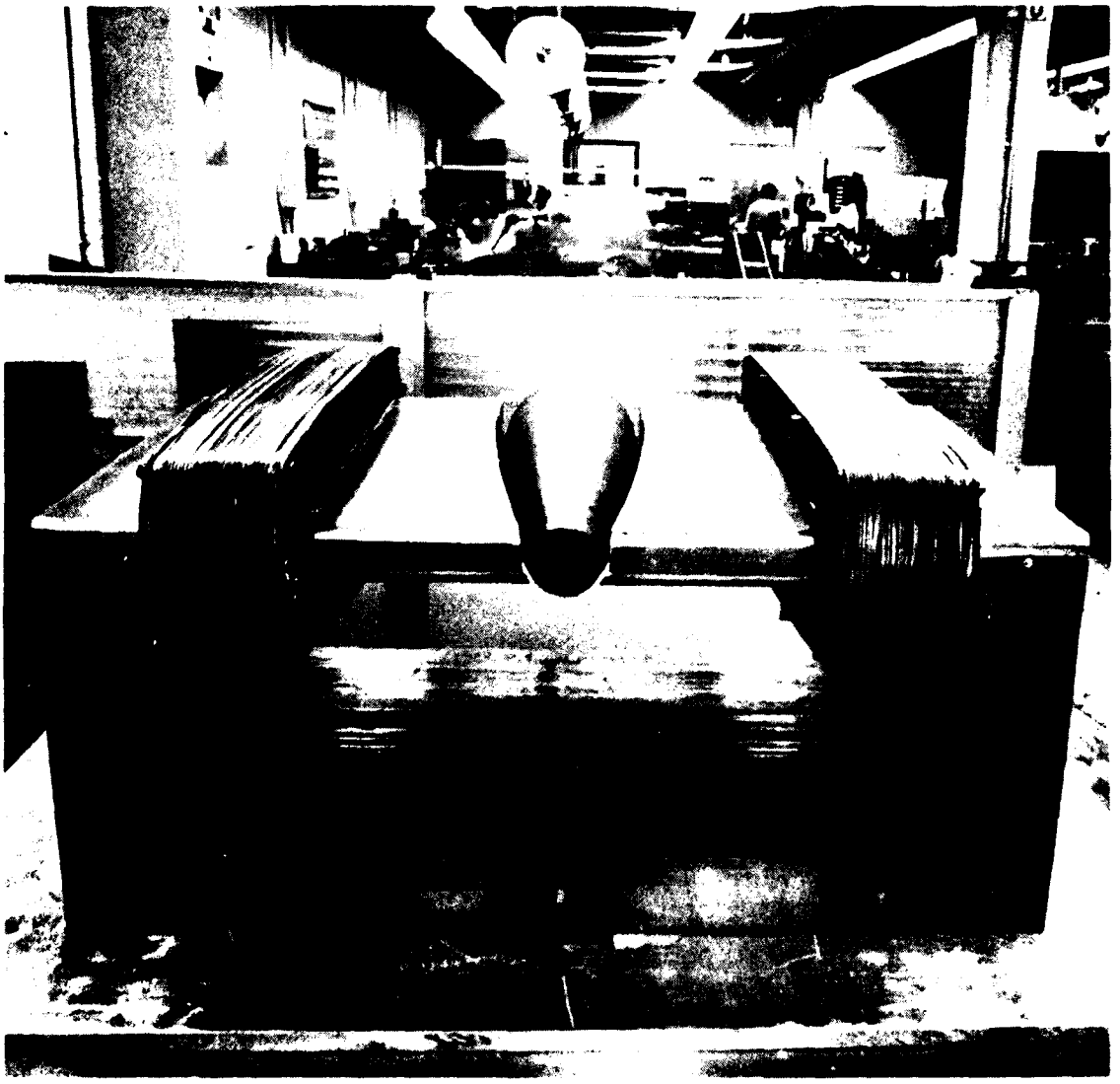

Fig. 16 End view of the electromagnet showing a M-549 projectile between the pole pieces.

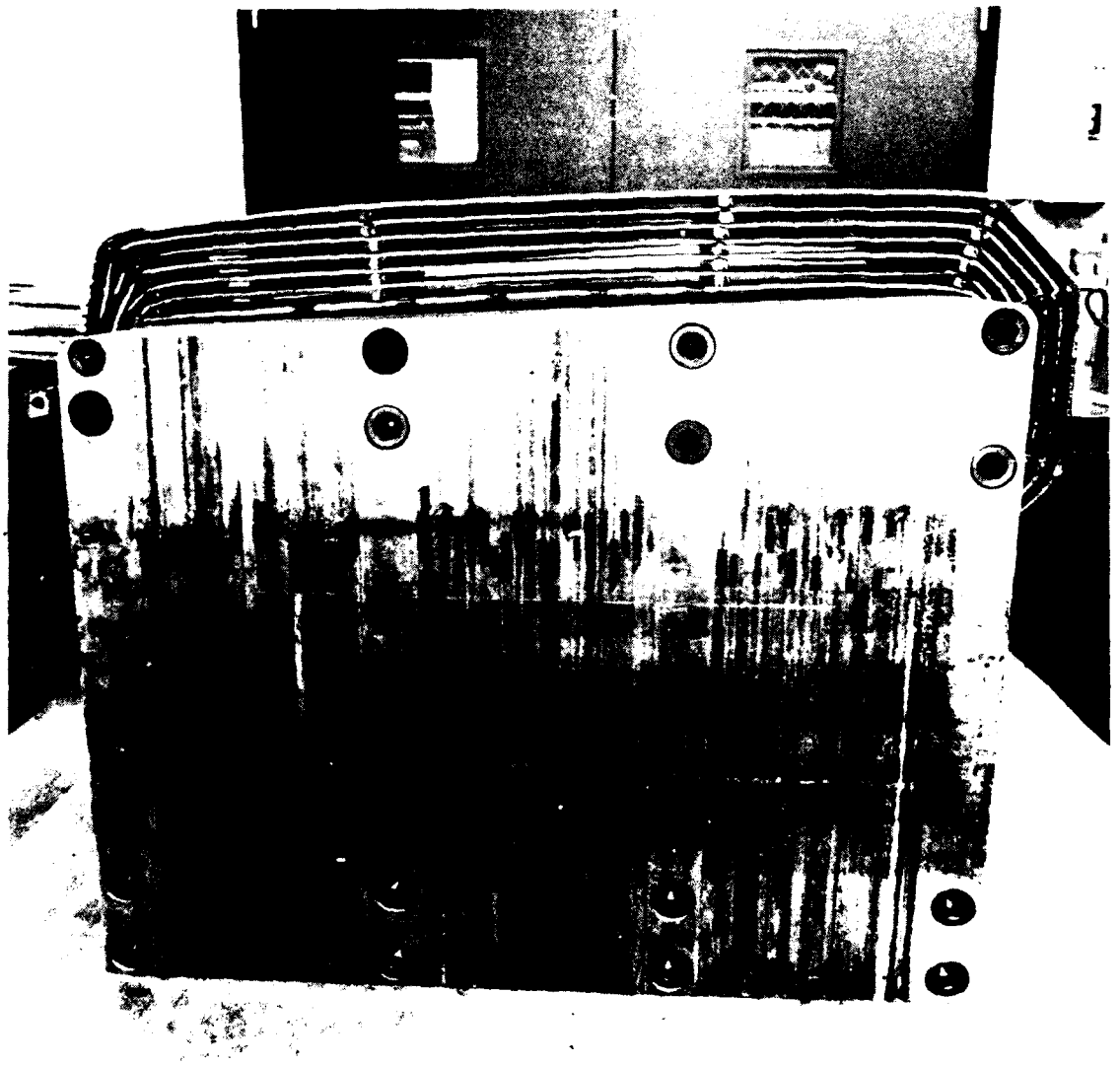

Fig. 17 Side view of electromagnet showing details of yoke laminations and coil design.

individual layers and forced air cooling will not be necessary when the magnetic fields are switched on and off for 30% of the time as required to inspect one projectile. The present power consumption based on continuous duty operation is approximately 1500 watts at 28 amperes. This can be reduced by approximately 75% to 375 watts, assuming a 30% duty cycle.

A provision will be included in the power supply design to minimize residual magnetization of the projectile due to hystersis effects after switching off the coil current. This can be accomplished by the inclusion of a suitable field sensing device in the air gap which would be part of a feedback system connected to the power supply. The inclusion of this device would reduce wear on the projectile handling machinery by eliminating residual magnetic forces.

Figures 18, 19, 20 and 21 summarize the measured magnetic flux density profiles along the walls and at the center of the base of the M-549 projectile as a function of coil drive current. In particular, Figs. 18 and 19 show the tangential flux density profiles at the top and the bottom of the M-549 projectile. The non-linear dependence of the flux density profiles in the magnet upon the drive current is clearly evident. In particular, it is seen from Figs. 18 and 19 that a magnetization level of approximately 200 Oe is present at the base of the projectile at approximately 28 amperes of magnet coil current. However, the magnetic flux densities in the ogive region exceed 450 Oe with a maximum flux density at the nose of approximately 900 Oe. These

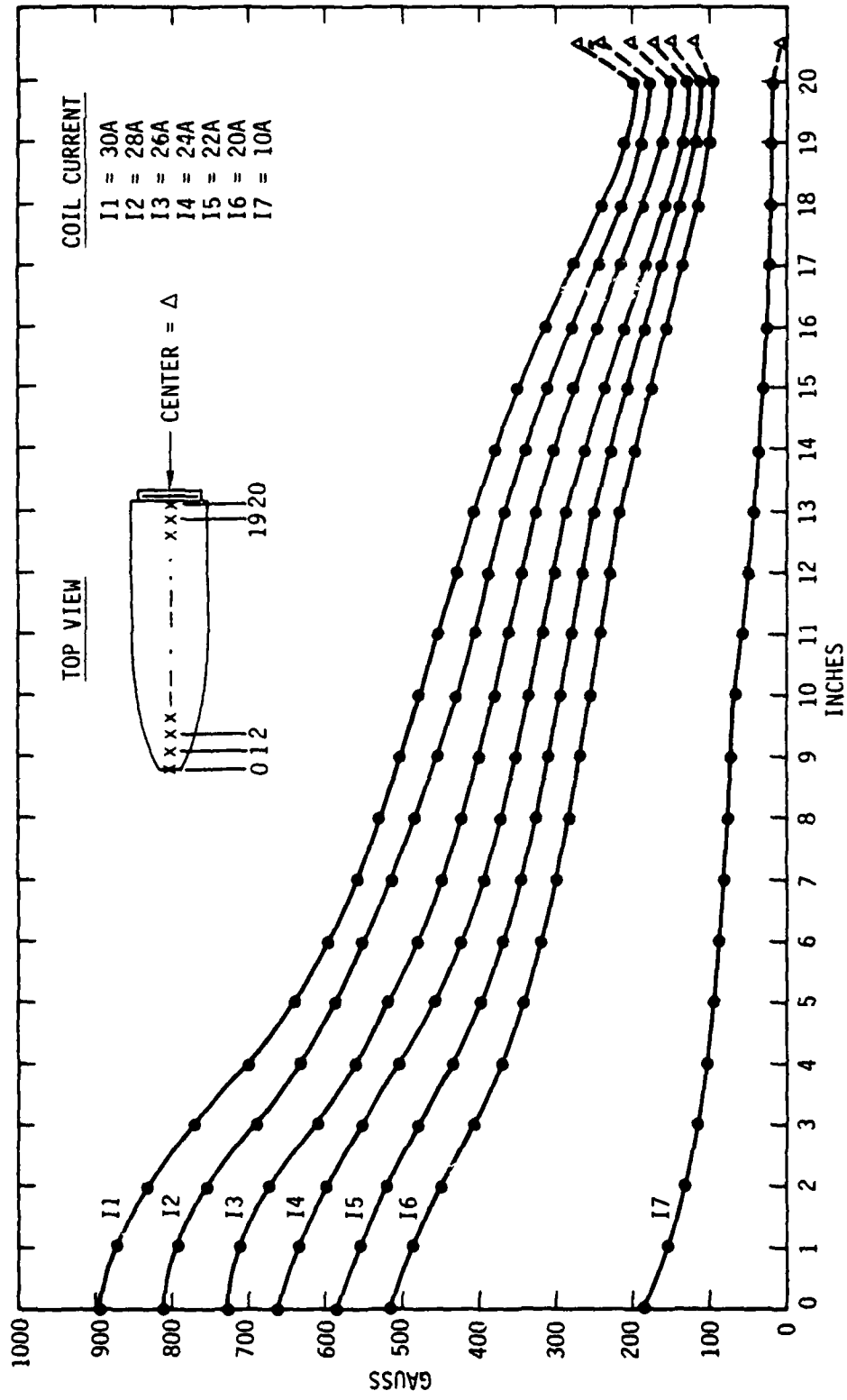

Fig. 18 Tangential magnetic field profile at the top of a M-549 projectile as a function of magnet coil current.

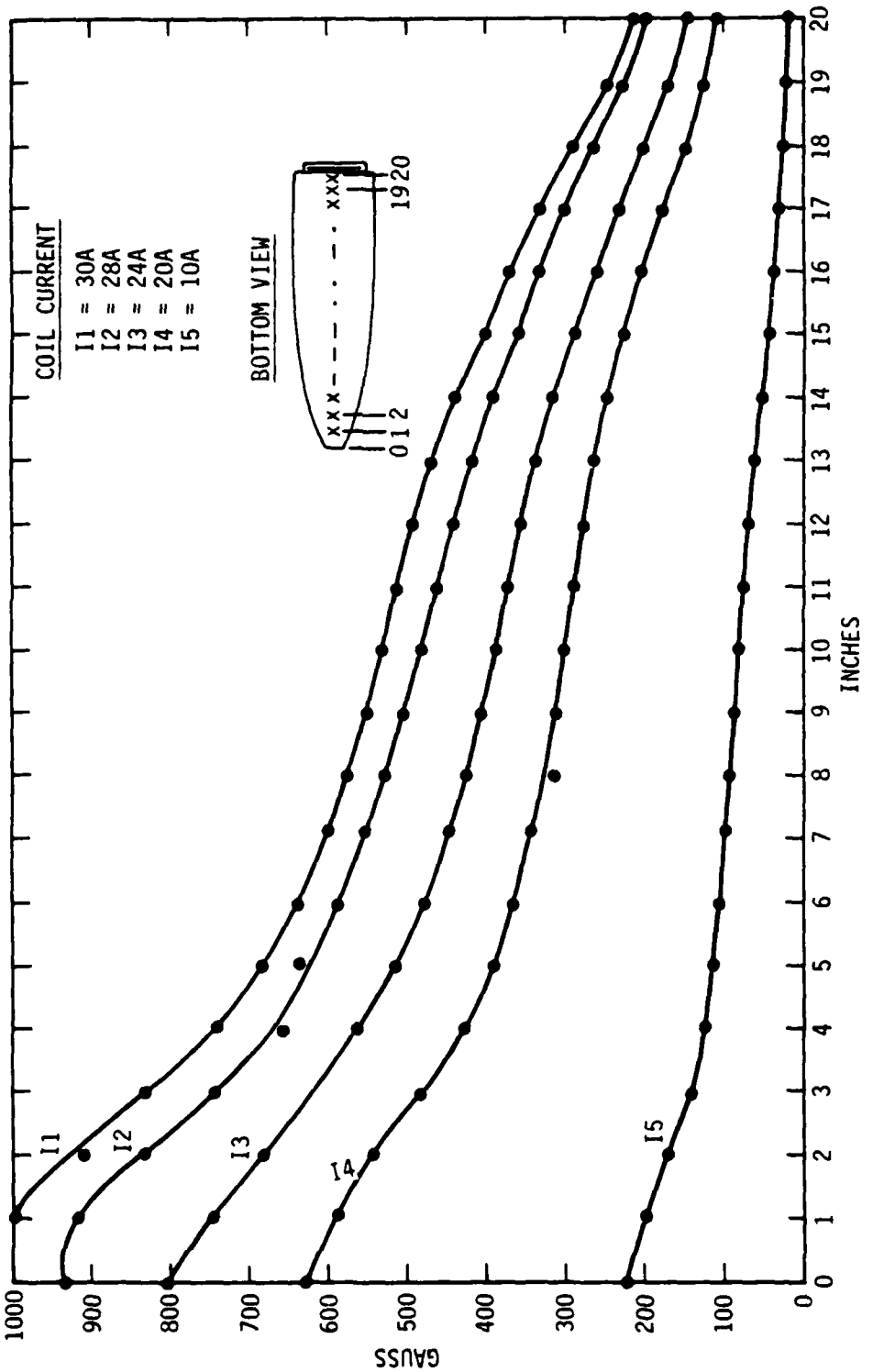

Fig. 19 Tangential magnetic field profile at the bottom of a M-549 projectile as a function of magnet coil current.

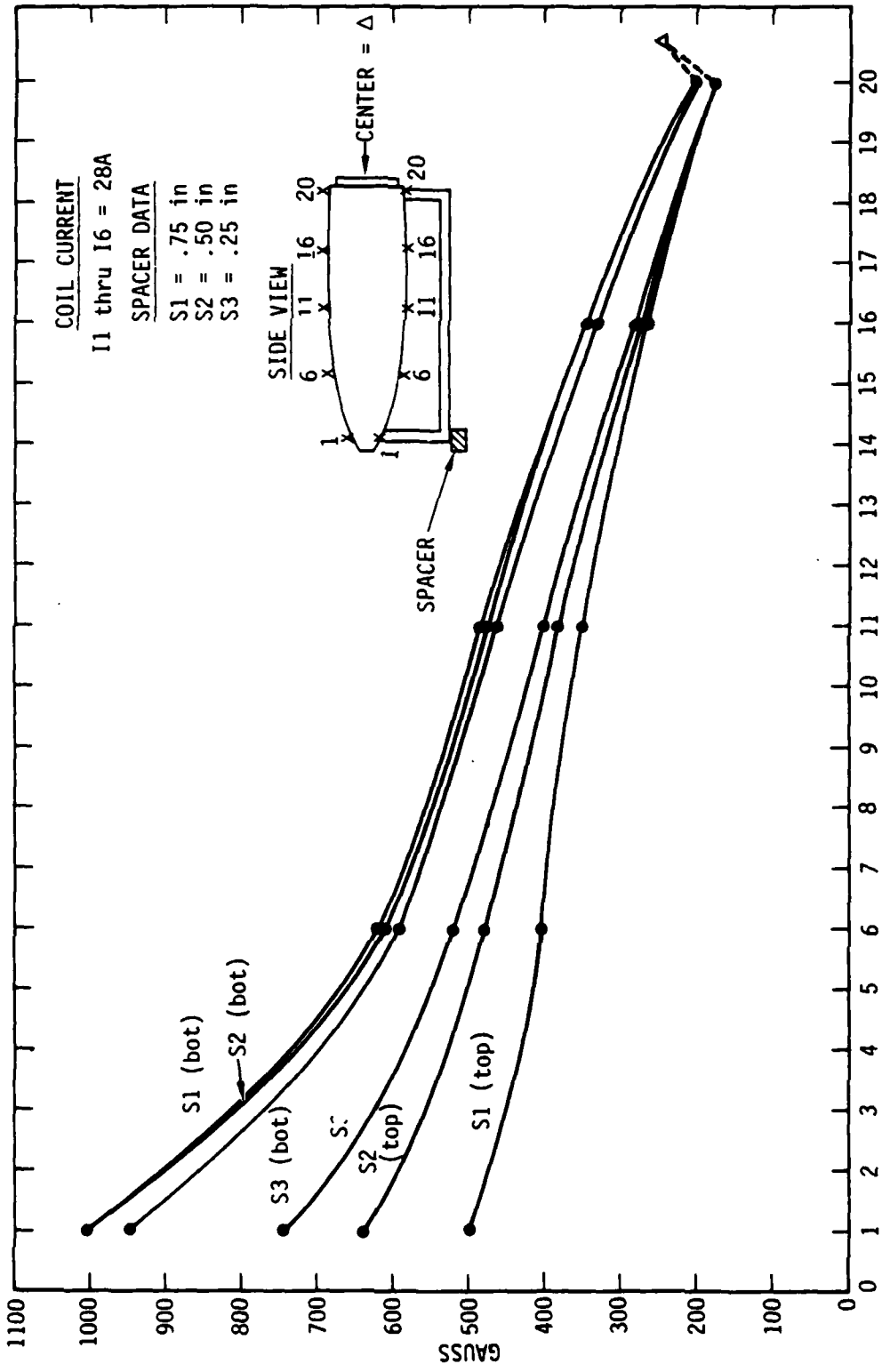

Fig. 20 Simulation of the effect of increasing the air Gap width by raising the nose of the M-549 projectile in the magnet by means of spacers.

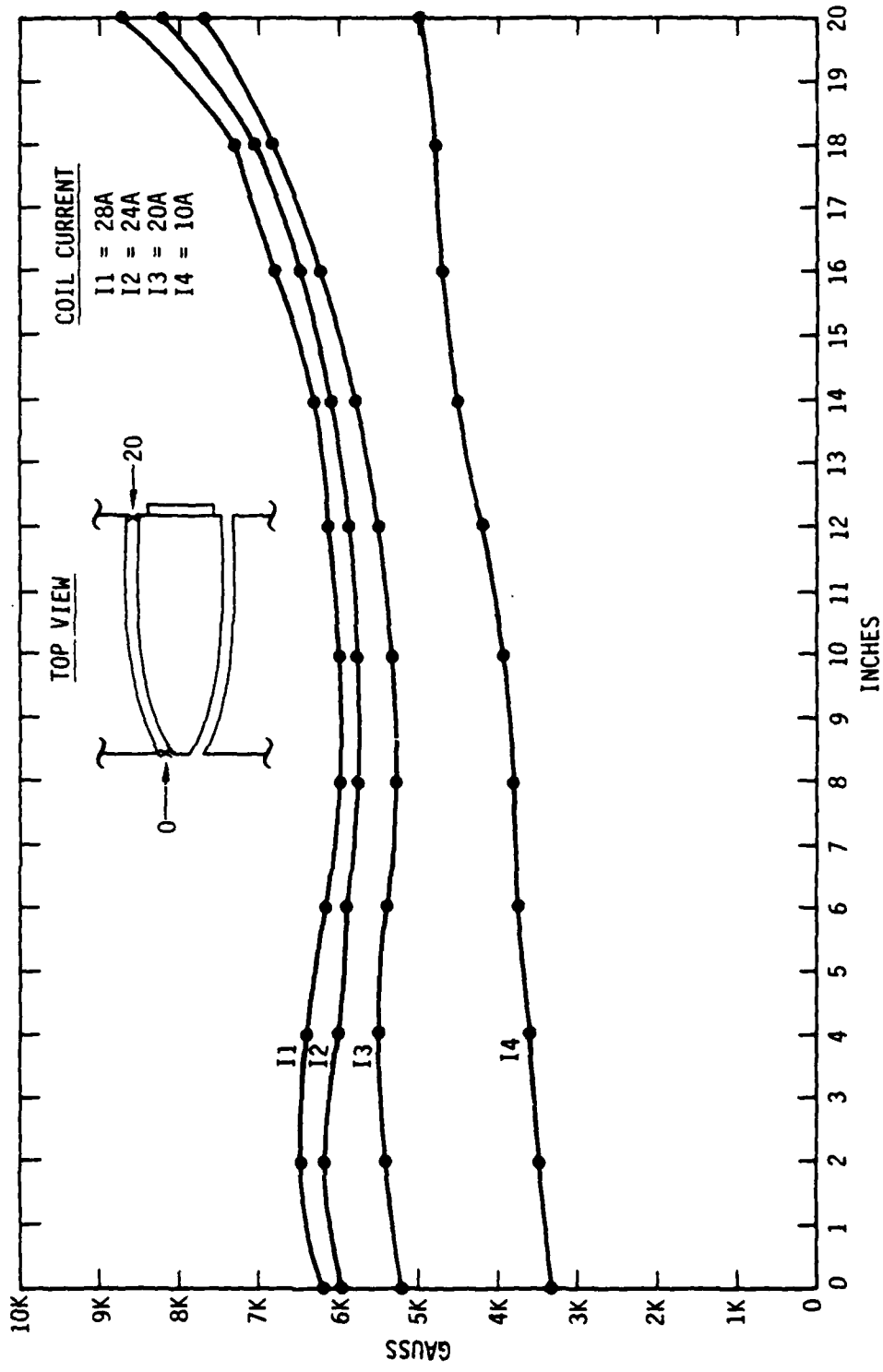

Fig. 21 Normal magnetic field profile in the air gap as a function of magnet coil current.

results were expected from initial analytical estimates and it is believed that the field profile in the ogive region can be easily trimmed by selectively increasing the magnetic reluctance of the yoke at the nose of the projectile. For example, increasing the air gap from ¼ inch to ½ inch at the nose should reduce the near parallel magnetic field level from 900 Oe to approximately 450 Oe, so as to bring the entire projectile within the ±3 dB transducer efficiency limits for magnetostrictive excitation.

The effect of widening the air gap at the nose can be simulated experimentally by raising the nose of the projectile above the normal position by means of a spacer. The results of this experiment are summarized by Fig. 20, which clearly illustrates the dramatic reduction in the field intensity at the nose of the projectile while showing only a modest decrease at the base.

Finally, measurements were made of the near-normal magnetic flux density in the air gap as a function of magnet coil current. The measured field levels, as shown in Fig. 21, fall between 6 and 10 kG which should be sufficient to insure adequate normal field magnetic bias for transducers placed in the air gap. In summary, it is believed that the present electromagnet design is satisfactory from the expected performance point of view. The necessary adjustments of the magnetic field profile will be carried out during the succeeding phase of this program.

D. Projectile Handling Machine Design

1. General Description

One of the major tasks of this program was to design a fully automated system that would remove 155mm M-549 (RAP) projectiles from the production line at Norris Industries, Vernon, California, manipulate these projectiles through an EMAT inspection station and, when acceptance criteria were met, position each back on the production line. This task, performed under subcontract by K.J. Law Associates, Inc., Farmington Hills, Michigan, is complete and includes a total of 59 fabrication drawings that describe in detail the design of the handling system. Major components and functions of this system are described below.

The entire inspection system, shown as a block diagram in Fig. 22, consists of 8 individual stations, each of which performs a specific task. The function of the handling machine itself is simply to carry each projectile through this series of stations. A section of this handling machine is shown in Fig. 23 schematically illustrating major components. The transfer of projectiles occurs by a walking-beam movement which simulates a closed square-wave as shown in Fig. 23. Specifically, projectiles, horizontally held in V-blocks at each station, are lifted by a hydraulically activated bell-crank that lifts the walking beam which then contacts projectiles and lifts them above the V-blocks. The walking beam is then hydraulically translated 18 inches downstream and is lowered thus locating each projectile one position further through the inspection system. The walking beam, now free of projectiles, translates 18 inches upstream to its original position ready to repeat this same motion.

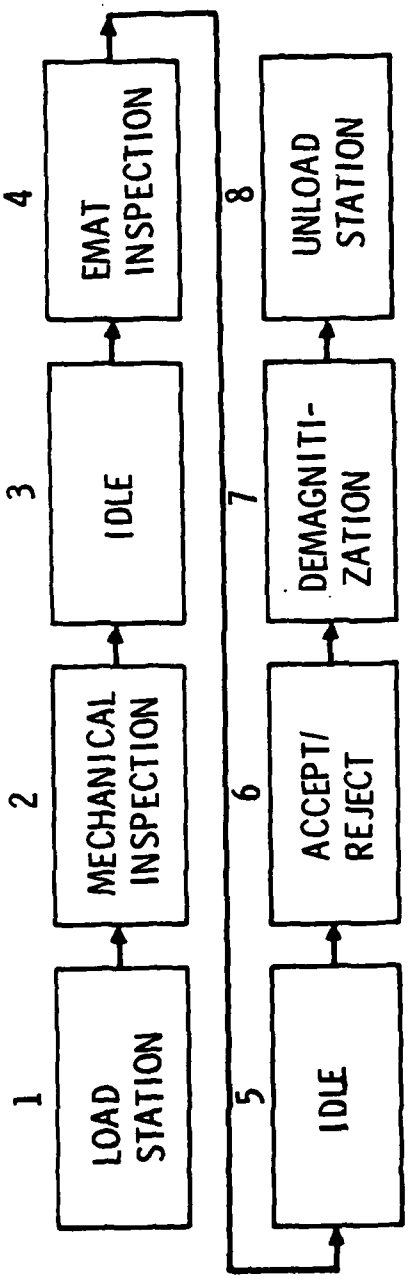

Fig. 22 Stations proposed for the EMAT ultrasonic inspection system.

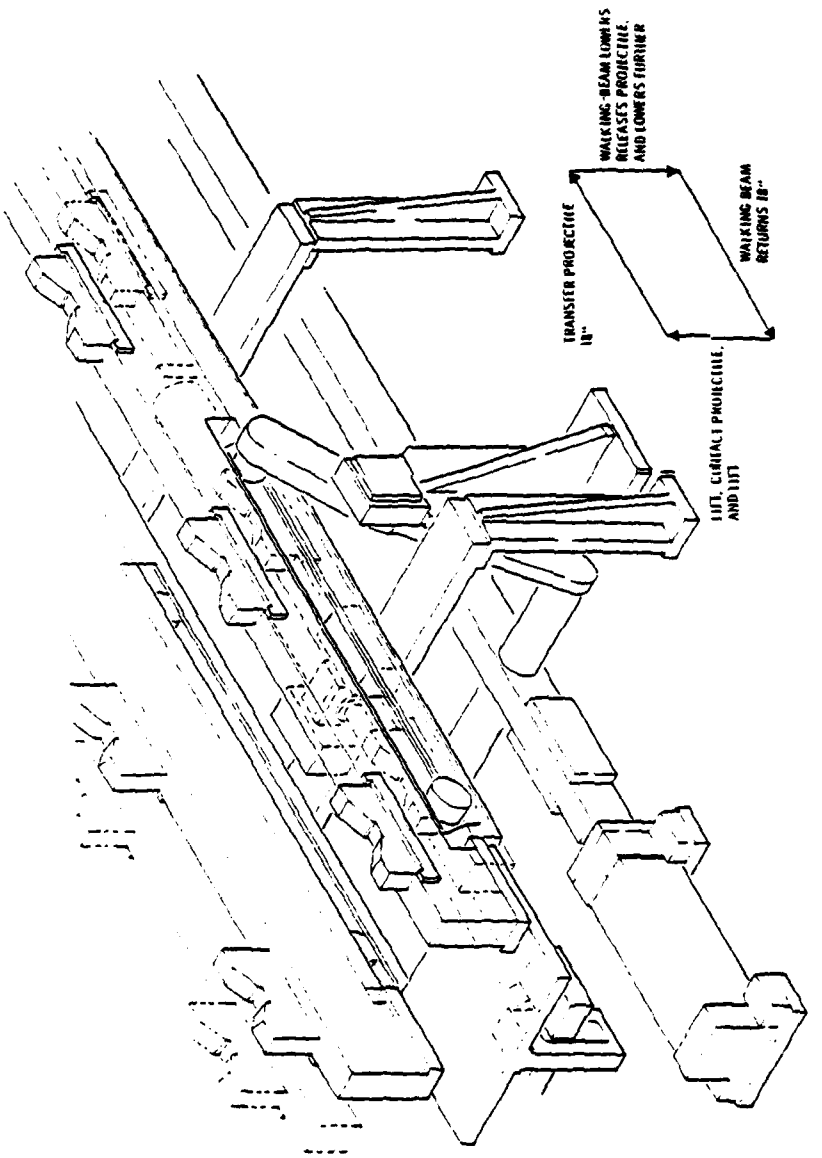

Fig. 23 Portion of the projectile handling system illustrating the closed-square-wave motion of the walking beam.

In addition to the walking beam, the mechanical machinery necessary for movement of projectiles through the EMAT inspection station has also been designed with an end view illustrated in Fig. 24. It is planned that this device: 1) grip the projectile from the ID of the nose with pressure applied to the shoulder of the base, 2) lift the projectile to a location ¼ inch from each electromagnet pole-piece, 3) rotate the projectile a set number of revolutions, and 4) remove the projectile from the magnetic field and place it back on the walking-beam. This device has also been designed by K.J. Law Associates and as such is an integral part of the handling system.

The system described above proposes to ultrasonically inspect M-549 projectiles in one inspection station. This can be accomplished by using 1) surface waves or eddy currents to inspect the outer surface of the base, 2) angle shear waves launched from the circumference through the base to inspect the interior of the wall in the base region, 3) angle shear waves launched in the longitudinal direction to locate ID & OD circumferentially oriented defects, and 4) angle shear waves launched circumferentially to inspect in the ogive and bourrelet regions for longitudinally oriented defects on the ID & OD and to inspect in the interior of the wall. This is a major departure from the previously proposed two-inspection station theory.(8) However, the improvements made in both electromagnet design and ultrasonic circuitry now suggest that it will be possible to inspect the entire projectile at one station. We feel this will both simplify and make more efficient ultrasonic inspection procedures necessary for inspection of the M-549 projectile.

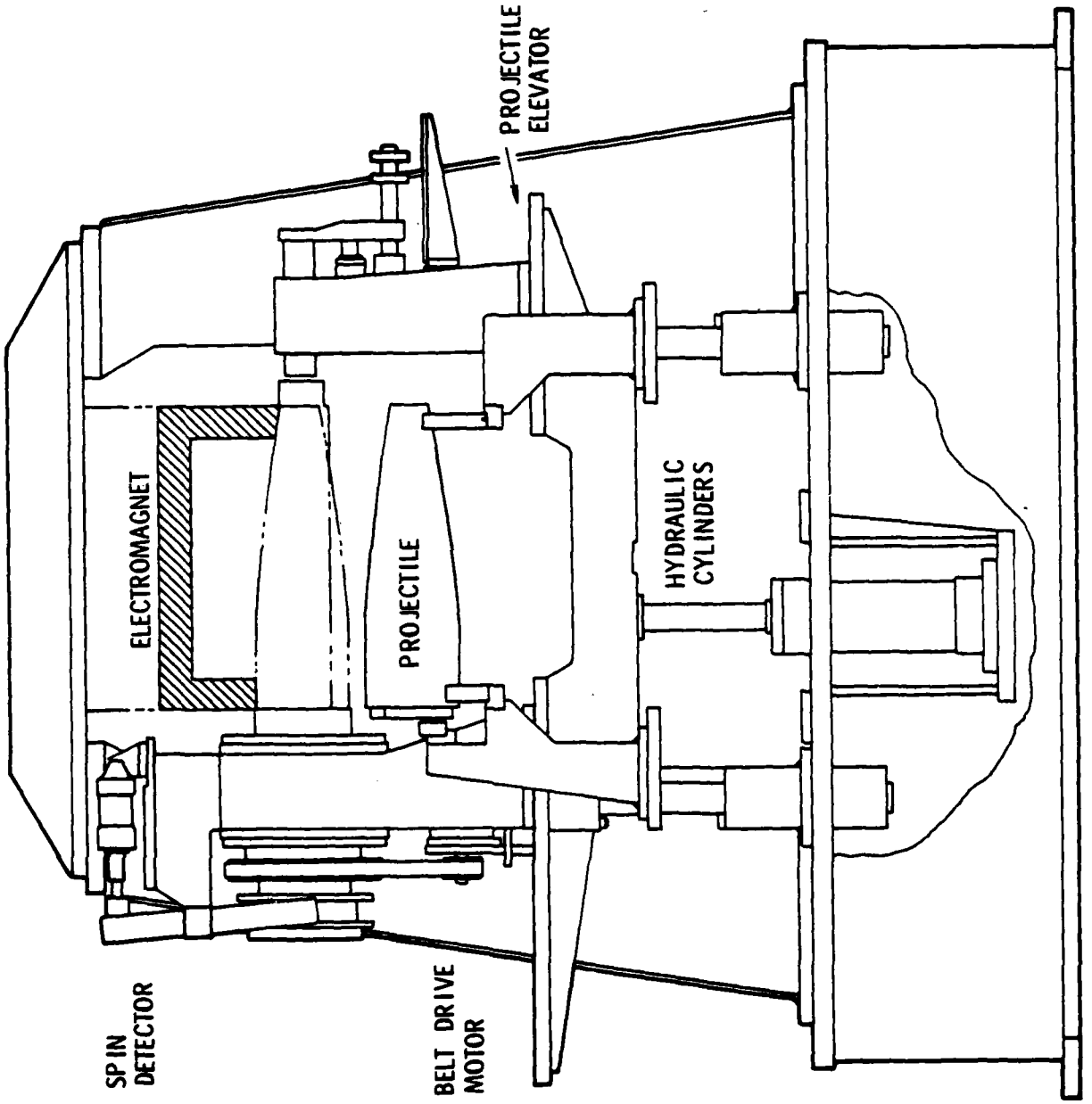

Fig. 24 Plane view of the EMAT inspection station.

It has been required that the automated handling system be compatible with both the EMAT inspection-procedure, and the Norris Industries M-549 production line at Vernon, California. The satisfaction of each of these requirements is discussed below.

2. Compatibility with EMAT Inspection Requirements

Although the EMAT transducer is noncontact, and thus successful inspection is not dependent upon the care normally necessary for parts prior to ultrasonic inspection, there are some simple precautionary procedures necessary to prevent the occurence of damage within the EMAT inspection station. For this particular inspection system, it is important that an oversized shell not be allowed to reach the EMAT inspection station. If this should occur, the possibility exists for damage to both the electromagnet and transducers when the projectile is lifted between the electromagnet pole-pieces. The potential for this occurrence is eliminated by locating the entire inspection system just subsequent to the dimensional inspection procedures already in practice at Norris Industries. The proposed position of the EMAT inspection system in relation to other operations in the M-549 production line is shown in Fig. 25. An anomalous shell, of dimensions sufficient to cause damage (~½ inch in diameter, oversized), would be easily detected during this inspection.

Similarly, metal fragments such as machine turnings, if allowed to ramain on the OD surface, could very likely damage the EMAT transducers and most certainly would effect inspection results. Although the parts are washed and manually handled for dimensional inspection prior to reaching the

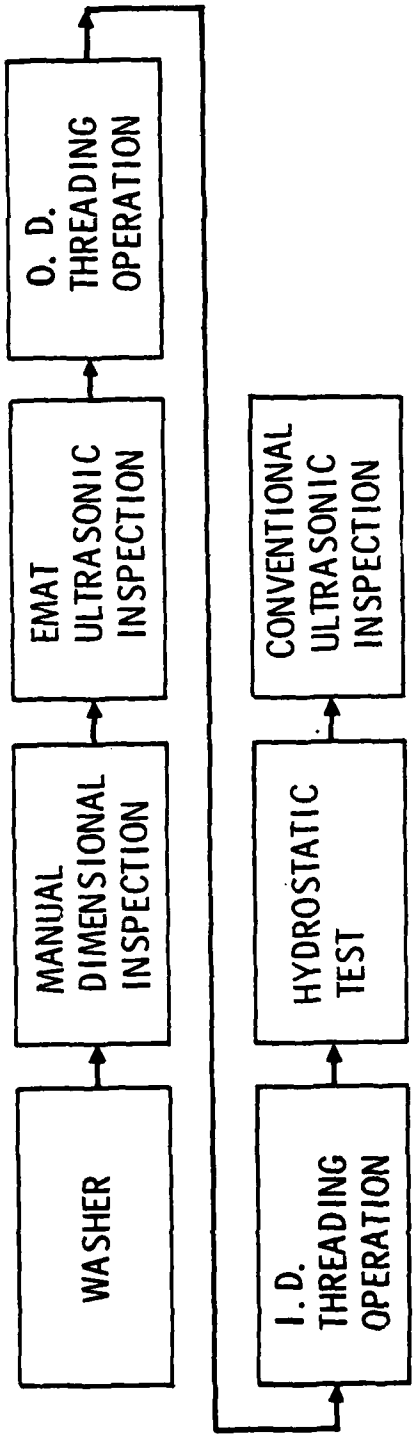

Fig. 25 Proposed location of the EMAT ultrasonic inspection system in the M549 production line.

inspection station, we felt it necessary to leave station 2, shown in Fig. 22, open for possibly locating a cleaning device if cleaning was found necessary in the future. Also, this station could be used to inspect for unremoved nose plugs. That is, upstream from the inspection station and prior to washing, plastic nose plugs are inserted into the ID of the projectile to prevent the collection of moisture. This plug can easily be removed during the dimensional inspection, however, the probability of this operation occasionally being omitted certainly exists. Since the projectile is gripped from the ID of the nose when lifted into the EMAT test station, it is mandatory that this plug be removed. For these reasons it is necessary to determine the presence of a nose plug prior to a projectile entering the EMAT inspection station. This operation could also be performed at station 2.

Idle stations 3 and 5 shown in Fig. 22 are necessary due to the dimensions of the electromagnet (89cm (35 inches) in length.) It is possible to use these stations for some purpose in the future, but at present they exist only to allow clearence for the EMAT inspection station. To get a feel for the structural nature of components being discussed, it should be remembered that the electromagnet alone weighs nearly one metric ton (~2000 lbs). The inspection station, which must support the electromagnet, has been designed accordingly.

Peculiar to the EMAT inspection procedure is the necessity to magnetize the part to be inspected. For the case of the ferromagnetic M-549 projectile, this requires a tangential magnetic field of 150 to 350 Oe to take advantage of the magnetostrictive enhancement of ultrasonic signals. This results in the inspected part retaining some level of residual magnetism.

Since the projectile is not completely machined at this stage (threading operations in the nose and base are still required), residual magnetism would make metal chip removal difficult during final machining. It may prove possible to demagnetize within the EMAT test station, however, as an alternative, station 7 has been set aside for locating a demagnetizing coil. A unit such as the SB demagnetizers produced by Magnaflux Corp. could be easily adapted to the walking beam. This unit imposes a continuously reversing magnetic field upon the part by passing it through a coil. Corresponding field reversals occur in the part along with a reduction in residual field strength as the part passes from the influence of the coil. The location of this coil in the production line is such that rejected projectiles will not be demagnetized thus providing a secondary precaution against rejected projectiles inadvertently being accepted for further processing.

3. Compatibility with the Norris Industries M549 Production Line

Throughout the course of this program, Science Center personnel have visited the Norris Industries facility at Vernon, Calif., to evaluate the most appropriate location for the EMAT inspection system in the M-549 production line. It is our objective to minimize any disturbance to the production line while at the same time providing for as complete an inspection as possible. It is not reasonable at this time to determine absolutely the appropriate location due to the potentially continuous state of change in the line; particularly since installation of this system is not scheduled for at least another 20 months. For this reason, it was to our benefit to design as

flexible a handling system as possible. Indeed, the system designed simply requires that a projectile be delivered to the first station. However, although the line may change, there is at this time an optimum location for the EMAT inspection system as shown in Fig. 25. The rationale for this location will not change and as such is discussed below.

For the sake of simplifying the handling system, it is most efficient to take advantage of existing procedures. For example, if it becomes necessary, a station has been set aside in the new system for cleaning of the projectile. However, it is simpler to position the EMAT inspection system downstream from the existing washer. Similarly, a dimensional inspection to identify anamolous projectiles could be included in the new system, but again, it is simpler to position the EMAT system downstream from the present dimensional inspection. Thus, in Fig. 25, the EMAT inspection system is shown in a location downstream from both the washer and dimensional inspection. Conversely, it is not possible at this time to ultrasonically inspect a threaded region. Accordingly, OD & ID threading operations are located after the EMAT ultrasonic inspection.

Initially, it is not the intent to eliminate the conventional ultrasonic test station, but to run both ultrasonic systems in parallel to evaluate the reliability of the EMAT system. Thus, two ultrasonic systems are shown in Fig. 25. The conventional ultrasonic inspection is currently the final step in the M-549 production line and as shown follows all machining, including threading operations. This is possible because current inspection standards do not require complete ultrasonic inspection of the projectile. That is, only specific locations are evaluated for soundness by ultrasonics

and this does not include threaded regions. It is anticipated that introduction of the EMAT inspection procedures will improve product reliability by inspecting the entire projectile with the only condition being that inspection be prior to threading.

V. DEMONSTRATION OF ULTRASONIC INSPECTION CAPABILITIES

The capability of detecting a number of artificial and natural flaws was demonstrated during this program. These results are presented below but are first preceded by a more general discussion of some of the properties of ultrasonic waves launched by EMATs, in the M-549 projectile, so that the results of this study can be related to those of other ultrasonic inspection programs.

A. Properties of Ultrasonic Waves Generated by Electromagnetic Transducers in the M-549

It is well known that periodic electromagnetic transducers of the type shown in Fig. 3 can excite and detect ultrasonic shear and longitudinal waves and that the direction of propagation of such waves can be determined from Snell's law.

$$\sin\theta_{S,L} = \frac{V_{S,L}}{fD} \tag{3}$$

where θ is the angle of the direction of propagation of the excited wave with respect to surface normal, V is the bulk phase velocity for shear and

longitudinal waves, f is the frequency, and D is the periodicity of the transducer. The subscripts S and L refer to wave type (i.e. shear or longitudinal). This relationship is only strictly obeyed when the ultrasonic signals are excited in a thick sample, i.e. when the length of the ultrasonic tone burst is shorter than the transit time between the bounding surfaces of the part being inspected. This is the case in the base region of the M-549 projectile, where the bounding surfaces are sufficiently far apart to prevent mutual coupling due to transverse resonance and a simpler analysis of the angle shear wave propagation characteristics is possible. However, this condition is not in general satisfied over a major portion of the M-549 projectile because typical wall thicknesses in the ogive and the bourrelet regions range from 1.15cm (.450 in) to 1.4cm (0.550 in) and do not exceed the length of typical ultrasonic tone bursts. These contain 8 RF cycles at 1.8 MHz carrier frequency and therefore extend over 4.6cm (1.8 in) in space. Because the inner and the outer surfaces of the projectile are coupled ultrasonically, it is not appropriate to use the Snell's law analysis to describe the propagation of quasi-plane sound waves within the "plate-like" wall of the projectile. The coupling between the surfaces changes the propagation characteristics of the ultrasonic waves, particularly their phase and group velocity characteristics as a function of frequency. In order to deal with this problem a new analytical procedure has been devised using a guided wave formulation. The analytical procedures were developed under previous IR&D and contract support and are summarized below.

1. Generation of Angle-Shear Waves in Thick Walled Sections of the M-549

This section summarizes the results of a theoretical calculation by Vasile and Thompson[4] of the angular dependence of the relative generation efficiency for normally polarized (SV) angle shear waves in a half-space. The results are important in that they can serve as a guide for optimum design and selection of frequencies of electromagnetic transducers operating in the base region of the M-549 projectile, where the bounding surfaces do not affect the plane wave behavior of the excited ultrasonic waves. Although the results apply strictly only in the case of a single-wire electromagnetic transducer, they can be especially generalized for multiple period transducers by multiplying by suitable array factors. The key features are summarized in a polar plot in Fig. 26

The calculation used to generate the plot of Fig. 26 assumes that the driving stresses due to the interaction of the eddy currents and the static magnetic field lines at the surface are directed along the surface (in-plane). This assumption is correct for Lorentz force excitation when the magnetic field bias is normal to the surface and is also true for magnetostrictive excitation when the magnetic field is parallel to the surface. These two cases cover all the situations anticipated in the projectile system.

It is seen from Fig. 26 that a maximum in the generation efficiency curve for shear waves occurs at an angle of approximately 30^{o} with respect

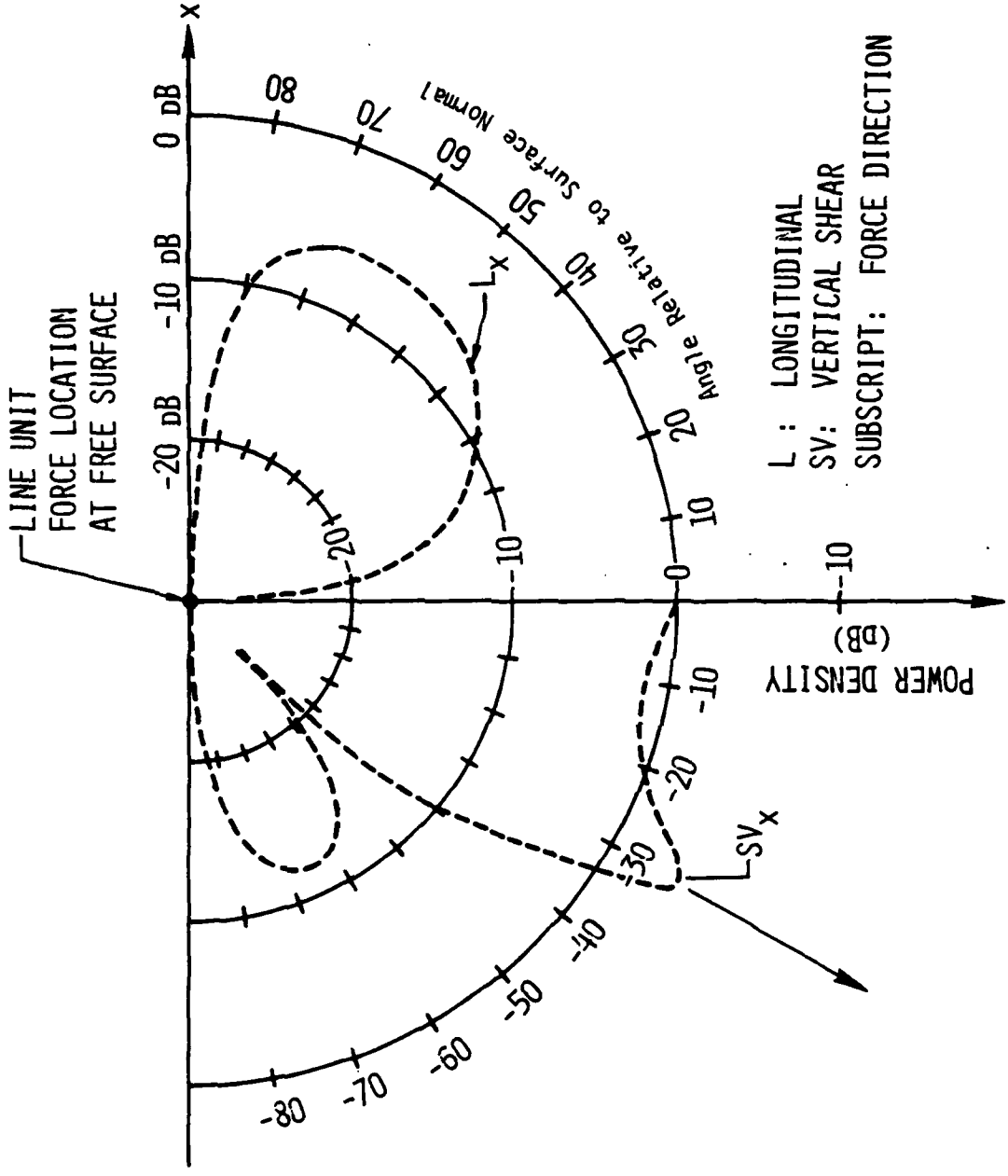

Fig. 26 Calculations of the angular dependence of the amplitude of both shear and longitudinal acoustic waves excited by a single wire EMAT.

to the surface normal. An electromagnetic transducer can be made to generate waves at this maximum providing its frequency of operation and periodicity are selected to satisfy Snell's law in accordance with Eq.(3).

A number of other important characteristics can also be deduced from Fig. 26. When an array is constructed, such as the meander coil, the ultrasonic field is formed by a superposition of translated radiation patterns such as shown in Fig. 26. The amplitude of the generated wave in the far field can then be shown to be the product of the function shown in Fig. 26 and an array factor which is unity when Eq.(3) is satisfied. To take advantege of the large shear wave generation at 30°, the transducer is tuned for this angle. For the same f and D, it is found that the radiated longitudinal wave is just passing from the evanescent to the propagating conditions; in fact this condition probably produces the large peak in efficiency. It is desirable to operate just below this point to ensure high efficiency without the presence of spurious signals that would be produced by the propagating longitudinal waves.

Note also that the generation efficiency for angle shear waves exhibits a sharp minimum occurring at approximately 45° with respect to the surface normal. A second relative maximum occurs at approximately 65° with respect to surface normal, but the efficiency is reduced by nearly 16 dB with respect to the main maximum at approximately 30°. It follows that practical electromagnetic transducers for generating and receiving angle shear waves at nearly maximum efficiencies must be restricted to operate slightly below 30° in order to avoid substantial longidutinal wave generation.

2. Generation and Propagation of Ultrasonic Signals in "Plate-Like" Walls of the M-549

The results of the calculations summarized in Fig. 26 are in good agreement with experiments on thick samples and have been used to arrive at several important experimental results. However, this analysis is unable to quantitatively predict the correct behavior in the presence of ultrasonic coupling between the inner and the outer surfaces of the M-549 projectile and a new waveguide analysis had to be developed as a transducer design tool. Some of the results of the waveguide analysis are presented in this section.

In order to understand the generation and propagation properties of sound waves in the ogive and bourrelet regions of the M-549 projectile, a guided wave approach was used.[6] That is, instead of analyzing the ultrasonic propagation in terms of multiple bounces of plane waves, it was analyzed as a superposition of ultrasonic wave guide modes of a finite thickness plate. By calculating the frequency spectra and the relative coupling efficiencies of higher order Lamb waves, the analysis addressed the origin and dispersion characteristics of multiple time domain responses produced by a single flaw. These results serve as a basis for proper design and placement of transducer elements for the ogive and bourrelet region to properly interpret the ultrasonic signals.

Figures 27 and 28 show the calculated frequency spectra for the higher order symmetric and antisymmetric Lamb waves present in the 1018 steel plate of 1.27cm (0.500 in) thickness when excited by a transducer having a period of .31cm (.120 in) and in the neighbourhood of 1.8 MHz carrier frequency. The characteristics of these spectra can be used directly in the

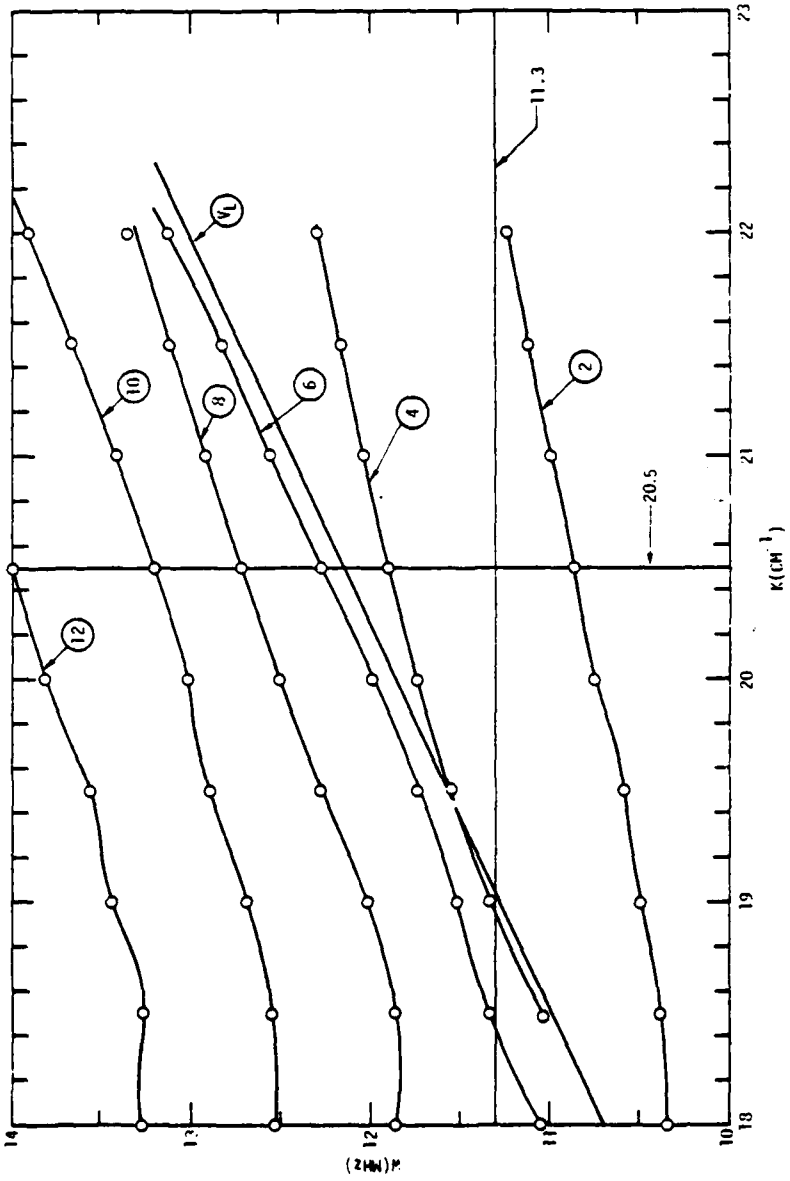

Fig. 27 Calculated frequency spectra of higher order symmetric Lamb modes in a 1018 steel plate of 0.500 inch in thickness in a region where maximum generation efficiency is obtained. The horizontal line corresponds to a frequency of 1.8 MHz.

SC5113.4FR

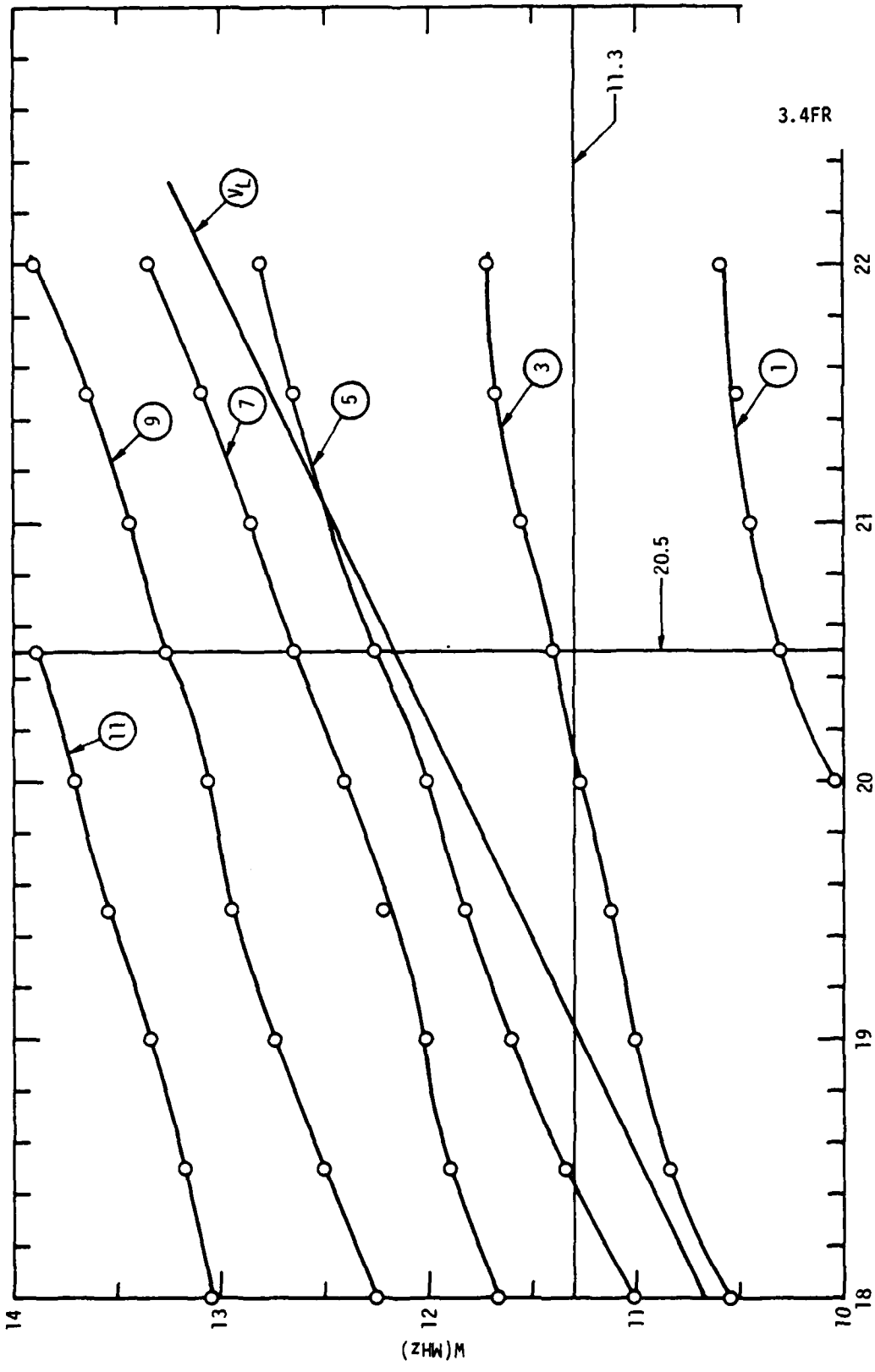

Fig. 28 Calculated frequency spectra of higher order anti-symmetric Lamb modes in a 1018 steel plate of 0.500 inch in thickness in a region where maximum transduction efficiency is obtained. The horizontal line corresponds to a frequency of 1.8 MHz.

TABLE 1.

Summary of Some Guided Mode Propagation Characteristics

Corresponding to the Frequency Spectra of Figs. 27 and 28.

#	Mode Type	MHz	f MHz	K CM^{-1}	V_{PH} Km/sec	V_G Km/sec	Y_X	Y_Z
1	A	10.30	1.63	20.5	5.025	2.24	1205.	206.
2	S	10.86	1.72	20.5	5.302	2.35	379.	240.
3	A	11.40	1.81	20.5	5.56	2.61	175.	353.
4	S	11.89	1.89	20.5	5.565	3.16	121.	1023.
5	A	12.26	1.95	20.5	5.98	3.73	179.	Very Large
6	S	12.26	1.95	20.5	5.984	5.55	Very Large	5658.
7	A	12.64	2.01	20.5	6.16	4.33	718.	1820.
8	S	12.70	2.02	20.5	6.19	4.10	326.	3383.
9	A	13.28	2.11	20.5	6.48	3.72	502.	1428.
10	S	13.21	2.10	20.5	6.44	3.68	353.	1948.
11	A	13.8	2.20	20.5	6.77	3.31	328.	1950.
12	S	13.90	2.22	20.5	6.81	3.37	577.	1104.

A: Asymmetric plate mode
S: Symmetric plate mode
: frequency
K: Propagation constant
V_{PH}: Phase velocity
V_G: Group velocity
Y_X, Y_Z: Bulk wave surface admittance coefficients in units of Nt/m^2-sec.

central portion of the M-549 projectile, but should be scaled according to the average thickness of the wall.

Numerical calculations showed that a maximum in the generation efficiency for plate modes occur when their longitudinal component passes from the evanescent to the propagating regime. In this respect the mechanism of excitation for plate modes is similar to that for plane shear waves in a very thick section of the projectile. However, important differences exist and must be understood for proper range gating and flaw reflectivities. Because the ultrasonic signals are of finite duration and the transducers are of finite spatial extent, the selection of a particular mode and exclusion of others is not possible. Strong coupling which exists between the modes causes their propagation characteristics to deviate substantially from that of uncoupled shear (SV) or longitudinal (P) waves. This is evidenced by the complex behavior of the dispersion curves of Figs. 27 and 28 which would be parabolic in the absence of the coupling between the modes. The strong coupling also results in large variations in coupling efficiencies, and phase and group velocities.

A number of propagation characteristics corresponding to the frequency spectra of Figs. 27 and 28 are summarized in Table I. The phase and group velocities were evaluated for a long electromagnetic transducer with .31cm (0.120 in) period assuming bulk shear and longitudinal wave velocities of 3.1 and 5.9 km/sec, respectively. The relative coupling efficiencies of the modes are also characterized by mode admittances. The amplitude of an ultrasonic signal is inversely proportional to this number. It is seen from the data that the group velocities, which determine the time delay of a

signal, range from 2.35 km/sec to 4.1 km/sec for the strongly coupled modes denoted with asterisks.

The results listed in Table I were confirmed by experiments on flat steel plates magnetized along the surface. For maximum magnetostrictive excitation, very similar effects were also observed in the M-549 projectile, but an exact comparison was not possible because of curvature and tapering of the wall thickness in the projectile.

The presence of several modes is evidenced by the dispersion of the ultrasonic wave into several signals traveling with different group velocities. This effect is illustrated in Fig. 29 which shows the photo of a dispersed ultrasonic signal at 1.8 MHz carrier frequency after a propagation distance of approximately 20cm (8 in). As shown in the next section, these effects are most pronounced for large propagation distances. However, as the flaws become closer to the transducer, the results approach the plane wave case.

An inspection of the frequency spectra shows that a degree of mode discrimination can be achieved by designing the electromagnetic transducer such that lines corresponding to inverse transducer periodicity and center frequency intersect on the first Lamb mode located below the longitudinal velocity. The corresponding range of angles for shear wave generation in a half-space lies between 30 and 34^{0} with respect to surface normal on Fig. 26. Of course, transducer parameters must be chosen consistently with material parameters such as shear wave velocity and Poisson's ratio.

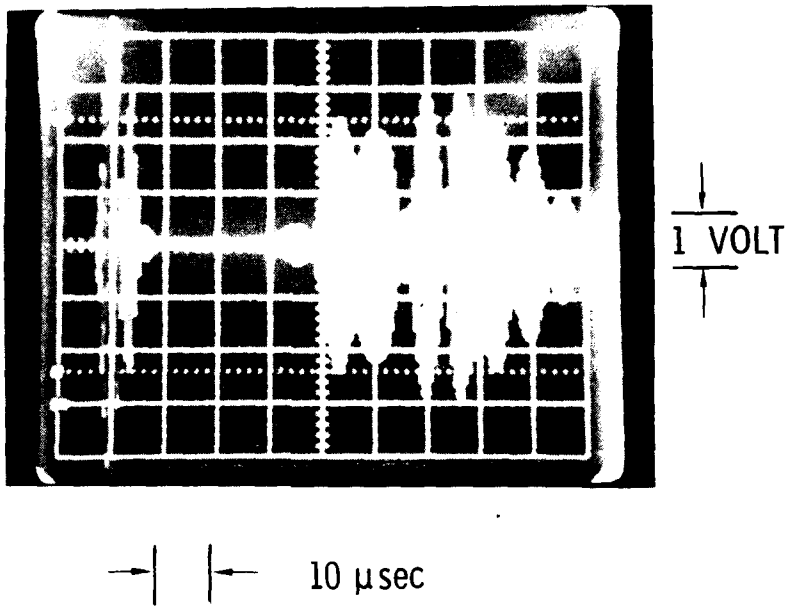

Fig. 29 Dispersion of ultrasonic signals in a 0.500 inch thick 1018 steel plate due to coupling of Lamb modes. The rf carrier frequency is 1.8 MHz and the input transducer is separated from the output transducer by approximately 8 inches.

The results described in this section are the key to the proper selection of range gate times and operating frequencies for transducers designed to operate in the ogive and bourrelet regions.

B. Performance of One Ultrasonic Inspection Channel

The development of a prototype electronics package, including a breadboard single-channel correlation receiver, has made it possible to set up a realistic demonstration of the operation of a single ultrasonic signal processing channel. The configuration of the experimental set up used in this demonstration is shown in Fig. 30. The experimental set up consists of an electromagnet for magnetic biasing of an M-549 projectile along the circumference as shown in Fig. 30, an electronic package including a single electromagnetic transducer for generating and receiving the ultrasonic signals, displays, and an M-549 projectile containing two simulated defects in the bourrelet region. A provision was made for permanently fixing the position and orientation of the electromagnetic transducer when the projectile was rotated around its axis of symmetry in the magnetic bias field to simulate the operation of an automated system.

The electronics package used in the demonstration consisted of subsystems already described in the preceeding sections of this report and a prototype correlation receiver as shown in Fig. 31. Additionally, a cathode ray tube oscilloscope and a four digit LED panel were used for displaying the received ultrasonic signals after linear preamplification, linear multiplication by a reference signal and integration respectively.

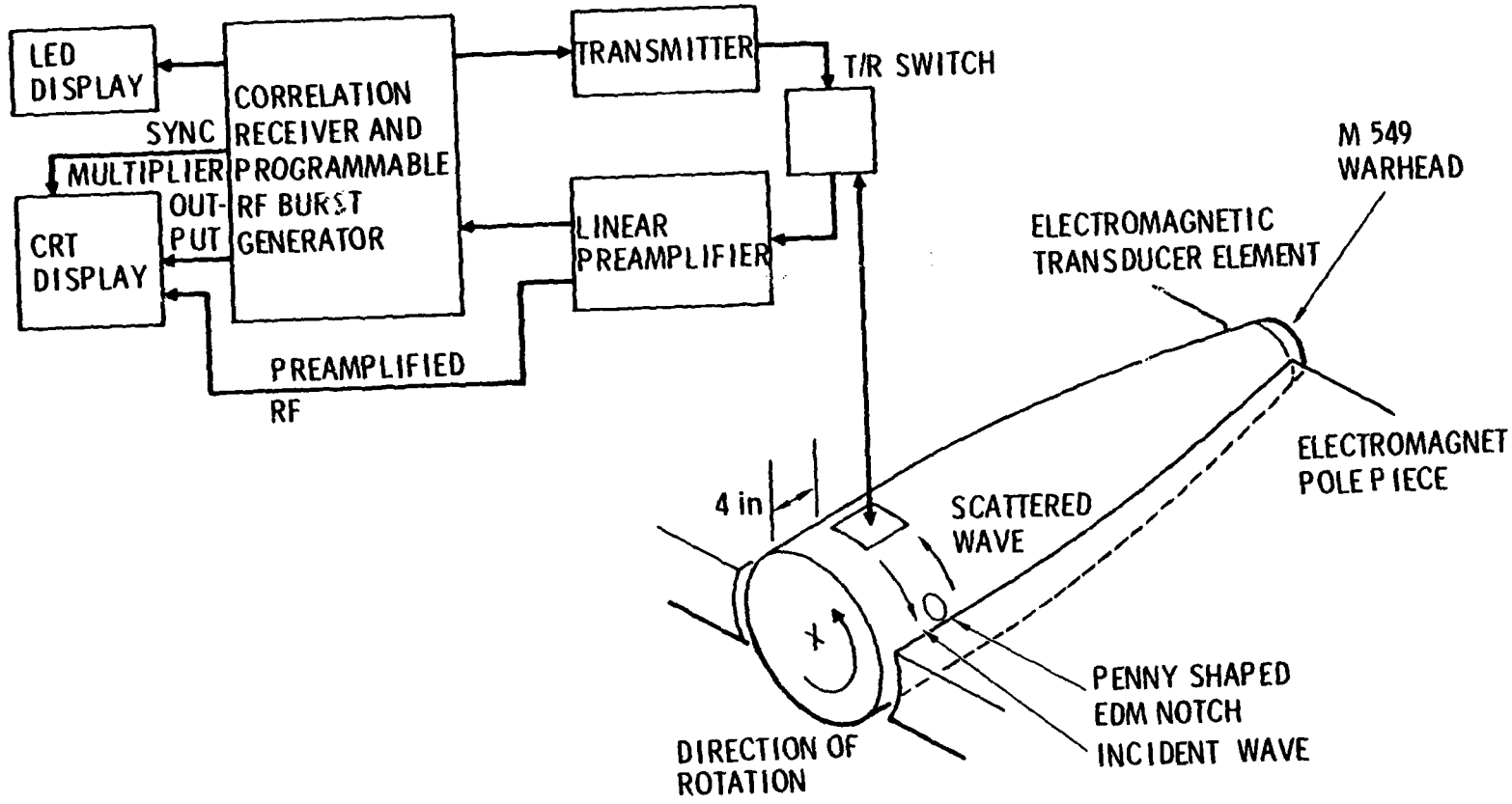

Fig. 30 Configuration used to test the performance of one ultrasonic signal processing channel, including a single channel correlation receiver.

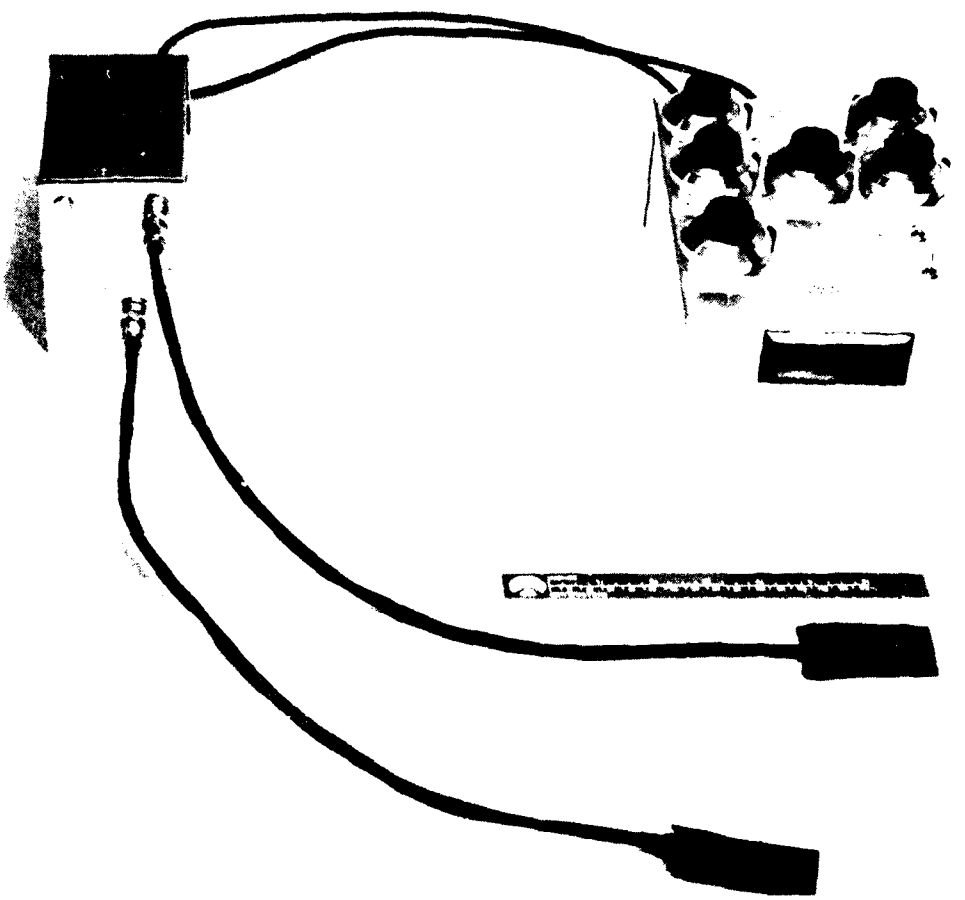

Fig. 31 Photo of the electronics package, including the correlation receiver and meander coil transducers.

This was done in order to illustrate the variety of waveforms involved in the signal processing and their interrelationships. The electronics package was tuned to a center frequency of approximately 1.8 MHz and the electromagnetic transducer was excited by a tone burst centered at this frequency and containing 8 cycles. The electromagnetic transducer was of the conventional meander coil geometry made by photo-etching a one ounce layer of copper deposited on a 0.0025cm (0.001 in) kapton substrate. A flexible black rubber pad was attached to the opposite side of the kapton substrate to help maintain conformity to the radius of curvature in the bourrelet region. The transducer coil contained eight full wave periods of 0.3cm (0.120 in) each and had an active acoustic aperture of 2.5cm (1.00 in). In addition, a 0.025cm (0.010 in) thick paper spacer was used as an electrical insulator and as a wear plate to maintain a nearly constant separation distance between the transducer and the wall of the M-549 projectile.

The beam axis of the electromagnetic transducer was purposely aligned along the circumference of the sample M-549 projectile in the bourrelet. This was done to maximize the illumination of a simulated defect over a large range as it passed below the fixed transducer in order to illustrate some of the key features of the detection process based on the use of a correlation receiver.

The two simulated defects in the bourrelet were produced by EDM (electron discharge machining), and were located 5 and 10cm (2 and 4 in) away from the base of the M-549 projectile. Both defects were aligned along the longitudinal direction and had an approximately penny-shaped cross section. The EDM notch located nearer to the base had a surface length of 0.95cm (0.374 in) and a maximum depth of 0.028cm (0.011 in). The second defect had a

surface length of 0.56cm (0.222 in) and a maximum depth of 0.09cm (0.035 in). Although both defects could be readily detected by the prototype signal processing system, the deeper defect was used for calibration purposes because its location in a region of nearly cylindrical gometry made it easier to track ultrasonically with a fixed transducer element over a longer distance.

A sequence of eight photos shown in Fig. 32 illustrates the detection process of the simulated defect with 0.56cm (0.222 in) surface length and 0.09cm (0.035 in) maximum depth as the M-549 projectile is rotated manually beneath the fixed electromagnetic transducer element. Before the experiment, the transducer beam axis and position were adjusted for maximum amplitude of the received ultrasonic signal after linear preamplification in all eight photos. In each photo, the upper trace shows the received ultrasonic waveform after preamplification and the lower trace shows the output of the multiplier with the center of the reference tone burst delayed so as to produce maximum integrator output for a 2.5cm (1.00 in) separation between the simulated defect and the center of the transducer element. As noted previously, this is analagous to the amplitude detection of a defect with a fixed time gate. The horizontal scale is 10 microseconds per division, while the verticle scales are 1 Volt per division. The rms electronic noise level is approximately .01 Volt. The final output of the correlation receiver is the integral of the multiplied output (lower trace). This value is presented as a function of the separation in Table II.

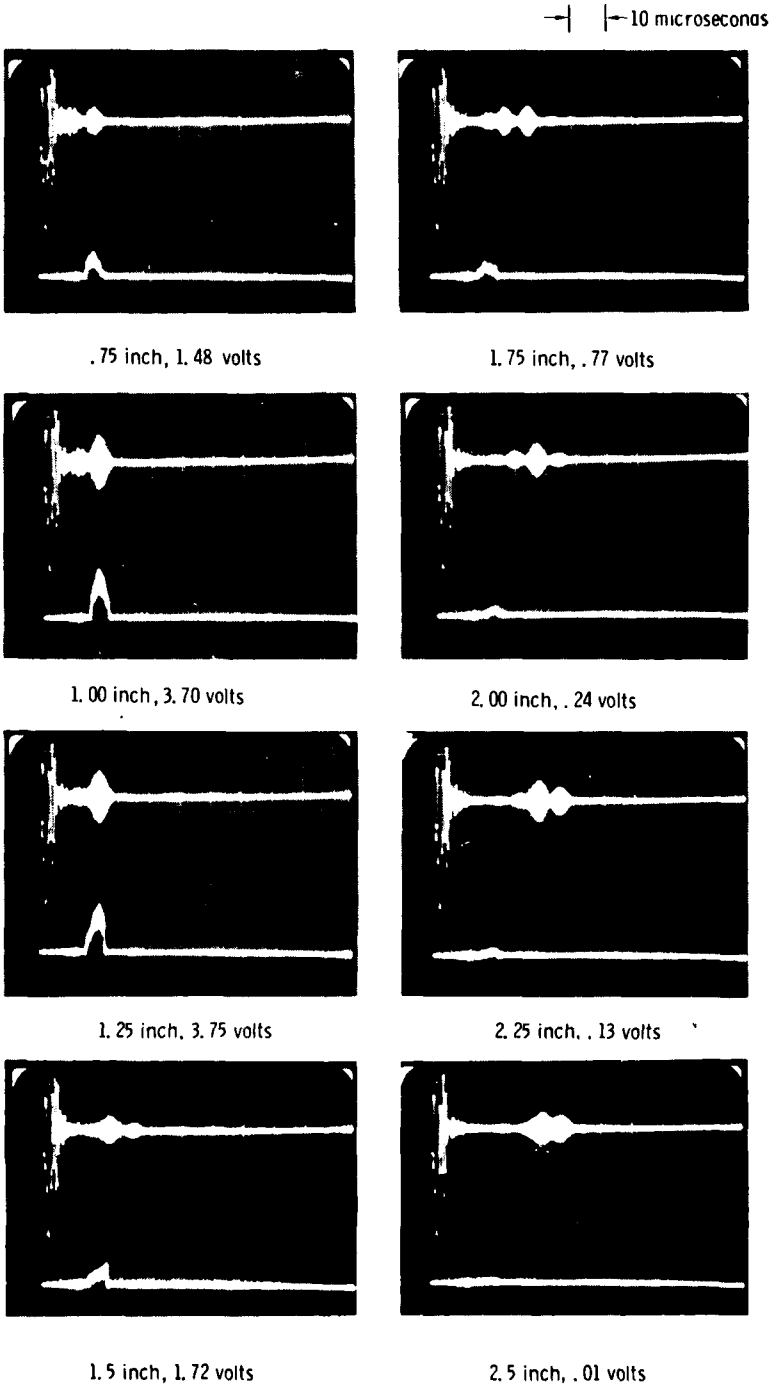

Fig. 32 Detection of a simulated defect as the M-549 projectile is rotated beneath a fixed electromagnetic transducer. The range gate of the correlation receiver is set for maximum output when the separation between the defect and transducer is approximately 2.5 cm (1 in).

TABLE II

Photo No.	1	2	3	4	5	6	7	8
Separation between center of transducer element & defect along circumference (inches)	0.75	1.00	1.25	1.50	1.75	2.00	2.25	2.50
Integrator output (volts)	1.48	3.70	3.75	1.72	0.77	0.24	0.13	0.01

A summary of correlation receiver outputs as a function of separation distance between the center of the transducer element and a defect (EDM notch) having a surface length of 0.56cm (0.222 in) and a maximum depth of 0.09cm (0.035 in) located 10cm (4 in) from the base and aligned along the longitudinal direction. The range gate of the correlation receiver is set to produce maximum output for a separation at 2.5cm (1.00 in). In the absence of a defect the output is $\pm$ 0.01 Volts.

A number of interesting features appearing in the photos have already been examined in the preceeding sections. In particular, the separation of the ultrasonic signals into separate wave packets has been attributed to the coupling between the inner and the outer surfaces of the projectile in the ogive and bourrelet. This effect is clearly shown in the sequence of photos of Fig. 32. For small propagation distances there is essentially one ultrasonic signal. However, the number of distinguishable wave packets increases as the separation between the transducer element and the defect

becomes progressively larger. The mutual interference between the discrete ultrasonic modes causes phase distortion which reduces the effectiveness of simple correlation receivers using a reference tone burst with linear phase characteristics. Because the distortion increases for larger separation distances it is advantageous to set the range-gate as soon as possible after the main bang, although some trade-offs are inevitable because of the time required for transducer "ringdown" after the transmit pulse.

The detection of two simulated defects at short transducer-defect separation distances is shown in Fig. 33. Two wave packets are distinguishable. One propagates essentially at the longitudinal wave velocity, the other at the shear wave velocity. The upper photo shows the detection of a defect having a surface length of 0.45cm (0.375 in) and a depth of 0.028cm (0.011 in). The defect is located approximately 5cm (2 in) from the base of the M-549 projectile where the mean wall thickness is approximately 1.4cm (0.550 in). This photo should be compared with the lower photo which shows the detection of the other defect having a surface length of 0.56cm (0.222 in) and maximum depth of 0.089cm (0.035 in), and located in a region where the mean wall thickness is only about 1.14cm (0.450 in) Note the greater separation between the two wave packets in the upper photo. This correlates with the different depths of the defects.

As an additional demonstration of the sensitivity of the electromagnetic transducers system to defects in the ogive and bourrelet, a comparison was made between our 1.8 MHz ultrasonic channel and a standard 2.25 MHz ultrasonic search unit using a 2.25 MHz piezoelectric transducer (PZT) with a 60^{o} plastic wedge. The results are summarized by the photos

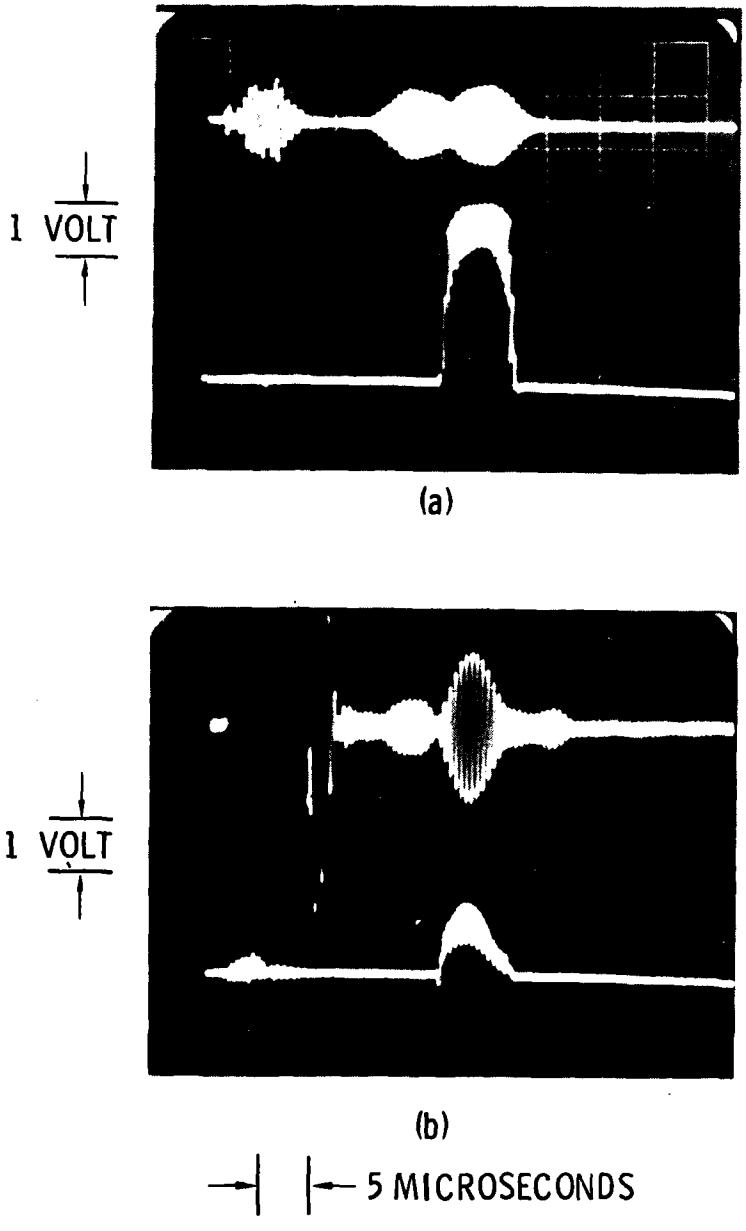

Fig. 33 Detection of OD simulated defects in the bourrelet with correlation receiver range gate set to produce maximum output for 2.5 cm (1 in) separation between transducer and defect. (a) upper trace: detection of a defect located 5 cm (2 in) from base and having 0.95 cm (0.375 in) surface length and 0.028 cm (0.011 in) depth. (b) lower trace detection of a defect located 10 cm (4 in) from base and having 0.56 cm (0.222 in) surface length and 0.09 cm (0.035 in) depth.

shown in Fig. 34. The upper photo corresponds to photo number 8 of Fig. 32. The middle photo shows the detection of the same defect taken after substituting the piezoelectric element in place of the electromagnetic element. The lower photo shows the same display as the photo directly above, except that the portion of the trace corresponding to the defect signature is absent following a 180^{o} rotation of the projectile. The horizontal time scales and the vertical scales are 10 microseconds and 1 volt per division respectively. The photos are different in that the RF signals received with the PZT element appear to contain fewer cycles because the exciting "pulse" consisted of essentially one RF cycle. On the other hand, the electromagnetic transducer was excited with a tone burst containing 8 cycles of RF in order to increase the peak signal-to-noise ratio on reception. The two sets of photos show similar features including the average time of arrival of the signals and their dispersal into discrete wave packets. It is also interesting to note that the effective "ring-down" time is shorter for the electromagnetic transducer system. The apparent long "ring-down" of the PZT system is caused by reverberations in the plastic wedge. The results of Fig. 34 show that the two transducer systems produce very similar ultrasonic outputs and that the detection is limited mainly by the propagation properties of the ultrasonic wave at a given frequency in the medium and its interaction with the defect. The excellent sensitivity of the electromagnetic transducer system compares well with that of the PZT system which is mainly limited by mechanical reverberation of the wedge and greater complexity of transduction. The PZT transducer reverberation signals due to the plastic wedge could be significantly reduced by using a water immersion system.

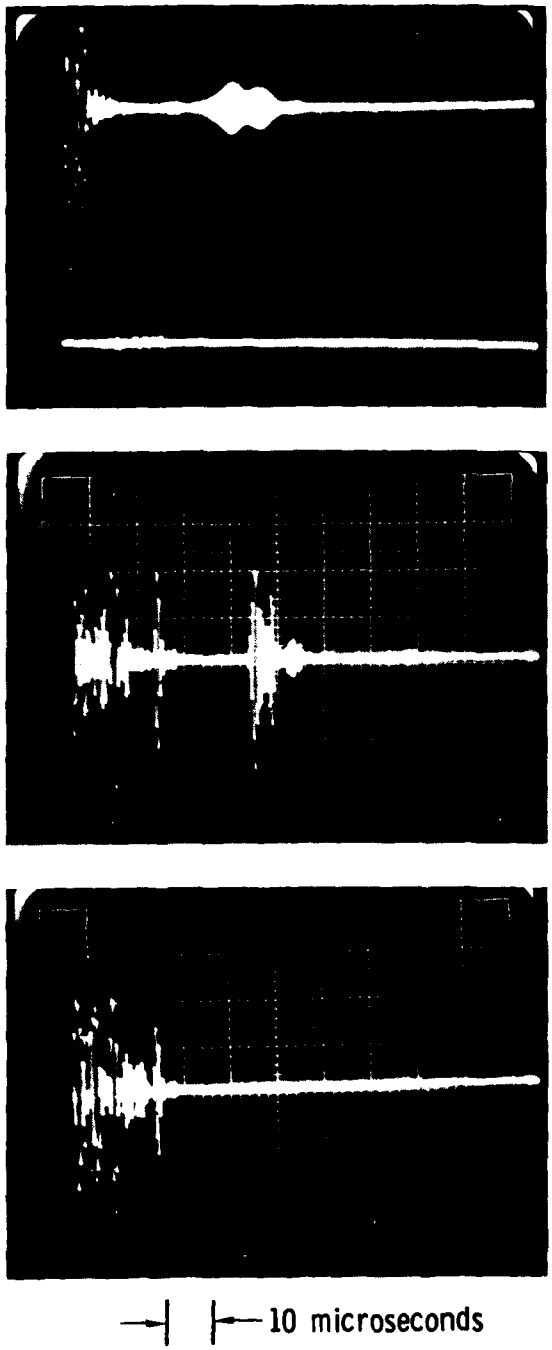

Fig. 34 Detection of an OD simulated detect with EMAT and piezoelectric wedge transducers. The transducer elements are 5.7 cm (2.25 in) away from the defect along the circumference in the bourrelet region and approximately 10 cm (4 in) away from base. (a) upper trace EMAT @ 1.8 MHz, (b) middle trace 60° wedge transducer @ 2.25 MHz, (c) lower trace same as above but projectile rotated 180°.

C. Survey of Detectability of Defects at Various Locations

Using the apparatus and procedures defined previously, measurements were made to demonstrate the ability of the system to detect both naturally occurring and artificial flaws in M-549 projectiles. Two sets of projectiles were used. One set of three projectiles fabricated by Flinchbaugh contained naturally occurring flaws which had been detected in a previous inspection using an immersion technique with piezoelectric transducers. These flaws were easily detected using the EMAT transducers. It would have been instructive to section these projectiles in order to characterize these natural flaws and to correlate resultant ultrasonic signals with signals corresponding to EDM notches. However, the second set of projectiles supplied by Norris Industries showed metallurgical differences which influenced the transduction efficiencies (see next section), and it was felt important to retain intact some samples of both types until the origin of this effect could be fully defined.

Accordingly, only one Flinchbaugh projectile was distructively evaluated. Projectile No. 31 was sectioned and in the exact location predicted an irregularly shaped notch was found on the I.D. surface. As noted, the shape was irregular reaching a maximum depth of 0.053cm (0.021in) over a length of 1.46cm (0.575in). Over most of this length the depth was considerably less than the .053cm maximum depth. The EMAT signal resulting from this material defect is shown in Fig. 35. The base with which this flaw can be discriminated from background noise is apparent. Similarly, naturally occurring defects have previously been located using EMAT techniques as illustrated in Figs. 6 and 7 of Ref. 1.

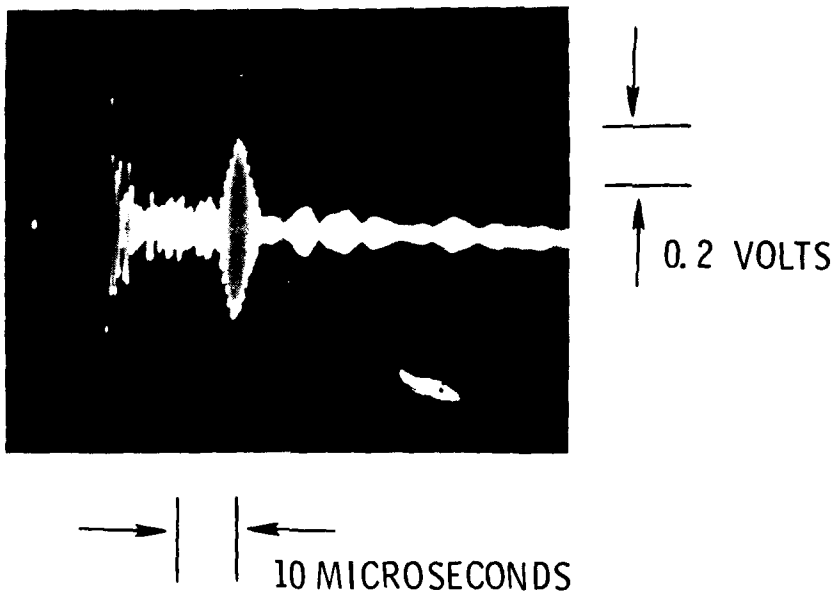

Fig. 35 Detection of a natural flaw located on the ID in the ogive region of an M-549 artillery projectile using EMAT technology.

In the second set of projectiles, produced by Norris Industries, a number of simulated defects were produced at various locations by electron discharge machining (EDM) to demonstrate the detection sensitivity of the electromagnetic transducer inspection system. Typical dimensions of the EDM notches ranged from 0.076 to 0.95cm (0.030 to 0.374 in) in surface length and 0.028 to 0.14cm (0.011 to 0.055 in) in depth. All notches were approximately 0.013cm (0.005 in) wide at the surface.

The majority of the simulated defects were placed on external surfaces along the ogive and bourrelet and oriented essentially along the axis of the M-549 projectile or, in a few cases, canted at various angles with respect to the axis. Two simulated defects were also placed on the inner surface along the circumferential direction. One small EDM notch having a surface length of only 0.05cm (0.020 in) was placed on the outer surface of the center of the base.

Angle shear and guided waves at 1.8 MHz were used to detect all of the simulated defects, except at the center of the base, with signal-to-noise ratios ranging from 30 to 40 dB. In all cases a single-ended (pulse-echo) system was used. The defect in the base has not yet been detected due to the greater geometrical complexity of that region. However, improvements are in progress in other programs which we believe will overcome this difficulty.

The experimental results are summarized in Table III, which give the relative position and orientations of the simulated defects as well as the peak-to-peak RF voltages of the received ultrasonic signatures. The RMS noise voltage level was approximately 0.007 Volts in all cases.

TABLE III

Summary of Ultrasonic Reflections from Various Simulated Defects on M-549 Projectiles. Data was Taken at 1.8 MHz

Simulated Defect No.	Distance From Base (inches)	OD / ID	Surface Length (inches)	Max. Depth (inches)	Cant Angle w/respect to axis	Output Level (V)	Field Configuration	Sample No.
1	6.5	O.D.	.146	.014	0	1.2	Parallel	88
2	8	O.D.	.158	.014	0	1.6	Parallel	88
3	9.5	O.D.	.186	.019	0	2	Parallel	88
4	9.5	O.D.	.256	.052	0	4	Parallel	88
5	11	O.D.	.116	.009	0	.8	Parallel	88
6	12.75	O.D.	.190	.022	0	2.8	Parallel	88
7	14.5	O.D.	.174	.015	0	1.2	Parallel	88
8	2	O.D.	.172	.020	10	.6	Parallel	85
9	2	O.D.	.177	.020	20	.2	Parallel	85
10	2	O.D.	.186	.018	30	.08	Parallel	85
11	2	O.D.	.374	.011	0	2.2	Parallel	09
12	3.5	O.D.	.222	.035	0	3.6	Parallel	09
13	5	O.D.	.105	.019	0	1.5	Parallel	09
14	3	O.D.	.179	.021	0	3	Parallel	51
15	5	O.D.	.157	.107	0	2	Parallel	51
16	2	I.D.	.030	?	90	.8	Normal	88
17	2	I.D.	.030	?	90	.6	Normal	88

AD-A112 162 ROCKWELL INTERNATIONAL THOUSAND OAKS CA SCIENCE CENTER F/G 19/1
RAPID ULTRASONIC INSPECTION OF ARTILLERY PROJECTILES.(U)
MAY 78 C M FORTUNKO, R B THOMPSON DAAK10-77-C-2020
UNCLASSIFIED SC5113.4FR NL

END
DATE FILMED
4 82
DTIC

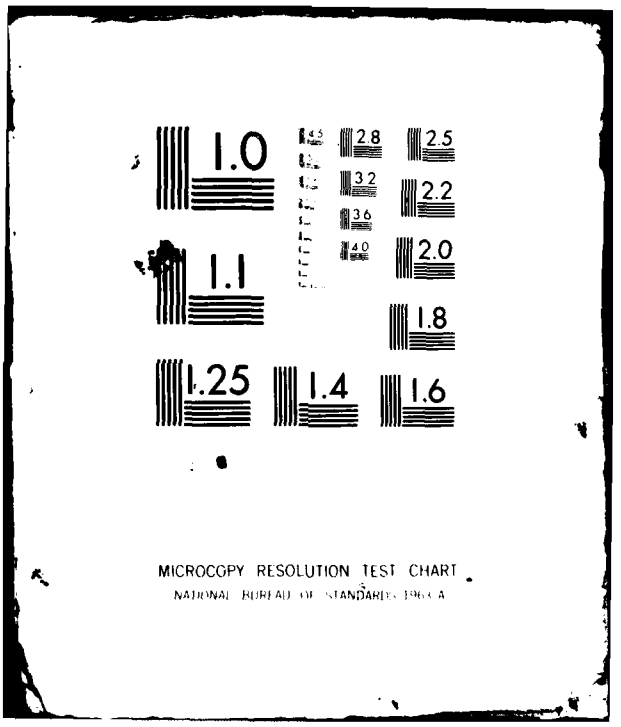
1.0
1.1
1.25
1.4
1.6
1.8
2.0
2.2
2.5
2.8
3.2
3.6
4.0
MICROCOPY RESOLUTION TEST CHART
NATIONAL BUREAU OF STANDARDS 1963 A

VI. EFFECTS OF SURFACE DECARBURIZATION ON ELECTROMAGNETIC TRANSDUCER EFFICIENCY

Hot worked steel products usually become somewhat decarburized during heating prior to a hot working operation. The depth and magnitude of decarburization depends on the hot working temperature, time at temperature, furnace atmosphere, reduction of area between the bloom and the finished size, and the type of steel. Considering the forming operations necessary to fabricate an M-549 artillery projectile, e.g. nosing operations in air at 829^{o}C (1525^{o}F), one would expect the high carbon steel used for this fabrication (1.1%C) to exhibit some degree of surface decarburization. Indeed, it has been found during this program that M-549 projectiles are decarburized and the presence of this surface decarburization influences, in an adverse manner, inspectibility. This section discusses this observation and proposes methods to improve inspectibility. This work was performed under industrial research and development funds.

1. Identification of Surface Decarburization on M549 Projectiles. - A chronological discussion of the discovery of this surface effect aids in understanding proposed solutions. Initially, M-549 projectiles fabricated by Flinchbaugh were used to evaluate the feasibility of ultrasonic inspection using EMAT technology. With these projectiles, ultrasonic signals were routinely launched from EMAT transducers and naturally occurring defects were readily located. During fabrication by Flinchbaugh, the projectiles had been machined on the OD surface and thus, any surface phenomena resulting from

prior heat treatments or hot working operations would have been removed. At a later date, projectiles fabricated by Norris Industries in a 1975 lot were received by the Science Center for feasibility evaluation. No difficulties were encountered in inspecting the body of the projectile, i.e., the area between the base and the location where the nose taper begins. This region is a machined surface and again, any surface conditions affecting inspectibility would have been removed. On this same projectile, in regions exhibiting a hot worked surface, ultrasonic signal intensities were found to decrease by a factor of 15 (23 dB) as compared to corresponding locations on machined projectiles. However, after removal of a thin layer by machining signal intensities were restored. Subsequently, this hot worked surface was evaluated by x-ray, metallography, scanning electron microscopy (SEM), hardness measurements and heat treatment studies. The results of this evaluation, which led to the conclusion that some degree of surface decarburization was present, are discussed below.

Of the analyses performed, SEM photos most clearly illustrated a difference in the morphology of a second phase precipitate. Figure 36 shows this difference illustrating a lack of Fe_3C precipitates in a region up to 0.025cm (0.010 in) from the hot worked surface whereas a uniform density of precipitates is evident throughout the thickness of the machined sample. It should be understood that we have no quantitative analysis of the carbon content as a function of depth from the surface. Our observations of "carburized" and "decarburized" are purely qualitative and are based on the presence or lack of observable Fe_3C precipitates.

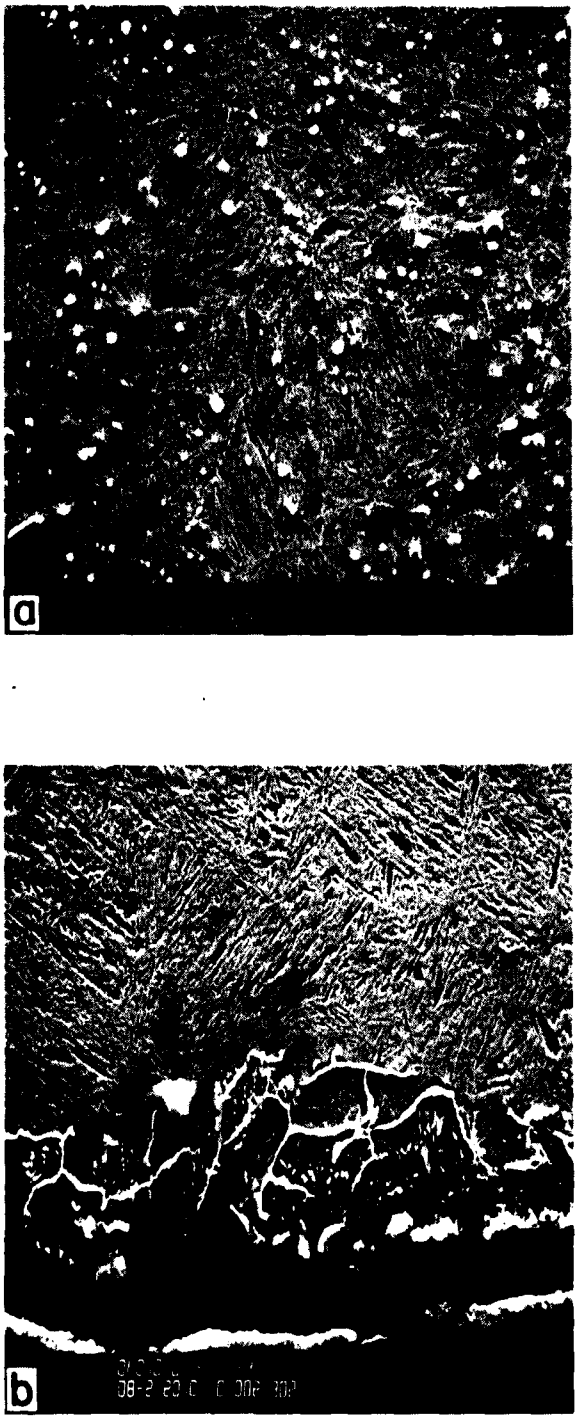

Fig. 36 Scanning electron micrographs illustrating (a) the Fe_3C precipitate distribution near the O.D. surface in a machined region of an M-549 projectile, and (b) lack of Fe_3C precipitates after a decarburization heat treatment of 829°C/4hrs. in air.

Surface hardness and micro-hardness results failed to support this decarburization observation. However, when hardness tests are used to evaluate carbon control, it should be remembered that maximum quenched hardness is attained at about 0.70%C in plain carbon steels, and at lower carbon contents in alloy steels. If variations in carbon content above that required to produce maximum hardness are significant, hardness measurements are not capable of evaluating carbon control.

X-ray diffraction techniques are capable of identifying the composition, crystallographic phases, and line peak shifts indicative of a change in lattice spacing. This technique is not capable of identifying the occurrence of surface reactions such as carburizing, decarburizing, nitriding, etc. However, its usefulness is its capacity to illustrate differences between the machined and hot worked surfaces for major compositional variations and for changes in crystallographic phases. Prior to x-ray, all parts were wire brushed to remove both layers of paint. Correspondingly, it was also shown that paint removal alone had no effect on ultrasonic signal intensity. A comparison of line scans for a recording of x-ray intensity vs scattering angle failed to reveal differences between the two surfaces in composition, phase, or characteristic Bragg angles. Similarly, x-ray analysis at different locations through the wall thickness using an x-ray spectra generated by electron bombardment in an SEM failed to show a difference in chemistry between the interior and the surface of the material.

It can be concluded from these x-ray results, that 1) there are no major compositional differences when considering elements with an atomic number >12, 2) crystallographic phases are the same, and 3) lattice

spacings are unchanged. It should be understood, however, that neither of the above techniques is capable of differentiating between surface reactions by lighter elements such as oxygen, nitrogen or carbon.

Based upon the carbon morphology observation, and negative x-ray results, a projectile was longitudinally sectioned such that each half contained both a machined surface and a hot worked surface. One half of this projectile was decarburized by heat treating at 829^{o}C/4 hrs (1525^{o}F) in air while the other half was carburized by heat treating at the same temperature in an endothermic base atmosphere with the dew point set to correspond to 1.1 points of carbon. Prior to this heat treatment, the machined surfaces were readily inspectable while signals launched on hot worked surfaces were reduced by a factor of 15. After carburization, both surfaces were inspectable whereas after decarburization, signal intensities were reduced for each surface condition. The sequence of operations corresponding to these results is shown in Fig. 37. This experiment very definitely identified the source of reduced transducer efficiencies. Not only could decarburization reduce signal levels, but inspectability of a decarburized surface could also be restored by heat treatments conducive to restoration of the original carbon level.

2. Solutions to Improve Inspection Capabilities. - There are two changes that can be made to production line procedures to eliminate this decarburized layer, that is, 1) machine the appropriate surfaces, and 2) recarburize by appropriate heat treatment. It is beyond the charter of this program to evalute the economic aspects associated with these procedures

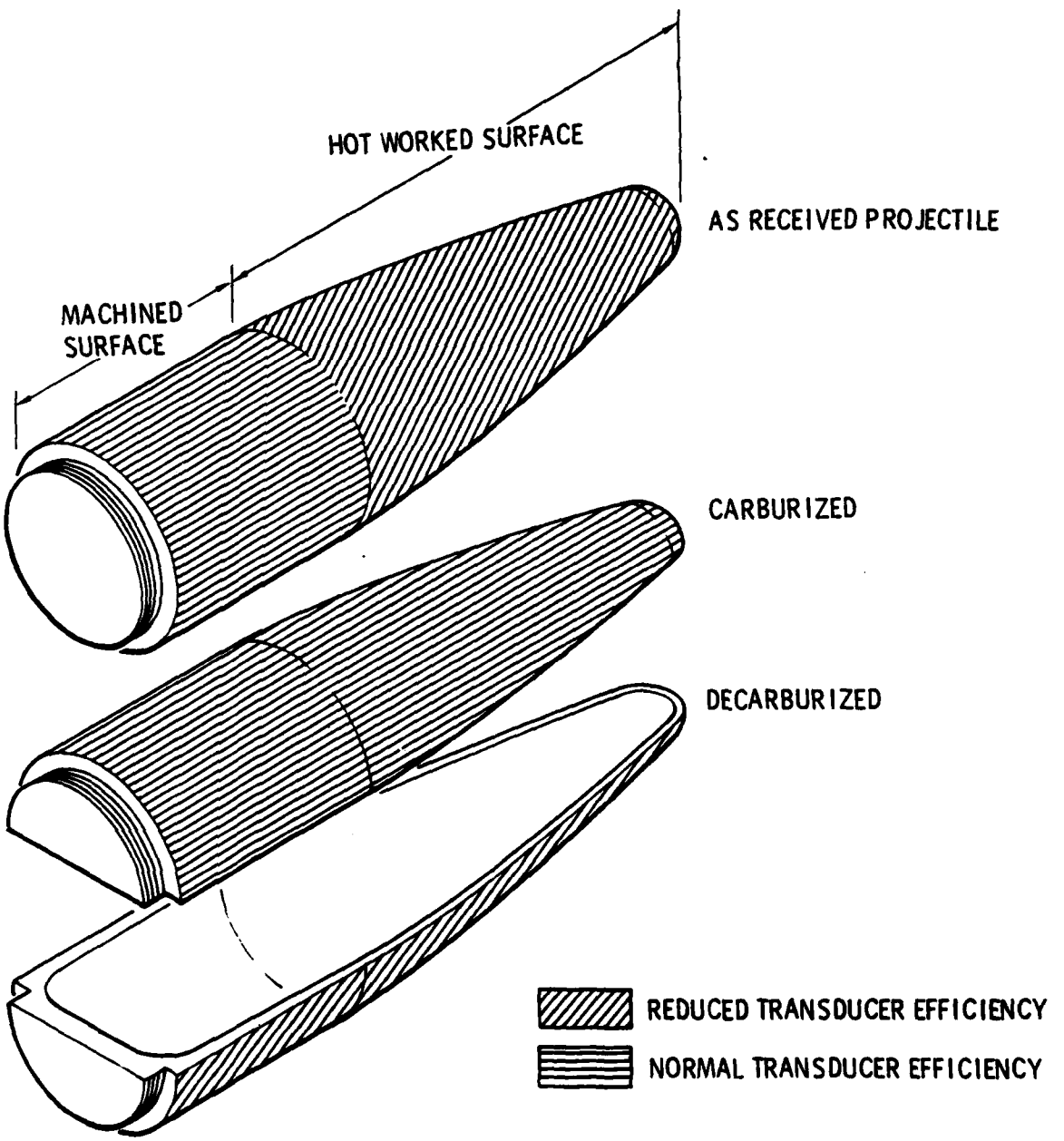

Fig. 37 Changes in transducer efficiency as a function of surface condition and heat treatment.

vs. benefits to be gained. However, due to the simplicity of the recarburization procedure, it merits further discussion concerning both the technique and how it could be applied to the M-549 production line.

Three types of atmospheres are generally used for carbon restoration, but of the three, endothermic base atmospheres with controlled dew points are the best understood and the most widely used in commercial practice. Typical quantities of gasses used in an endothermic atmosphere include 40% H_2, 19% CO and 40% N_2. With regard to dew point, at a certain temperature, for a given pressure, a mixture of gasses will precipitate its moisture content. The exact temperature at which the moisture precipitates is referred to as the dew point. The dew point will thus reflect the chemical balance of various components comprising the reacted products. A relationship between dew point, furnace temperature and carbon level for carbon steels is available.(9) Thus, by control of dew point a "carbonaceous" atmosphere can be controlled to either carburize or decarburize.

As we have illustrated in the above experiment, it would be a simple matter to adjust the dew point during final heat treatment of M-549 projectiles to restore carbon levels to the 1.1%C content of the original material. This would not add an additional heat treatment to current production practices, but would simply require adjusting the dew point to correspond to 1.1 points of C.

A third alternative to circumvent the effects of decarburization results from the discussion presented on the electromagnet design (Section IV-C). In this discussion, it was illustrated that ultrasonic inspection with EMAT transducers could be done in either a tangential or normal magnetic

field. It was shown that in the tangential field, decarburization severly reduced transducer efficiencies whereas when operating in a normal magnetic bias field decarburization had no apparent effect. If it should prove unfeasible to restore the surface carbon content in the M-549 projectile to levels sufficient for EMAT inspection in a tangential field, then inspection procedures could be altered to inspect in the orthogonal field. This alternative is recommended only as a second course of action since it is not anticipated that the inspection of future projectiles will be hindered by decarburization. Future systems would certainly take advantage of benefits to be gained by inspection in the tangential magnetic field, and it is recommended that this inspection system demonstrate these capabilities.

3. Variables Associated With Surface Decarburization. - The variables associated with decarburization and the extent to which they reduce inspectability have yet to be evaluated. For example, in addition to a decrease in efficiency with EMAT transducers, inspection of M-549 projectiles with a decarburized surface layer also proved to be unsuccessful with eddy current techniques. For the case of eddy current inspection, the background noise level increased approximately one order of magnitude due to decarburization and was sufficiently variable as to inhibit calibration of the instrument. For the case of EMAT inspection in two different lots of projectiles, the ultrasonic signal amplitudes differed by a factor of three. Apparently, variables such as depth, magnitude and gradient of a decarburized layer could in some manner influence the sensitivity of the eddy current and EMAT inspection techniques, and probably other magnetic techniques as well.

It is not known by what mechanism decarburization affects the noise level in eddy current inspection, or how the ability to launch ultrasonic signals is affected and indeed a complete scientific investigation of this phenomena has not yet taken place. However, it is possible to make some strong inference as to its origin.

By way of review, the following facts are known in the EMAT case:

1. A mathematical model exists showing that the efficiency of transducers is directly proportional to certain magnetostrictive coefficients of materials. Direct comparison to experimental measurements of efficiencies and magnetostrictive coefficients in four iron-nickel alloys, Armco iron, cold drawn 1018 steel, Invar, and nickel have been in quantitative agreement with the model.
2. On all low carbon steels studied to date (perhaps 10-15 alloys) comparable efficiencies have been observed except in two cases.
3. In an isothermally transformed HF-1 steel having a pearlitic structure, very weak signals were observed. This material had a lamellar structure which is known to substantially affect magnetic properties. Although measurements have not been made, it appears that the magnetostrictive constants are substantially reduced. The microscopic mechanism may be related to the difference in the magnetic properties of the Fe and Fe_3C phase combined with the lamellar structure. When the material is

magnetized, free magnetic poles on the boundaries between the two phases will be energetically unfavorable, thereby restricting the magnetic states that are assumed.

4. In quenched and tempered HF-1 steel, this problem has not been observed except in the decarburized condition discussed above. Again it appears likely that the magnetostrictive constants have somehow been changed.

It is clear that a number of variables associated with decarburization have not as yet been evaluated. To more completely understand this surface effect and to be able to establish a mechanism, it will be necessary to quantitatively determine the extent to which variables such as depth, magnitude and gradient of decarburization influence transducer efficiencies.

VII. SUMMARY

In a previous study,[1] the feasibility of detecting simulated defects in M-107 projectiles and naturally occurring defects in the M-393 projectile using EMAT transducers was demonstrated. The objectives of the present program were (1) to establish the applicability of the EMAT inspection principles to a second projectile, the M-549 (RAP), (2) to layout an inspection system based on these principles, (3) to make detailed designs of specific components, and (4) to construct some components and evaluate their

performance. These results have all been successfully completed as reviewed below.

The fact that the M-549 does not have a rotating band somewhat simplifies the inspection, since now the majority of the projectile is a cylinder (with tapered nose). Consequently, it is believed that a single inspection station, rather than the two station system previously discussed, can be used to inspect essentially the entire projectile. Such a system would be built around a multi-stage mechanical handling system designed for both movement of the projectiles into and out of the inspection station and for performing auxilliary operations, as needed, such as cleaning, dimensional check, rejection of faulty projectiles, and demagnetizing. Detailed fabrication drawings, making use of a walking beam movement to translate the projectiles, have been prepared by K.J. Law Associates, Inc. under subcontract.

The ultrasonic inspection itself is performed while the projectile is in the gap of a large electromagnet which places the entire projectile at the proper magnet bias for optimum transduction efficiency. Inspection is performed by a fixed raster of transducers, which automatically track the projectile and are electronically multiplexed as the projectile is rotated, thus ensuring full coverage. During the previous feasibility phases, a magnet was designed for the M-107, but it was found to have certain deficiencies. During this phase, a new magnet for the M-549 was designed and constructed, which overcomes these deficiencies. This electromagnet will be available for direct incorporation in the prototype system to be constructed during the next phase.

The system will be fully automated under the control of a central processing unit. This central processor will control the handling machinery, the rotation of the projectile in the magnet gap, the activation of the magnet power supply, and the timing of the firing of the individual transducers. In addition, it will process the received ultrasonic signals, compare them to rejection levels stored in a look-up table, and control the machinery to remove defective projectiles from the line. No operator intervention will be required.

As a part of this program, two complete ultrasonic channels were designed, constructed, and evaluated. These are made up of both the meander coil transducers and custom electronics including a high power transmitter, a low noise receiver, a transmit-receive switch, and a correlation receiver. The output of the correlation receiver is a gated signal amplitude analogous in many functional ways to the output of a fixed gate in a standard ultrasonic unit. However, it is superior because it provides both optimum matched filtering and rejection of transient electronic noise which can be anticipated in production facilities. These ultrasonic channels had a dynamic range of approximately 70 dB.

Using these components, the ultrasonic detectability of a variety of defects in the M-549 projectile was investigated. EDM notches having depths as small as 0.023cm (0.009 in) were detected with excellent signal to noise ratios. These notches were located in both the ogive and bourrelet, in the inner and outer surfaces, with axial and circumferential orientations. (No axial notches were placed on the inner surfaces.) Some further work is needed in the base region to overcome geometrical complexities, but it is believed

that this will be solved with the aid of results from ongoing, related programs. Additionally, naturally occurring defects were located using EMAT techniques and verified by destructive analysis.

One unanticipated problem was encountered during the program. It was found that on certain M-549 projectiles, inspectability was hindered by the presence of a decarburized surface layer in unmachined regions. Analysis of production procedures indicates that this can be overcome by either a) machining the projectile exterior, b) slightly modifying the environment during heat treatment to recarburize to initial carbon levels or, c) redesigning the electromagnet to make use of the normal magnetic field, for which transduction efficiencies are uninfluenced by decarburization. It is felt that approach b) is the most desirable alternative since it is believed to represent only slight changes in production procedures while retaining the flexibility of the system described herein.

VIII CONCLUSIONS AND RECOMMENDATIONS

The feasibility of applying the EMAT inspection technology to the M-549 projectile has been demonstrated in both this program and also during the feasibility study (Ref. 1). Based on the successful completion of this phase, it is recommended that Phase III of this program, the construction of a fully automatic prototype system and its installation on a production line, be initiated at the earliest possible time.

IX. REFERENCES

1. R.B. Thompson, "Rapid Ultrasonic Inspection of Artillery Projectiles," Final Report SC5067.7FR on Contract Number DAAA25-76-C-0381, Frankford Arsenal, U.S. Army, January, 1977.

2. R.B. Thompson, "Electromagnetic, Noncontact Transducers," Ultrasonics Symp. Proc. (IEEE, N.Y., 1973) p. 385.

3. R.B. Thompson, "Noncontact Transucers," Ultrasonics Symp. Proc. IEEE, Phoenix, 1977, p. 74.

4. C.F. Vasile, R.B. Thompson, "Periodic Magnet Noncontact Transducers Theory and Application," Ultrasonics Symp. Proc., IEEE, Phoenix, 1977, p. 14.

5. C.M. Fortunko, R.B. Thompson, "Rapid Inspection of Artillery Projectile with Electromagnetic Transducers," Ultrasonics Symp. Proc., IEEE, Phoenix, 1977, p. 134.

6. R.B. Thompson, "A Model for the Electromagnet Generation of Ultrasonic Guided Waves in Ferromagnetic Metal Polycrystals," IEEE Trans. on Sonics and Ultrasonics, Vol. 80-25, Jan. 1978, p. 7.

7. Di Franco and Rubin, "Radar Detection," Prentice-Hall, Inc., Englewood Cliffs, N.J., 1968, Chapter 5.

8. Rockwell International Science Center, Proposal No. SC2815T, January, 1977.

9. _____, Metals Handbook, "Heat Treating, Cleaning and Finishing," 8th Ed., Vol. 2, p. 69.

X. FIGURE CAPTIONS

Fig. 1 Distribution of currents and forces on the lattice of a metal part contributing to generation of ultrasonic signals under normal field bias.

Fig. 2 Variation of ultrasonic amplitude in a 1018 steel plate at 130 kHz. The amplitude is maximized at approximately 300 Oe. Curves are theoretical results.

Fig. 3 Principle of generation of surface waves and angle bulk waves by meander coil electromagnetic transducers.

Fig. 4 Block diagram of the planned system for processing of ultrasonic signals, control of projectile handling machinery and making of accept-reject decisions.

Fig. 5 Time diagram of analog signal processing steps and conversion of the analog data to digital format for further processing of the central data and control processors.

Fig. 6 Circuit diagram of a 1.8 MHz transmitter power amplifier module.

Fig. 7 Transmitter power amplifier output waveforms, (a) collector current on one transistor (10 amp/div, 2μsec/div), (b) transducer current (10 amp/div, 2μsec/div).

Fig. 8 Circuit diagram of a 1.8 MHz receiver preamplifier.

Fig. 9 Functional block diagram of a correlation receiver using a timed delayed replica of the input signal to demodulate the received ultrasonic signal.

Fig. 10 Correlation receiver response for different integration time constants.

Fig. 11 Typical waveform observed at the a) input and b) output of the multiplier circuits at 500 kHz.

Fig. 12 Photograph of a single channel receiver breadboard.

Fig. 13 Magnet configuration for inspecting the M-549 projectile.

Fig. 14 Dependence of transducer generation efficiency on parallel magnetic field in the presence and absence of decarburization.

Fig. 15 Tangential magnetic field as measured on a ¼ scale model of the M-549 projectile. The projectile model neglected the tapering in the ogive.

Fig. 16 End view of the electromagnet showing a M-549 projectile between the pole pieces.

Fig. 17 Side view of electromagnet showing details of yoke laminations and coil design.

Fig. 18 Tangential magnetic field profile at the top of a M-549 projectile as a function of magnet coil current.

Fig. 19 Tangential magnetic field profile at the bottom of a M-549 projectile as a function of magnet coil current.

Fig. 20 Simulation of the effect of increasing the air gap width by raising the nose of the M-549 projectile in the magnet by means of spacers.

Fig. 21 Normal magnetic field profile in the air gap as a function of magnet coil current.

Fig. 22 Stations proposed for the EMAT inspection station.

Fig. 23 Portion of the projectile handling system illustraing the "closed square-wave" motion of the walking beam.

Fig. 24 Plane views of the EMAT inspection station.

Fig. 25 Proposed location of the EMAT ultrasonic inspection system in the M-549 production line.

Fig. 26 Calculation of the angular dependence of the ultrasonic amplitude of both shear and longitudinal acoustic waves excited by a single wire EMAT. These results can be extended to multiple wire EMATs by multiplication by suitable array factors.

Fig. 27 Calculated frequency spectra of higher order symmetric Lamb modes in a 1018 steel plate of 0.500 inch in thickness in a region where maximum generation efficiency is obtained. The horizontal line corresponds to a frequency of 1.8 MHz.

Fig. 28 Calculated frequency spectra of higher order anti-symmetric Lamb modes in a 1018 steel plate of 0.500 inch in thickness in a region where maximum transduction efficiency is obtained. The horizontal line corresponds to a frequency of 1.8 MHz.

Fig. 29 Dispersion of ultrasonic signals in a 0.500 inch thick 1018 steel plate due to coupling of Lamb modes. The RF carrier frequency is 1.8 MHz and the input transducer is separated from the output transducer by approximately 8 inches.

Fig. 30 Configuration used to test the performance of one ultrasonic signal processing channel, including a single channel correlation receiver.

Fig. 31 Photo of the electronics package, including the correlation receiver and meander coil transducers.

Fig. 32 Detection of a simulated defect as the M-549 projectile is rotated beneath a fixed electromagnetic transducer. The range gate of the correlation receiver is set for maximum output when the seperation between the defect and the transducer is approximately 2.5cm (1 in).

Fig. 33 Detection of OD simulated defects in the bourrelet with correlation receiver range gate set to produce maximum output for 2.5cm (1 in) separation between transducer and defect. (1) upper trace: detection of a defect located 5cm (2 in) from base and having 0.95cm (0.375 in) surface length and 0.028cm (0.011 in) by H_2. (b) lower trace detection of a defect located 10cm (4 in) from base and having 0.56cm (0.222 in) surface length and 0.09cm (0.035in) depth.

Fig. 34 Detection of an OD simulated detect with EMAT and piezoelectric wedge transducers. The transducer elements are 5.7cm (2.25 in) away from the defect along the circumference in the bourrelet region and approximately 10cm (4 in) away from base. (a) upper trace EMAT @ 1.8 MHz, (b) middle trace 60^{o} wedge transducer @ 2.25 MHz, (c) lower trace same as above but projectile rotated 180^{o}.

Fig. 35 Detection of a natural flow located on the ID in the ogive region of an M-549 artillery projectile using EMAT technology.

Fig. 36 Scanning electron micrographs illustrating a) the Fe_3C precipitate distribution near the O.D. surface in a machined region of an M-549 projectile, and b) lack of Fe_3C precipitates after a decarburization heat treatment of 829^{o}C/4hrs. in air.

Fig. 37 Changes in transducer efficiency as a function of surface condition and heat treatment.